

**Isotopic and geochemical characteristics of the British Empire
Granite as indicators of magma provenance and processes of melt
generation in the Mount Painter Inlier, South Australia.**

Narelle L. Neumann

(B.A.)

This thesis is submitted as partial fulfilment for the
Honours Degree of Bachelor of Arts

Department of Geology and Geophysics
University of Adelaide

November 1996

National Grid Reference (SH - 54) 6737

1:100 000

ABSTRACT

The production of granitic magmas at shallow to midcrustal depths by anatexis of crustal material requires a significant thermal perturbation of the normal crustal geothermal regime. Thermal perturbations leading to anatexis may be initiated by crustal thickening associated with deformation, intrusion and/or upwelling of heat sources from lower crust or mantle regions or by anomalous concentrations of heat-producing elements, U, Th and K. This thesis explores the origin of shallow to mid-crustal peraluminous granites within the Mount Painter Inlier, together with their relationship to older granite suites, as indicators of magmatic processes during crustal deformation of the Delamerian Orogeny.

The geochemical and isotopic characteristics of granites and gneisses of the Mount Painter Inlier indicate two distinct periods of granitic evolution involving different source regions and magmatic processes. Proterozoic granites and gneisses reflect magmatic sources and processes similar to those involved in the evolution of other Australian anorogenic Proterozoic terrains, although extreme concentrations of U, Th and K suggest an important role for element concentration within accessory minerals during granite genesis. Field relationships, together with geochemical and isotopic characteristics of the Palaeozoic(?) British Empire Granite indicate evolution from a complex mixture of surrounding metasediments and granites in a number of possible scenarios. The additional thermal energy required to produce the British Empire Granite from partial melting of this package at depths of approximately 12 to 15 km is consistent with perturbed thermal regimes resulting from anomalous internal heat production due to the extreme concentration of U, Th and K within the Proterozoic units.

CONTENTS

Terminology and Abbreviations

Lists of Tables, Figures and Plates

Page No.

CHAPTER 1 - INTRODUCTION

1.1 Introduction	1
1.2 Previous Investigations, Aims and Thesis Outline	2

CHAPTER 2 - REGIONAL GEOLOGY

2.1 Regional Setting of the Mount Painter Inlier	4
2.2 Geological Setting of the Paralana Plateau - Yudnamutana Gorge - Mawson Plateau Area	4
2.3 Lithological Descriptions	5
2.4 Structural Framework	9
2.5 Conclusions	10

CHAPTER 3 - MAJOR AND TRACE ELEMENT GEOCHEMISTRY

3.1 Geochemical Characteristics of Mount Painter Inlier Suites	11
3.2 Geochemical relationships between Mount Painter Inlier Units	13
3.3 Geochemical Characteristics of the Neoproterozoic Adelaidean Units	14
3.4 Geochemical Comparisons to other Australian terrains	14
3.5 Conclusions	14

CHAPTER 4 - RADIOGENIC ISOTOPE GEOCHEMISTRY AND GEOCHRONOLOGY

4.1 Zircon systematics	15
4.1.1 Zircon Pb-Pb data and interpretations	16
4.1.2 Zircon backscattered electron imagery and microprobe analysis	17
4.2 Whole Rock Rb-Sr and Sm-Nd systematics	17
4.2.1 Rb-Sr and Sm-Nd isotope results	18
4.2.2 Rb-Sr isotope analysis and interpretations	19
4.2.3 Sm-Nd isotope analysis and interpretations	19
4.3 Conclusions	21

CHAPTER 5 - RADIOACTIVE ELEMENT CONCENTRATIONS IN THE MOUNT PAINTER INLIER

5.1 Anomalous U, Th and K enrichment in the Mount Painter Inlier	22
5.2 Origin and processes controlling heat-producing element distribution and concentration	23
5.3 Absolute Crustal Heat Production within the Mount Painter Inlier	26
5.4 Conclusions	27

CHAPTER 6 - BRITISH EMPIRE GRANITE PROVENANCE AND IMPLICATIONS FOR MAGMATIC PROCESSES WITHIN THE MOUNT PAINTER INLIER

6.1 Potential British Empire Sources	28
6.2 Origins and potential thermal perturbations initiating crustal anatexis and British Empire Granite production	29
6.3 Implications for British Empire Granite Provenance	32
6.4 Conclusions	32

REFERENCES

ACKNOWLEDGMENTS

APPENDICES

- A : Geological Map of Paralana Hot Springs - Mawson Plateau area
- B : Sample Location Map
- C : Thin Section Descriptions
- D : Thins section photomicrographs
- E : Summary of Geochemical Data Set
- F : Summary of Zircon Pb-Pb Data
- G : Summary of Zircon Microprobe Data
- H : Summary of Isotopic Data
- I : Isotopic mixing curve calculations
- J : Major, trace and radiogenic isotope element analysis techniques

K : Zircon separation and analysis techniques

L : Radiometric image of the Mount Painter Inlier

M : Heat production calculations for the Mount Painter Inlier

LIST OF TABLES

Table 2.1 Comparison of lithological names used for units in the Paralana Plateau-Mawson Plateau Area

Table 3.1 Summary of whole rock analysis for selected Mount Painter Inlier units

Table 4.1 Summary of $^{207}\text{Pb}/^{206}\text{Pb}$ isotopic data

Table 4.2 Summary of geochemical characteristics of British Empire Granite and Paralana Granodiorite zircons and apatites

Table 4.3 Summary of Rb-Sr and Sm-Nd isotopic data for selected lithologies of the Paralana Hot Springs-Mawson Plateau area

Table 5.1 Average Heat production values for Mount Painter Inlier Units

LIST OF PLATES

Plate 1a Augen-textured Gneiss with cross cutting pegmatite

Plate 1b Steeply dipping mylonitised Paralana Creek Metasediments and Paralana Granodiorite

Plate 1c Migmatitic Paralana Granodiorite with ptigmatic K-feldspar veins

Plate 1d Strongly folded migmatitic Paralana Granodiorite with biotite schlieren

Plate 1e Undeformed Paralana Granodiorite with K-feldspar enclaves

Plate 1f Pegmatitic Granite with rafts of residual foliated biotite schlieren

Plate 1g British Empire Granite surrounded by migmatitic Freeling Heights Quartzite

Plate 1h Raft of Freeling Heights Quartzite within British Empire Granite

Plate 2a View of the Tail and Mawson Plateau from Paralana Plateau

Plate 2b View south from Mawson Plateau

Plate 3a British Empire Granite zircon from Mawson Plateau

Plate 3b British Empire Granite apatite from Mawson Plateau

Plate 3c Paralana Granodiorite-British Empire Granite Mix zircon

Plate 3d Paralana Granodiorite-British Empire Granite Mix zircon

-
- Plate 3e** Paralana Granodiorite zircon from the Tail
Plate 3f Paralana Granodiorite zircon from the Tail
Plate 3g Paralana Granodiorite zircon from Paralana Plateau
Plate 3h Paralana Granodiorite zircon from Paralana Plateau

LIST OF FIGURES

- Figure 1.1** Location of the Mount Painter Inlier in South Australia
Figure 2.1 Location of the study area within the Mount Painter Inlier
Figure 3.1 Multi-element comparison between MPI gneissic and metasedimentary units
Figure 3.2 Multi-element comparison between Tail-Body granites and metasediments
Figure 3.3 Multi-element comparison between Tail-Body granites and Adelaidean cover
Figure 3.4 Harker diagrams for selected Mount Painter Inlier units
Figure 3.5 Trace element comparison diagrams for selected Mount Painter Inlier units
Figure 3.6 Granite suite discrimination diagrams
Figure 3.7 Granite tectonic discrimination diagrams
Figure 3.8 Multi-element comparison between Mount Painter Inlier and Gawler Craton units
Figure 3.9 Multi-element comparison between Mount Painter Inlier and Gawler Range Volcanics units
Figure 3.10 Multi-element comparison between Mount Painter Inlier and Southern Adelaide Fold Belt
Figure 4.1 Pb-Pb age discrimination diagram for Paralana Granodiorite from the Tail
Figure 4.2 Rb-Sr isochron for British Empire Granite
Figure 4.3 Nd isotopic evolution through time for selected Mount Painter Units
Figure 4.3 Nd isotopic evolution through time for Mount Painter Inlier units, Wooltana Volcanics and Adelaidean sediments
Figure 4.5 Radiogenic isotope variations between Mount Painter Inlier units at 470 Ma and 800 Ma
Figure 4.6 Radiogenic isotope comparison to trace element concentrations at 470 Ma
Figure 5.1 U, Th and K comparisons between Mount Painter Inlier units and other Australian terrains
Figure 6.1 Geothermal models for the Mount Painter Inlier

TERMINOLOGY AND ABBREVIATIONS

Below is listed a list of abbreviations used throughout this document

BEG	British Empire Granite
bt	biotite
CHUR	Chondritic Uniform Reservoir
DM	Depleted Mantle
ϵ Nd	Epsilon Nd
Ma	Mega-anna, = Million years before present
Ga	Giga-anna, = Billion Years before present
GRV	Gawler Range Volcanics
FHQ	Freeling Heights Quartzite
fspar	feldspar
HREE	Heavy Rare Earth Elements
k-feldspar	potassium feldspar
LFB	Lachlan Fold Belt
LREE	Light Rare Earth Elements
MBI	Mount Babbage Inlier
MPI	Mount Painter Inlier
MPB	Mount Painter Block
mu	muscovite
PCM	Paralana Creek Metasediments
Peg G	Pegmatitic Granite
PG	Paralana Granodiorite
plag	plagioclase
ppm	parts per million
qtz	quartz
REE	Rare Earth Elements
T_{CHUR}	Model age from CHUR
T_{Model}	Model age from Depleted Mantle

Chapter One

INTRODUCTION

1.1 Introduction

Continental crustal melting and production of granitic magmas within shallow to midcrustal levels requires a significant perturbation of crustal steady-state geothermal conditions (England and Thompson, 1984). The processes of lithospheric-scale heating as a conductive response to deformation, localisation of heat associated with advective upwelling of magmas or hot fluids, or depression of the crustal melting point by the introduction of hydrous fluids, all potentially produce granitic magmas. In addition, heat produced by anomalous radioactive element concentrations within the crust may drive deformation and initiate partial melting (Chamberlain and Sonder, 1990; Lathrop *et al.*, 1994). As anatexis in an open-system requires additional crustal energy to initiate partial melting, a mantle perturbation must occur before crustal melting can occur (Lathrop *et al.*, 1994). In contrast, melting in a closed-system implies additional energy can be found within the crust itself, with no mantle involvement necessary. Therefore if the extent of mantle or lower crustal contribution to a magma can be identified by geochemical and isotopic characteristics, constraints on possible thermal sources and also closed- or open system anatexis can be derived (Lathrop *et al.*, 1994).

The peraluminous nature of the British Empire Granite (Teale, 1979; Schaefer, 1993) within the high temperature-low pressure polydeformed Proterozoic Mount Painter Inlier, South Australia (Figure 1.1) suggests that this granite is unlikely to be derived directly from lower crust or mantle rocks. Previous studies by Wall (1995) have shown that the Mount Painter Inlier is extremely enriched in radioactive elements, with the resulting heat generation potentially providing additional thermal energy required to initiate crustal melting represented by the British Empire Granite. This geochemical and isotopic study of the British Empire Granite therefore determines the provenance material and emplacement time of this magmatic body in order to identify the thermal energy source and define crustal magmatic processes within the Inlier.

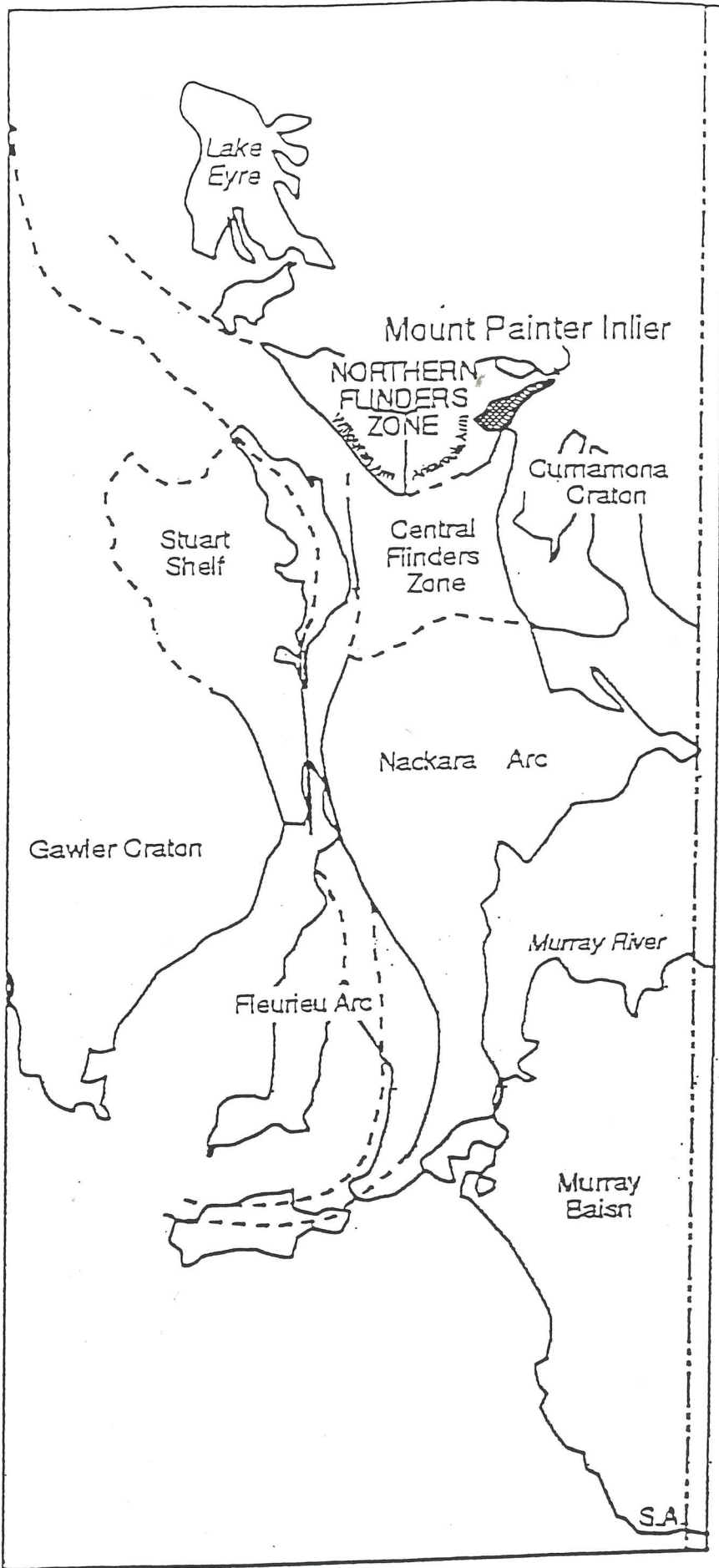


FIGURE 1.1 : LOCATION OF THE MOUNT PAINTER INLIER, SOUTH AUSTRALIA

1.2 Previous Investigations, Aims and Thesis Outline

Driven by the potential for discovery of significant copper and uranium mineral deposits, the Mount Painter Inlier has been a focus of geological studies and mining exploration since the late 1800's. Investigations concerning the geochemistry, geochronology and structure of the Inlier have been undertaken by Teale (1995), Teale (1993a,b), Sheard *et al.* (1992), Coats and Blissett (1971) and Bowes (1953) and by University of Adelaide Honours students including Wall (1995), Slade (1995), Huston (1995), Schaefer (1993), Teasdale (1993), Blight (1977) and Roberts (1976). Likewise, stratigraphic and sedimentological characteristics of the Neoproterozoic cover sequence and its relationship to basement have been discussed by Mildren and Sandiford (1995), O'Halloran (1992), Coats and Blissett (1971), and Bingemer (in prep.).

Although some investigation of the Palaeozoic intrusives (British Empire Granite, Mudnawatana Tonalite, Gordan Springs Granodiorite) has been undertaken in the past (Schaefer, 1993; Teale, 1979; Coats and Blissett, 1971; Coats *et al.*, 1969), little is known about the source, petrogenesis and crystallisation age of the British Empire Granite or its relationship to Delamerian metamorphism and deformation. In addition, previous studies of Proterozoic granites, gneisses and volcanics (Schaefer, 1993; Teale, 1993a, b) have failed to explore the magmatic processes responsible for the anomalously high concentrations of U, Th and K within basement units, nor their potential impact on the regional thermal regime during subsequent generation of the British Empire Granite. The Mount Painter Inlier therefore provides an ideal setting to investigate the processes which may initiate shallow to mid-crustal anatexis during Delamerian deformation.

This research project explores the mineralogy, geochemistry and geological setting of the British Empire Granite, together with its relationship to both the basement and cover sequence in order to identify the material from which the granitic melt was derived, the time of crystalline emplacement and mechanisms of melting. Lithological and structural characteristics and relationships of Proterozoic and Palaeozoic granites, gneisses and metasediments within the Paralana Hot Springs-Mawson Plateau region are discussed in Chapter 2. Geochemical classifications, similarities and distinctions between the Proterozoic and Palaeozoic units, together with comparisons of other well-defined Australian terrains, are outlined in Chapter 3 in order to identify processes which produce the lithological characteristics observed. Chapter 4 explores the geochronology of the Proterozoic and Palaeozoic units, with zircon isotopic systematics constraining magmatic crystallisation ages,

and interpretation of Rb-Sr and Sm-Nd isotopic signatures indicating potential provenance sources of the British Empire Granite.

Chapter 5 investigates the origin of anomalous U, Th and K concentrations in Proterozoic granites, gneisses and volcanics relative to other anorogenic Proterozoic terrains, together with processes that may produce such anomalies. Calculations and implications of the resulting elevated crustal heat production on the thermal regime of the Mount Painter Inlier are also discussed. Chapter 6 explores different provenance scenarios for the British Empire Granite, together with possible thermal perturbations which provide the additional thermal energy required for crustal anatexis, and resulting implications for the magmatic and structural evolution of the Mount Painter Inlier.

Chapter Two

REGIONAL GEOLOGY

An important precursor to any discussion of magmatic evolution within the Mount Painter Inlier is the identification of characteristics and relationships between different lithological units. An area located on the southeastern boundary of the inlier (Figure 2.1) provides the focus for this discussion and allows investigations of the relationship between British Empire Granite, Proterozoic units and Delamerian deformation. This chapter provides lithological classifications and descriptions based on field studies in the region. In addition, the structural framework of this region will be briefly addressed.

2.1 Regional setting of the Mount Painter Inlier

The Mount Painter Inlier located in the northern Flinders Ranges, South Australia (Figure 1.1) consists of Mesoproterozoic and possibly Palaeoproterozoic metasediments, granites and gneisses (Figure 2.1) which display a complex intrusive, metamorphic and deformational history (Flint, 1993; Teale, 1993a). Unconformably overlying this crystalline basement complex is a Neoproterozoic (Adelaidean) cover sequence which includes clastic and carbonate sediments and volcanics deposited within the Adelaide Geosyncline. Deformation and heating associated with the Delamerian Orogeny approximately 450-500 Ma ago resulted in metamorphism of the cover sequence around the inlier, with associated intrusions of granitoids into the Mount Painter and Mount Babbage Inlier and Adelaidean metasediments (Preiss, 1987).

2.2 Geological setting of the Paralana Hot Springs-Yudnamutana Gorge-Mawson Plateau Area

The Paralana Hot Springs-Yudnamutana Gorge-Mawson Plateau region contains Proterozoic granites, gneisses, volcanics and metasediments in a northeast-southwest trending and southwest plunging antiform (Appendix A). This sequence is intruded by the essentially undeformed British Empire Granite. The north-easterly trending Paralana Fault system defines the eastern boundary of the Inlier. It is believed that there has been intermittent

FIGURE 2.1

Schematic map of the Mount Painter Inlier and Mount Babbage Inlier, northern Flinders Ranges, South Australia. The Paralana Hot Springs-Yudnamutana Gorge-Mawson Plateau study area is located within the boxed area, with a geological map in Appendix A representing this area in more detail.

Unit 1 represents Mesoproterozoic and possibly Palaeoproterozoic basement rocks of the Mount Painter and Mount Babbage Inliers, including granites, gneisses, volcanics and metasedimentary successions.

Units 2 to 5 are Neoproterozoic (Adelaidean) cover sediments comprising the Callana, Burra, Umberatana and Wilpena Groups respectively.

Unit 6 represents the British Empire Granite body, and the Paralana Granodiorite Tail identified in this study.

The area to the east of the Mount Painter Inlier is dominated by Tertiary sediments.

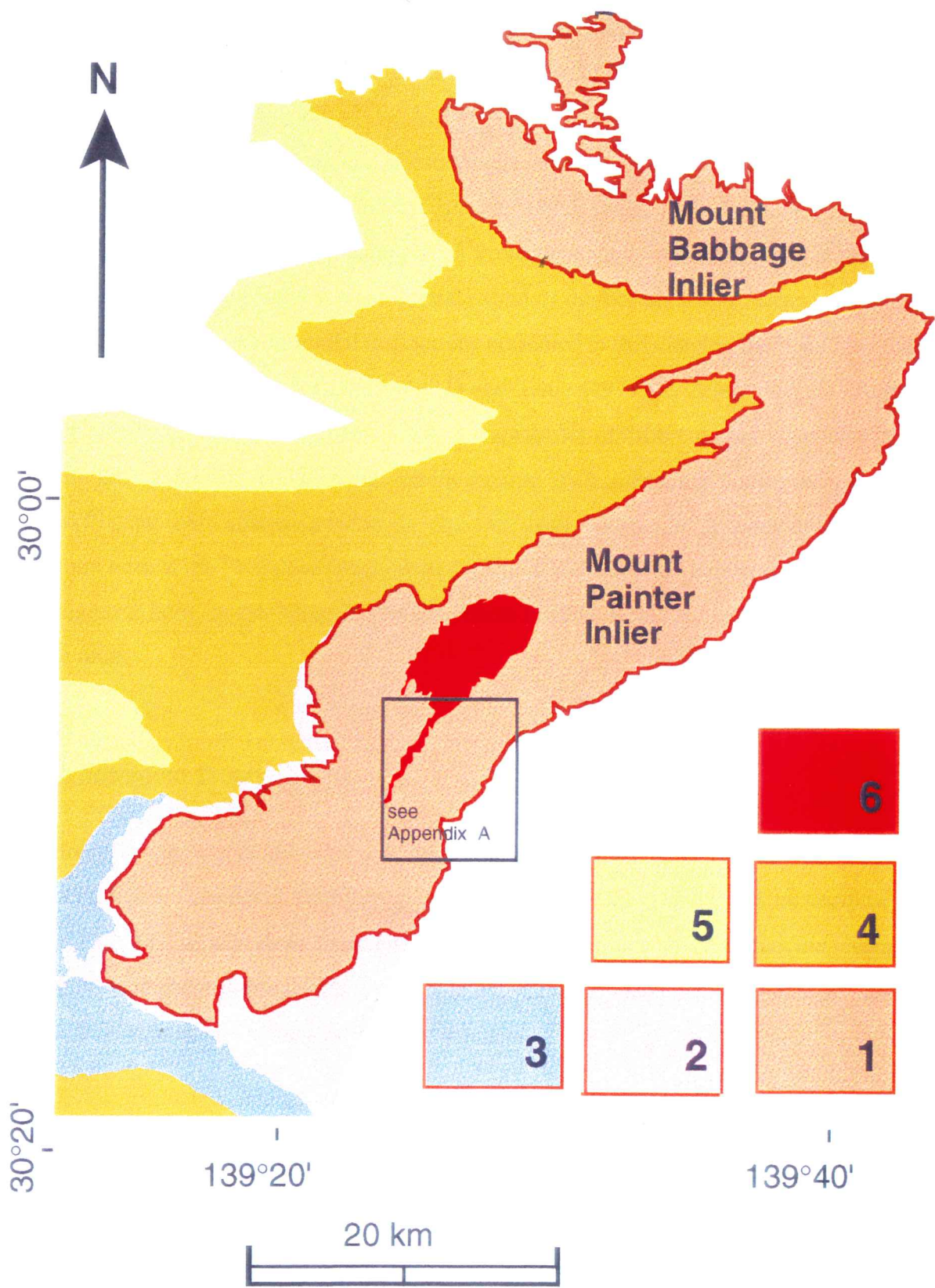


FIGURE 2.1 : LOCATION OF THE STUDY AREA WITHIN THE MOUNT PAINTER INLIER

activity along this fault zone since the Proterozoic (Teasdale, 1993; O'Halloran, 1992; Schaefer, 1993; Teasdale *et al.*, 1995).

Due to contradicting lithological classifications presented in previous studies of the Mount Painter Inlier (Coats *et al.*, 1969; Coats and Blissett, 1971; Teale, 1979; Teale, 1993a, b) it has been necessary to revise the classification of all Proterozoic and Palaeozoic units in this region (Table 1.1). Of particular interest is the spatial extent of the British Empire Granite. Based on mineralogical, textural and structural distinctions presented in this chapter, the body mapped by Coats *et al.* (1969), Coats and Blissett (1971) and Teale (1979) as British Empire Granite is shown to consist of two distinct magmatic bodies, probably of different ages. Specifically, it is proposed that a narrow body of deformed granitic rock extending southwards from the Mawson Plateau (here after referred to as “the Tail”) and the granitic gneisses of the Paralana Plateau are termed the “Paralana Granodiorite”. The British Empire Granite is restricted to the main magmatic body on the Mawson Plateau. These lithologies will henceforth be discussed as separate units.

2.3 Lithological Descriptions

Mineralogical and structural characteristics of major lithologies within the structural framework will be discussed briefly to classify major granitic, gneissic and metasedimentary units and identify relationships between different units in order to constrain the magmatic, sedimentary and deformational history of the Inlier. Lithologies of the study area are listed in order of their appearance in the stratigraphic column.

Paralana Creek Metasediments

Paragneisses are the lowest unit of the mapped area and comprise of a series of migmatitic metasediments ranging from quartzites to pelitic metasediments and aluminous quartzites with biotite schists and sillimanite-bearing interlayers. Compositional, mineralogical and textural distinctions within this series result from variations in initial bulk composition reflecting changes in original sedimentary facies environment. This migmatitic and metasedimentary unit is part of the Palaeoproterozoic ‘Freeling Heights Quartzite’ of Coats *et al.* (1969) and is hereafter referred to as the “Paralana Creek Metasediments.”

	Coats <i>et al.</i> , 1969; Coats and Blissett, 1971	Teale, 1979, 1993a, b	Paralana Plateau - Mawson Plateau Area
Palaeozoic	Mudnawatana Granite	Gordan Springs Granodiorite Mudnawatana Tonalite British Empire Granite	British Empire Granite
Mesoproterozoic	Wattleowie Granite Terrapinna Granite Yerila Granite Mount Neill Granite Porphyry	Nooldoonooldoona Trondjemite Wattleowie Granite Mount Neill Granite Unit 3 - Volcanics, schists, quartzite (including Pepegoona Porphyry) Unit 2 - Quartzite, schist (including Freeling Heights and Mount Adams Quartzite) Unit 1 - Phyllite, schist (including Yargdlin Phyllite)	Paralana Granodiorite (?) Mount Neill Granite in northern area Felsic Volcanics in southern area Freeling Heights Quartzite
Palaeoproterozoic	Freeling Heights Quartzite Brindana Schist Pepagoona Porphyry Mt Adams Quartzite Yagdlin Phyllite	Unit 5 - Quartzite Unit 6 - Metavolcanic-granitic gneiss Unit 4 - Metasediments Unit 3 - Layered Gneiss Unit 2 - Augen Gneiss Unit 1 - Migmatites	Hot Springs Granitic Gneisses Paralana Creek Metasediments

Table 1.1 : Comparison of lithological names used for units in the Paralana Plateau - Mawson Plateau Area

Hot Springs Granitic Gneisses

This suite comprises of massive K-feldspar gneisses and augen-textured gneisses with distinctions based on variations in mineralogy and deformation fabrics. Massive K-feldspar granitic gneisses located at Paralana Plateau, Yudnamutana Gorge and the eastern margin of the Tail were originally named Terrapinna Granite (Coats *et al.*, 1969) but have since been re-classified and broadly correspond to the Palaeoproterozoic Suite 1 of Teale (1993a). This medium-grained, massive, dark pink-coloured granitic gneiss ranges from massive granite to gneisses containing a strong biotite foliation. At the Paralana Plateau, a repeated outcropping sequence of Hot Springs Gneisses and Paralana Granodiorite on a 10 metre scale show no

intrusive relationships and thus may reflect tight folding associated with probable Delamerian folding events focussed at the nearby Paralana Fault.

The Massive K-feldspar Gneiss Suite is spatially related to Augen-textured Gneisses (Suite 2 from Teale, 1993a). The Augen-textured Gneisses are located at the Paralana Plateau, Hot Springs Gorge, eastern and central tail region and intrudes Paralana Creek Metasediments in Paralana Creek. This gneissic sequence is dominated by black and white/pink gneisses containing K-feldspar and plagioclase augens within a strong biotite foliation, with significant potassium and magnetite enrichment (Plate 1a). In Yudnamutana Gorge, this unit is associated with an orange/red-coloured augen gneiss characterised by large quartz augens recording a pervasive fabric within a K-feldspar dominated matrix. Although no field relationship is observed between units within the Hot Springs Gneiss suite, geochemical similarities discussed in Chapter 3 suggest they are part of the same magmatic suite with compositional and textural distinctions reflecting variations in melt proportion during genesis.

Freeling Heights Quartzite

Freeling Heights Quartzite is observed at the western margin of the Tail and Mawson Plateau. This unit is characterised by fine-grained cross-bedded quartzites containing internal dark mineral banding, mica-rich interbeds and conglomerate beds in the basal unit at the western Tail. The Freeling Heights Quartzite appears less deformed than Paralana Creek Metasediments, recording dominantly muscovite-grade metamorphism with brittle faults accommodating deformation, suggesting a Delamerian signature and constraining maximum burial depths experienced by this and surrounding units (Preiss, 1995; E. Paul, *pers. comm.*, 1996). At the Tail, the quartzite boundary with the Paralana Granodiorite is marked by a 30m wide gradational zone of migmatites and pegmatitic granites. The depositional vertical thickness of this unit is estimated at 3.6 km (E. Paul, *pers. comm.*, 1996).

Felsic Volcanics and shallow intrusives

The Felsic Volcanic Suite identified within the eastern and southern study region corresponds to the Mesoproterozoic Mount Neill Porphyry (Coats *et al.*, 1969) and represents a large range of distinct textural lithologies produced in a sub-extrusive setting. The most volumetrically significant unit in the study area is a porphyritic granite containing clasts ranging in size from 1 to 5 cm within a siliceous matrix. At Paralana Hot Springs, the suite is characterised by a purple hematitic and siliceous matrix which may represent the brecciated porphyry described from this area by Coats and Blissett (1971). The strong foliation fabric characteristic of the Hot Springs Gneisses is not observed within the Felsic Volcanics,

PLATE 1a

Strongly foliated K-feldspar dominated augen-textured gneiss of the Hot Springs Gneiss Suite cross cut by undeformed pegmatite on Paralana Plateau.

PLATE 1b

Vertically dipping, strongly mylonitised Paralana Creek Metasediments (left) and Paralana Granodiorite (right) of the Paralana Fault Zone.

PLATE 1c

Ptygmatic K-feldspar veins developed within biotite schlieren at the western boundary of the Paralana Granodiorite Tail.

PLATE 1d

Alternating bands of pale pink K-feldspar leucosomes and dark grey biotite-dominated melanosomes folded into "M" and "W" folds around large leucosome pods within Paralana Granodiorite at the western boundary of the Tail.

PLATE 1e

Restitic K-feldspar situated within undeformed massive Paralana Granodiorite at the Paralana Plateau.

PLATE 1f

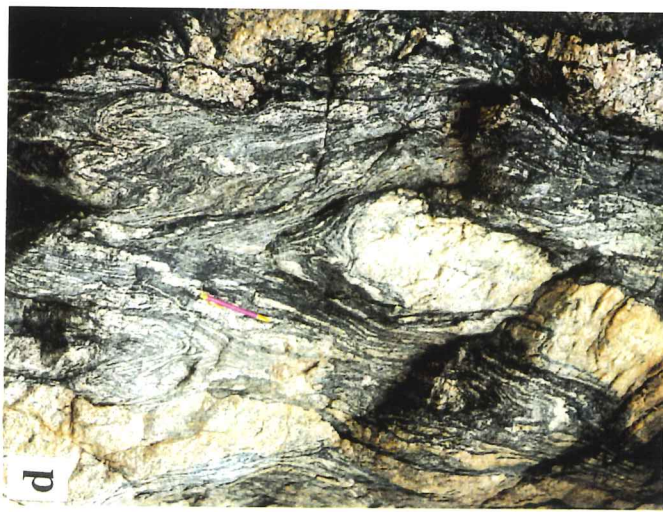
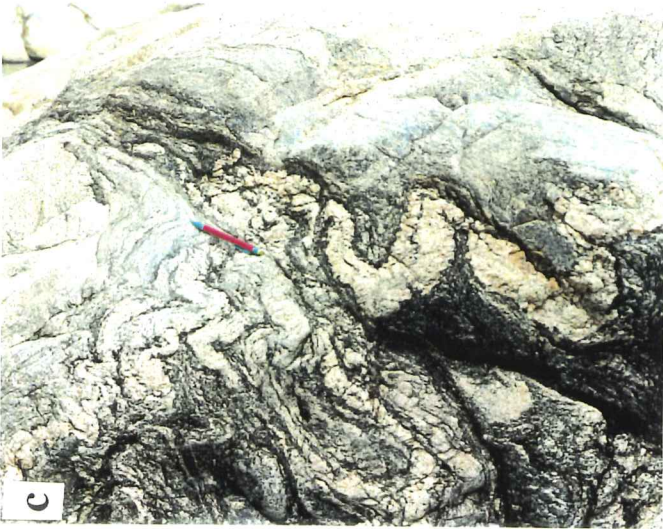
Massive undeformed Pegmatitic Granite at the western Tail boundary with pods of strongly foliated residual biotite schlieren.

PLATE 1g

British Empire Granite enclosed within migmatitic Freeling Heights Quartzite containing distinct dark mineral banding. Minor migmatitic quartzite pods exhibiting a minor foliation are also situated within the granite.

PLATE 1h

Rafts of Freeling Heights Quartzite within British Empire Granite at the Tail-Body junction, with granite containing a subtle restitic foliation .



suggesting that this porphyry has not recorded the same number of deformational events as the gneisses and therefore imposing a maximum relative age for the suite.

Paralana Granodiorite

As discussed in the introduction, the Paralana Granodiorite is located at Paralana Plateau, Yudnamutana Gorge, the Tail and southern Mawson Plateau. This unit is characteristically a medium to coarse-grained massive granite-granodiorite containing plagioclase, quartz and biotite with minor K-feldspar and hornblende. Textural and compositional characteristics are similar to the Gordon Springs Granodiorite identified by Teale (1979).

On the Paralana Plateau, Paralana Granodiorite intrudes Hot Springs Gneisses at a shallow angle to gneissic foliation, with subsequent isoclinal tight folding producing repeated 'interfingered' sub-parallel outcrop of the two units. The occurrence of numerous Paralana Granodiorite pods up to 10m thick between Paralana Plateau and the Tail represent dyke-like offshoots from the main granodiorite intrusive which are slightly discordant to bedding and foliation of the Paralana Creek Metasediments.

The eastern boundary of the Tail displays a clear gradation from Paralana Creek Metasediments with increasing migmatisation to Paralana Granodiorite. The Tail comprises Paralana Granodiorite together with minor Hot Springs Gneisses and quartzitic migmatitic pods. The western boundary of the Tail with the overlying Freeling Heights Quartzite is marked by pegmatitic granites up to 50m thick. On a local scale, the Paralana Granodiorite varies greatly in appearance from homogeneous granodiorite exhibiting a subtle biotite foliation to migmatites containing tight isoclinal folding of biotite schlieren around K-feldspar boudins and ptygmatic leucosome veins (Plate 1c and 1d). Minor zones of K-feldspar pegmatite located within this unit probably represent residual material segregated during granodiorite crystallisation (Plate 1e).

Due to its minimal deformed/folded thickness at both Paralana Plateau and the tail, the initial pre-Delamerian granodioritic intrusion may represent a thin continuous sheet-like body emplaced sub-parallel to bedding/foliation developed in Proterozoic metasediments and gneisses. Later folding and subsequent erosion producing the numerous discontinuous outcropping sequence observed.

PLATE 2a

Westerly view from Paralana Plateau, showing extensive Hot Springs Gneiss outcrop in the foreground. The Paralana Creek Metasediments in the center of the view produce subtle lower topography with the granite escarpment in the mid-ground marking the eastern boundary of the north-south trending Paralana Granodiorite Tail. The southern extent of the Tail is marked by the British Empire Mine located within the overlying rugged Freeling Heights Quartzite range forming the high background topography. In the north, the Mawson Plateau represents the southern extent of British Empire Granite.

PLATE 2b

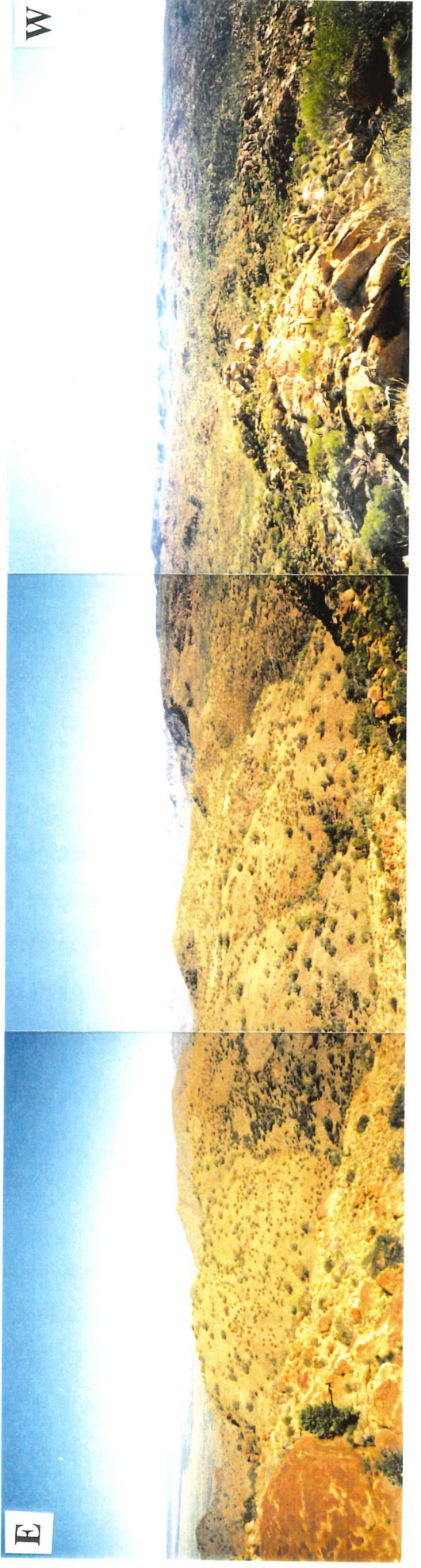
Panoramic view of the southern Mawson Plateau looking south from the southeastern boundary of the British Empire Granite-Paralana Granodiorite junction. The British Empire Granite produces elevated flat topography with tors and boulders dominating the landscape surface. In the central mid-ground the Freeling Heights Quartzite range containing the British Empire Granite Mine can be seen, indicating the extent of the field area. Note the dramatic change in topography from the basement Mount Painter Inlier to the surrounding Tertiary plain illustrated in the left of the photo.

N



S

W



E

British Empire Granite

The British Empire Granite is coarse-grained, granular K-feldspar, muscovite, plagioclase, quartz-bearing with minor biotite and tourmaline. The body dips shallowly to the west, with diffuse gradual contact boundaries of the southwest section of the body to the surrounding units suggesting minimal migration during generation. The western boundary of the granite with the overlying Freeling Heights Quartzite is gradational, spanning approximately 150m and characterised by an increase in the proportion of feldspar megacrysts and incorporation of large *in situ* migmatized quartzite rafts (Plate 1g and Plate 1h). At Mawson Plateau, the eastern contact of the granitic body with metasediments also reflects a rapid gradation from migmatitic quartzite to Pegmatitic Granite (with minor quartzitic rafts) through finer-grained granite to typical British Empire Granite. South along the same contact, Paralana Granodiorite appears between the Granite and underlying metasediments, marking a northern point of the Tail and thus a change in mineralogy from K-feldspar and muscovite to the plagioclase and biotite- dominated phases defining the granodiorite. The two-mica transition zone between the two units is hereafter referred to as the Paralana Granodiorite-British Empire Granite mixture zone.

Pegmatitic Granite

The Pegmatitic Granite is an undeformed and very coarse-grained, semi-massive, K-feldspar and quartz unit dominated by K-feldspar megacrysts and located at the western boundary of the Tail and Paralana Plateau. Locally, this unit contains large rafts of biotite schlieren (Plate 1f) indicating derivation from a metasedimentary sequence. Furthermore, its spatial relationship with the British Empire Granite suggests that this volumetrically minor unit may represent 'residual' melt produced during magmatic crystallisation and therefore indicate the south-most extent of the British Empire Granite.

2.4 Structural Framework

Mount Painter Inlier records a complex and repeated metamorphic and deformational history recording events ranging 1700 Ma to 350 Ma with Proterozoic events signifying maximum P-T conditions of 740-760° C and 4.5-5.5 kb (Teale, 1993a). The Adelaidean cover records amphibolite-grade metamorphism representing maximum temperatures of about 550°C (M. Sandiford, *pers. comm.*, 1996) during the Delamerian Orogeny, with basement units preserving moderate slaty cleavages, open to tight folding and reverse to strike-slip movement along the Paralana Fault Zone (Preiss, 1995)

The structural framework of the Paralana Plateau-Mawson Plateau area is dominated by a northeast-southwest trending large-scale anticlinal fold which strikes parallel to the Paralana Fault Zone closing to the south-south west (Appendix A). The Paralana Fault Zone marks the eastern extent of the Inlier in the Hot Springs region with mylonitic metasediments, Paralana Granodiorite and pegmatites tightly folded implying high-strain events probably prior to Delamerian folding (Plate 1.b). Furthermore, variations in strain and deformational structures between Paralana Plateau and the Tail reflect a strain gradient from tight isoclinal folding at Paralana Plateau to flat-lying Paralana Creek Metasedimentary units east of the Tail. Therefore the distribution of Paralana Granodiorite is consistent with structural repetition associated with the anticline, where the granodiorite together with Hot Springs Gneisses outcrop on both limbs of this structure. As the regional anticline is of probable Delamerian age, incorporation of the Granodiorite within this structure implies a pre-Delamerian intrusive event.

Previous studies (Coats and Blissett, 1971; Teale, 1979) have concluded that the undeformed nature of the British Empire Granite suggests post-Delamerian evolution and thus a Palaeozoic crystallisation age. However, the coarse-grained nature of the granite may inhibit the development of deformation fabrics. Furthermore the shallow westerly dip of this granitic body may reflect subtle folding within the regional anticline, where British Empire Granite outcrop within the eastern limb of the anticline would be 'cut-out' of the observed sequence by the Paralana Fault.

2.5 Conclusions

The Mount Painter Inlier consists of a suite of Proterozoic granites, gneisses and metasedimentary pelites and quartzites recording a pre-Delamerian deformational and metamorphic history. This sequence is overlain by Proterozoic Freeling Heights Quartzite, and intruded by sub-extrusive Felsic Volcanics and Mount Neill Granite. Delamerian folding formed a regional south-southwest plunging anticline and produced a decreasing strain gradient west from the Paralana Fault Zone. In contrast to previous investigations, field evidence strongly suggests the British Empire Granite body and Paralana Granodiorite Tail are separate lithological units; incorporation of the Paralana Granodiorite within Delamerian folding implies this unit represents a pre-Delamerian magmatic event. In comparison, the British Empire Granite does not exhibit any deformational fabrics, suggesting either generation during late- or post-Delamerian deformation or pre-folding evolution with structural repetition about the regional Delamerian anticline not observed due to the Paralana Fault.

Chapter Three

MAJOR AND TRACE ELEMENT GEOCHEMISTRY

Major and trace element characteristics are powerful tools for interpreting granite genesis because they constrain source regions and magmatic evolution of igneous suites, as well as identifying and evaluating changes in magmatic characteristics through time. This chapter presents results of XRF whole rock analysis carried out on magmatic and metasedimentary rocks from the study area. Both major and trace element analysis was undertaken in order to constrain the source region and magmatic evolution of the British Empire Granite, explore the geochemical relationship between the Paralana Granodiorite and British Empire Granite and evaluate changes in magmatic evolution between the Proterozoic and Palaeozoic. Petrological features of major units are discussed in Appendix C with textures illustrated in photomicrographs of Appendix D. Whole rock analytical techniques are described in Appendix J, with selected major and trace element data listed in Table 3.1 and the complete data set in Appendix E.

3.1 Geochemical characteristics of Mount Painter Inlier Suites

Hot Springs Gneiss Suite

Both the Massive K-feldspar and Augen-textured Gneisses are extremely enriched in U and Th, together with elevated Light Rare Earth Elements (LREE), Rb, Nb, Zr and Y (Figure 3.1). In particular Figure 3.4 indicates Zr, Ti and V depletion with progressively evolved rocks, while constant Rb concentrations over a wide range of SiO₂% (Figure 3.5) are consistent with resitite-dominated magmas (Wyborn *et al.*, 1992). An A-type character (Figure 3.6) is reflected by Aluminium Saturation Index values of <1.1 and high Ga/Al and Zr + Nb + Ce + Y values (Whalen *et al.*, 1987; Chappell and White, 1992). These workers suggest magma derivation from H₂O-absent source regions, representing either later melts of previously melted parent material or unusual mafic melt fractionates. Tectonic discrimination plots from Pearce *et al.* (1984) indicate within-plate granite genesis (Figure 3.7).

Table 3.1a : Summary of Whole Rock Analysis for Hot Springs Gneiss and Mount Neill Granite

	Hot Springs Granitic Gneisses				Augen-textured Gneiss				Mount Neill Granite	
	Massive K-feldspar Gneiss	HSF	PCh	HSM	ECa	PCTa	A1015-HV-57	HV-48		
SiO2%	74.62	71.33	72.29	72.10	73.49	70.33	70.52	75.86		
Al2O3%	13.66	13.53	14.08	13.33	14.09	13.32	14.28	13.35		
Fe2O3%	2.31	2.31	2.51	3.68	1.35	2.03	3.77	0.82		
MnO%	0.00	0.03	0.02	0.02	0.01	0.05	0.01	0.01		
MgO%	0.25	0.63	1.18	1.08	1.21	2.38	0.32	1.31		
CaO%	0.13	1.71	1.32	1.37	0.92	0.50	0.23	0.27		
Na2O%	6.63	4.87	5.09	4.37	4.29	2.29	3.22	6.28		
K2O%	0.72	1.31	1.40	2.40	3.83	7.00	5.93	1.00		
Ti2O%	0.28	0.50	0.50	0.50	0.36	0.43	0.51	0.37		
P2O5%	0.05	0.09	0.09	0.08	0.08	0.09	0.09	0.06		
SO3%	0.00	0.00	0.00	0.00	0.00	0.00	0.00	0.00		
LOI%	0.60	0.39	0.77	0.54	0.43	0.44	0.86	0.47		
TOTAL%	99.26	99.28	99.25	99.48	100.06	98.85	99.76	99.79		
ASI	1.15	1.08	1.15	1.09	1.09	1.09	1.18	1.12		
K2O/Na2O	0.109	0.275	0.549	0.549	0.893	3.057	1.842	0.159		
Ga/Al*1000	3.058	2.891	2.483	3.077	3.595	3.178	3.931	3.896		
Zr+Nb+Ce+Y	824.800	1258.200	1346.300	1044.100	1196.600	1514.900	1332.600	650.500		
Rb ppm	54.7	79.9	111.6	190.6	325.3	645.8	429.8	88.2		
Ba	162	163	214	281	75	239	574	148		
Th	284.6	485.3	435.2	149.1	326	423.2	117.2	92.1		
U	65.8	88.8	130	32.9	84.2	118.7	126.5	14.9		
Nb	107.3	23	103.5	39.1	80.8	61	62.7	32.2		
K	5977.1	10874.9	11622.1	19923.6	31794.7	58110.4	49227.8	8301.5		
La	150	332	308	163	218	371	248	101		
Ce	295	600	583	366	516	771	485	200		
Pb	13.2	26	39.1	23.3	28.4	48.9	11.3	9		
Sr	32.3	137.6	153.3	110.5	56.8	37.7	46.7	56.4		
P	218.2	392.8	392.8	349.1	349.1	392.8	392.8	261.9		
Nd	95	186	189	123	164	218	136.9	34.2		
Zr	344.4	564	547.8	515.6	485.8	487.1	637.7	321.2		
Ti	1678.6	2997.5	2997.5	2997.5	2158.2	2577.8	3057.4	2218.1		
Y	78.1	71.2	112	123.4	114	195.8	147.2	97.1		
Sc	3.1	4.1	6	9	7.3	8.6	8	7.6		
Cr	4	0	0	1	1	1	2	8		
V	12	25	18	14	16	20	7.2	22.5		
Co	68	79	65	66	44	52	81.9	67.1		
Ga	22.1	20.7	18.5	21.7	26.8	22.4	29.7	27.1		
Cu	16	7	5	12	6	11	19	10		
Zn	11	18	13	15	7	24	25	7		
Ni	0	0	0	0	0	0	5	5		

All samples prefixed A1086- except A1015- (Schaefer, 1993) and 948- (Foden unpubl. data in Schaefer, 1993)

Table 3.1b : Summary of whole rock analysis of metasediments

	Freeling Heights Quartzite		Paralana Creek Metasediments	
	NC3	NC4	948-92-FHQ1	948-92-FHQ3
SiO2%	89.98	87.79	84.10	31.50
Al2O3%	4.63	5.72	7.42	24.91
Fe2O3%	2.78	2.34	2.16	14.28
MnO%	0.01	0.01	0.03	0.07
MgO%	0.21	0.44	1.87	16.59
CaO%	0.01	0.02	0.01	0.23
Na2O%	0.06	0.16	0.14	0.35
K2O%	1.47	2.26	2.75	7.73
Ti2O%	0.17	0.22	0.27	0.72
P2O5%	0.01	0.02	0.01	0.19
SO3%	0.00	0.00	0.00	0.00
LOI%	0.68	0.74	0.91	2.77
TOTAL%	100.02	99.71	99.67	99.34
ASI	2.71	2.08	2.30	2.66
K2O/Na2O	24.500	14.125	19.643	22.086
Ga/Al*1000	2.163	1.784	3.362	2.929
Zr+Nb+Ce+Y	130.200	177.000	186.300	657.800
Rb ppm	81.8	137.5	274.9	1059.5
Ba	448	443	181	375
Th	6.5	8.7	9.7	29.5
U	1.3	1.5	1.3	1.7
Nb	5.5	8.4	17.6	18.4
K	12203.2	18761.4	22829.1	64170.5
La	14	22	4	75
Ce	30	43	7	141
Pb	1	2	3.8	8.4
Sr	6.5	5.5	6.2	5.7
P	43.6	87.3	43.6	829.2
Nd	84	16	2	50
Zr	84	112	136.3	405.2
Ti	1019.1	1318.9	1618.6	4316.4
Y	10.7	13.6	25.4	93.2
Sc	2.1	2.9	6.4	10.1
Cr	11	12	50	39
V	25	17	28.1	76
Co	84	91	53.3	59.2
Ga	5.3	5.4	13.2	38.6
Cu	7	3	0	0
Zn	1	2	50	168
Ni	0	0	8	39

Table 3.1c: Summary of Whole Rock Analysis for Parana Granodiorite and British Empire Granite

	Parana Granodiorite		Tail		Qtz Parana Granodiorite		Parana Plateau		HSP		Tail		Parana Granodiorite		British Empire Granite		948-92-BE2		948-92-BE3		948-92-BE4		Southern Region		Northern Region		Pegmatitic Granite	
	HSD	FSE	FCI	PO	PP18	HSP	JF1	FC2	MP1	948-92-BE2	948-92-BE3	948-92-BE4	NC5	NC7	MP8	MP5	FCV											
SiO ₂ %	75.70	71.38	69.84	69.52	73.93	73.50	71.59	70.33	75.17	77.10	76.19	76.56	73.54	74.90	74.73	74.65	74.22											
Al ₂ O ₃ %	13.96	16.10	16.11	17.38	15.42	15.64	16.30	16.53	14.33	12.84	13.30	13.04	14.30	14.16	14.19	13.89	13.66											
Fe ₂ O ₃ %	0.261	1.48	2.02	1.25	0.61	0.55	1.39	2.14	0.65	0.49	0.57	0.77	0.65	0.77	0.65	0.76	0.48											
MnO%	0.01	0.01	0.01	0.01	0.00	0.01	0.02	0.02	0.01	0.02	0.02	0.00	0.01	0.01	0.01	0.02	0.01											
MgO%	0.42	0.68	0.89	0.77	0.17	0.39	0.63	0.92	0.18	0.14	0.14	0.08	0.33	0.34	0.22	0.23	0.21											
CaO%	1.28	2.66	3.31	2.98	1.14	1.85	2.44	3.33	0.48	0.50	0.56	0.48	0.50	0.60	0.60	0.65	0.34											
Na ₂ O%	5.54	5.74	3.02	5.91	6.68	5.93	5.68	4.56	3.50	3.29	3.14	3.14	3.31	4.57	3.06	3.08	2.75											
K ₂ O%	1.44	1.10	3.97	1.13	1.10	1.21	1.03	1.33	4.38	4.52	4.66	5.59	6.18	3.17	5.27	4.85	6.96											
Ti ₂ O ₅ %	0.06	0.20	0.29	0.15	0.06	0.07	0.13	0.30	0.05	0.05	0.06	0.03	0.06	0.11	0.08	0.07	0.05											
P ₂ O ₅ %	0.06	0.06	0.04	0.04	0.02	0.05	0.05	0.04	0.05	0.10	0.09	0.07	0.07	0.06	0.07	0.08	0.06											
SO ₃ %	0.00	0.00	0.00	0.00	0.00	0.00	0.00	0.00	0.00	0.00	0.00	0.00	0.00	0.00	0.00	0.00	0.00											
LOI%	0.41	0.31	0.42	0.47	0.38	0.43	0.44	0.56	0.74	0.47	0.49	0.26	0.41	0.35	0.61	0.61	0.29											
TOTAL%	99.31	99.72	99.74	99.63	99.51	99.61	99.71	100.07	99.41	99.44	99.37	99.44	99.36	99.72	99.59	98.88	99.02											
ASI	1.07	1.04	1.05	1.06	1.08	1.08	1.09	1.10	1.26	1.16	1.16	1.08	1.10	1.09	1.20	1.21	1.08											
K ₂ O/Na ₂ O	0.260	0.192	1.315	0.191	0.165	0.204	0.181	0.292	1.408	1.416	1.416	1.780	1.867	0.694	1.722	1.575	2.531											
Ga/Al*1000	2.261	1.900	1.900	2.463	2.463	2.139	1.948	1.978	2.561	2.561	2.561	2.145	1.956	2.109	2.424	2.585	1.729											
Zr+Nb+Ce+Y	216.900	178.200	233.400	185.800	155.900	249.500	158.300	223.300	143.800	110.400	105.200	67.900	63.300	89.600	159.800	155.800	47.200											
Rb ppm	79.4	90.9	177.4	81.7	56.6	67.8	62.9	57.4	220.2	293.8	327.6	250.3	330.8	180.4	357.5	389.6	334.6											
Ba	113	176	534	234	134	71	198	404	209	152	317	241	660	404	197	201	845											
Th	3.3	3.3	8.2	24.3	22.4	38.6	4.6	8.9	16.6	8.8	10.2	10.4	6.6	5.2	14.5	13.1	5.2											
U	5.4	1.5	0.8	3.1	7.9	7.2	1	1.7	31.5	24.8	14.9	15.7	2	1.9	24.5	19.6	2.2											
Nb	6.8	6.5	6.8	10.7	13.3	10.3	10.2	4.9	21.1	19.4	20.2	4.5	12.9	16	30.7	35.1	8.6											
K	11954.1	9131.6	32956.9	9380.7	9131.6	10044.8	8550.5	11041.0	36360.5	37522.7	36684.9	46405.3	51303.2	26315.7	43748.8	40262.2	57778.3											
La	19	12	19	26	17	35	12	18	13	8	8	8	5	5	12	12	5											
Ce	44	24	39	51	32	71	20	37	27	21	15	13	12	12	26	27	12											
Pb	9	6.2	6.2	7.1	8.9	12.7	10.9	7.4	20.5	22.7	24.3	27.2	24.5	18	35.3	33.4	15.4											
Sr	190.4	609.2	883	513.9	184.8	207	447.6	810.1	52.5	38.3	47.6	61.5	178	178	51.6	101.1	196											
P	87.3	261.9	174.6	173.6	174.6	218.2	218.2	174.6	436.4	436.4	392.8	305.5	305.5	261.9	261.9	349.1	261.9											
Nd	12	10	14	18	12	23	8	17	11	8	5	5	3	4	9	9	2											
Zr	103.7	130.7	181.9	87.3	79.4	45.7	118.5	177.1	57.2	38.3	37.4	28.6	18.4	51.6	55.3	46.4	13.1											
Ti	359.7	1199.0	1738.5	899.2	359.7	419.6	779.3	1798.5	299.7	299.7	359.7	179.8	359.7	659.4	479.6	419.6	299.7											
Y	62.4	17	5.7	36.8	31.2	122.5	9.6	4.3	38.5	31.7	32.6	21.8	20	10	47.8	47.3	13.5											
Sc	1.7	2.6	4.3	3.2	1.3	2.6	3.7	4.3	3.3	3.4	4	1.8	2.4	2.7	5.6	5.3	1.1											
Cr*	2	2	1	3	0	0	0	4	0	31	29	29	0	1	0	3	3											
V	5	16	21	15	6	6	5.1	28	5	8	4	3.8	7	8	0	5	6											
Co	71	65	64	81	67	72	75	61	73	30.1	44.4	35.9	75	74	75	60	74											
Ga	16.7	18.7	16.2	18.3	20.1	17.7	16.8	17.3	17.2	17.4	18	14.8	14.8	15.8	18.2	19	12.5											
Zn	14	18	17	17	13	6	16	8	8	2	2	-	10	9	8	13	8											
Cu	5	30	25	7	14	5	11	26	4	11	10	4	4	5	7	12	5											
Ni	0	0	0	0	0	0	0	0	0	4	-	2	0	0	0	0	0											

All samples prefixed A1015- (Schaefer, 1993) and 948- (Foden unpubl. data in Schaefer, 1993)

Figure 3.1 : Multi-element comparison between MPI gneissic and metasedimentary units

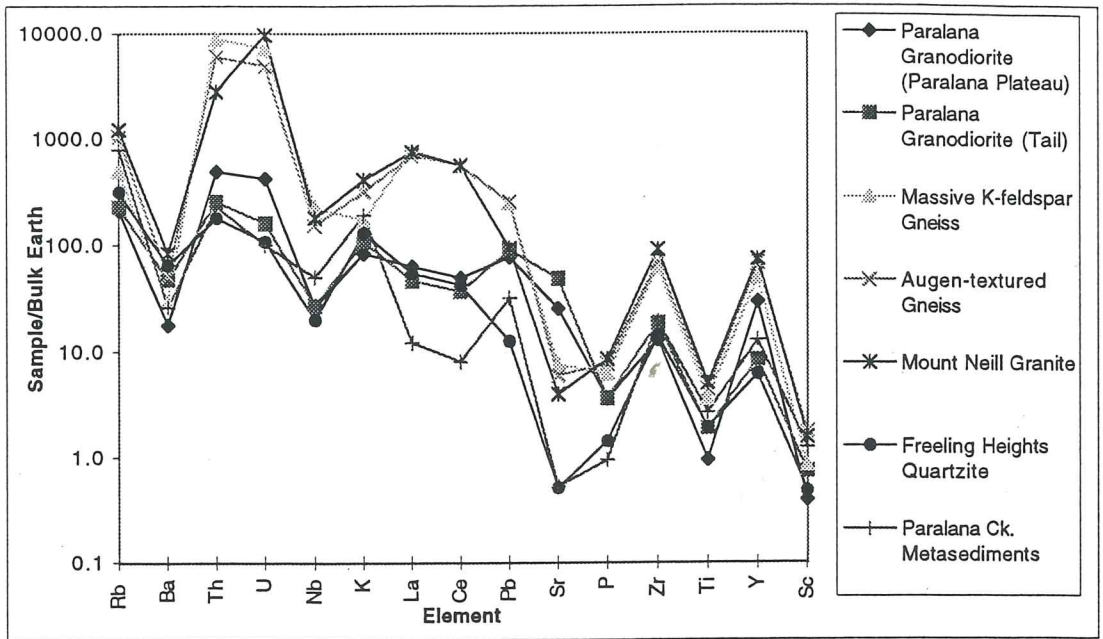


Figure 3.2 : Multi-element comparison between Tail-Body granites and metasediments

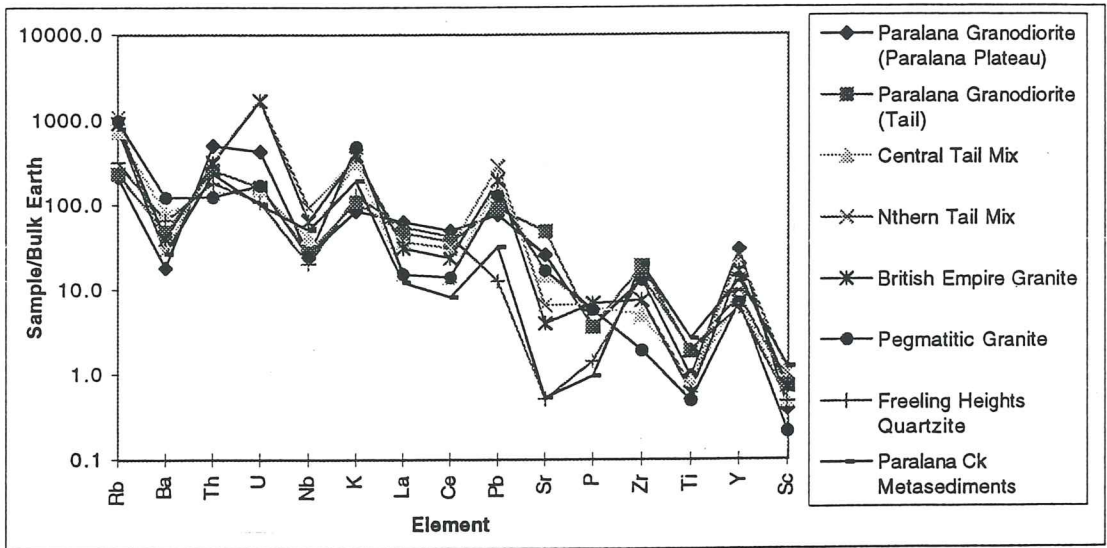


Figure 3.3 : Multi-element comparison between Tail-Body granites and Adelaidean cover

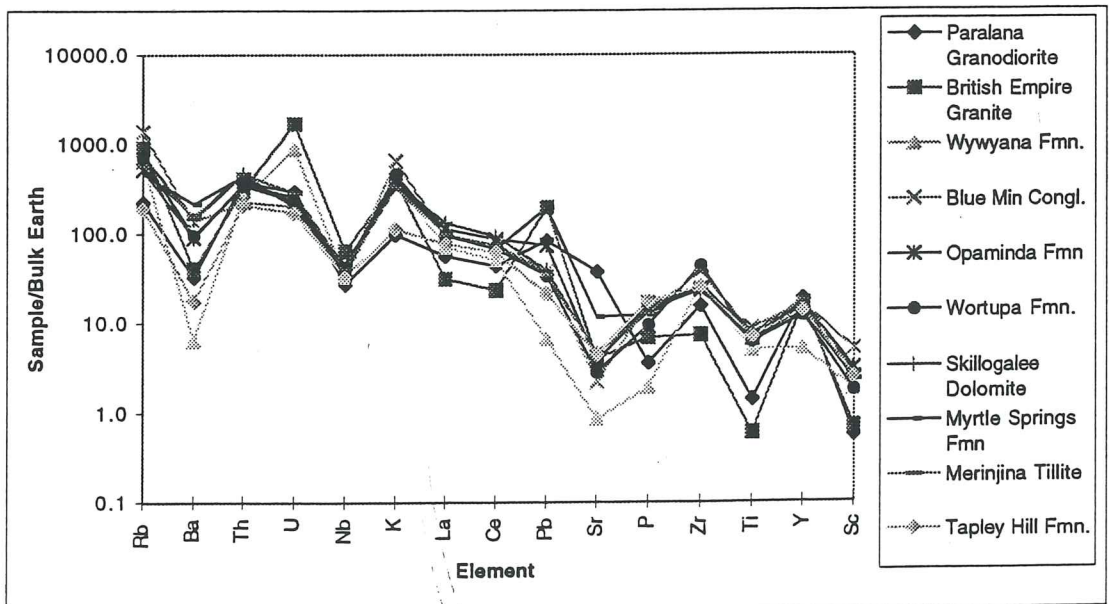
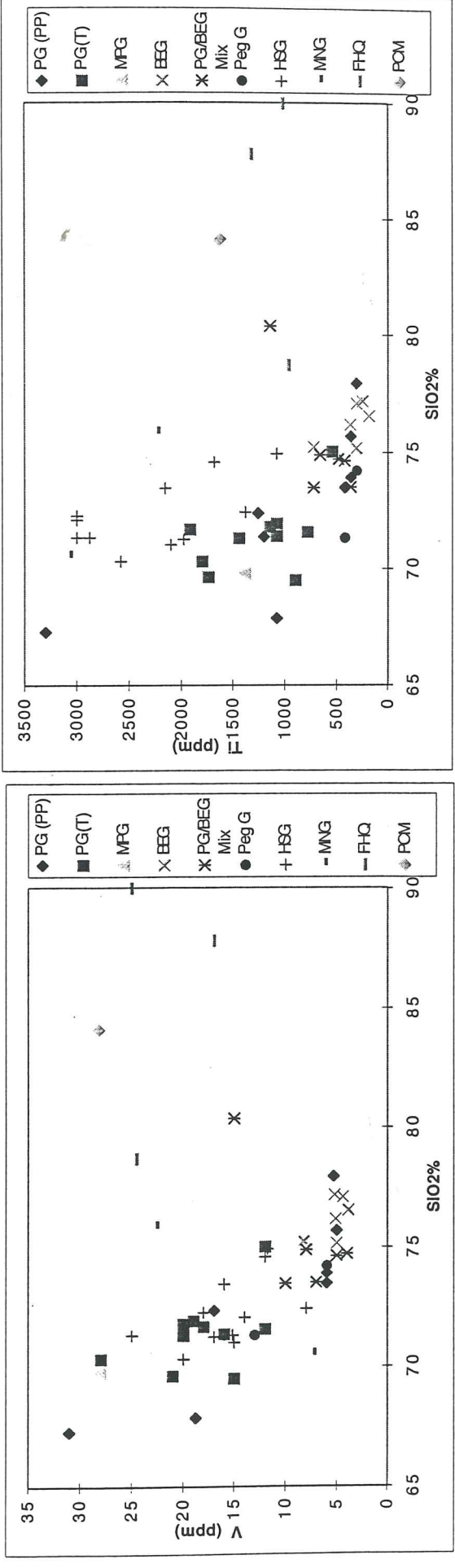
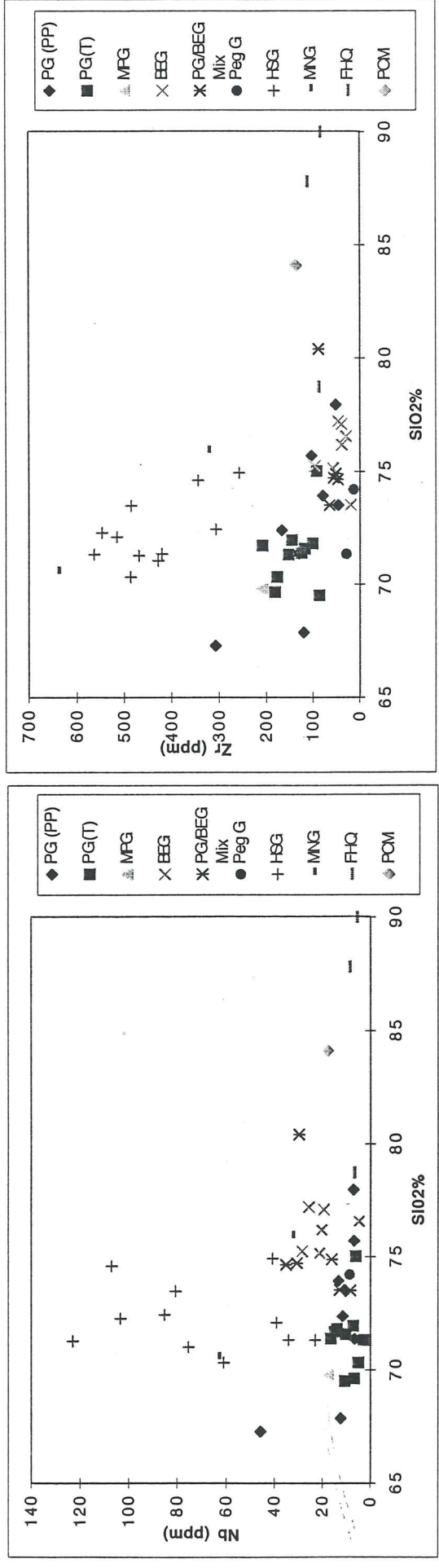


Figure 3.4 : Harker diagrams for selected Mount Painter Inlier units



PG=ParalanaGranodiorite, PP=Paralana Plateau, T=Tail, MFG=Migmatitic Paralana Granodiorite, BEG=British Empire Granite, Peg G=Pegmatitic Granite, HSG=Hot Springs Gneiss, MNG=Mount Neill Granite, FHQ=Freeing Heights Quartzite

Paralana Creek Metasediments and Freeling Heights Quartzite

These metasedimentary sequences contain low values for most trace elements in the multi-element plot, especially low LREE, U, Sr and P values (Figure 3.1 and 3.2), with high silica and low FeO, MgO and CaO values reflecting massive clean quartzite characteristics.

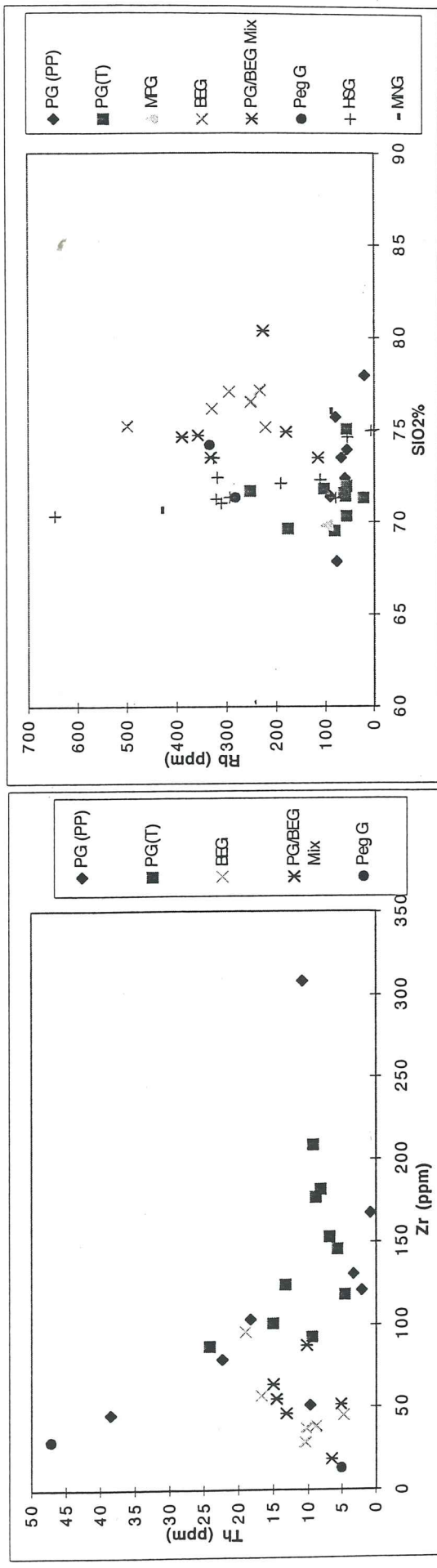
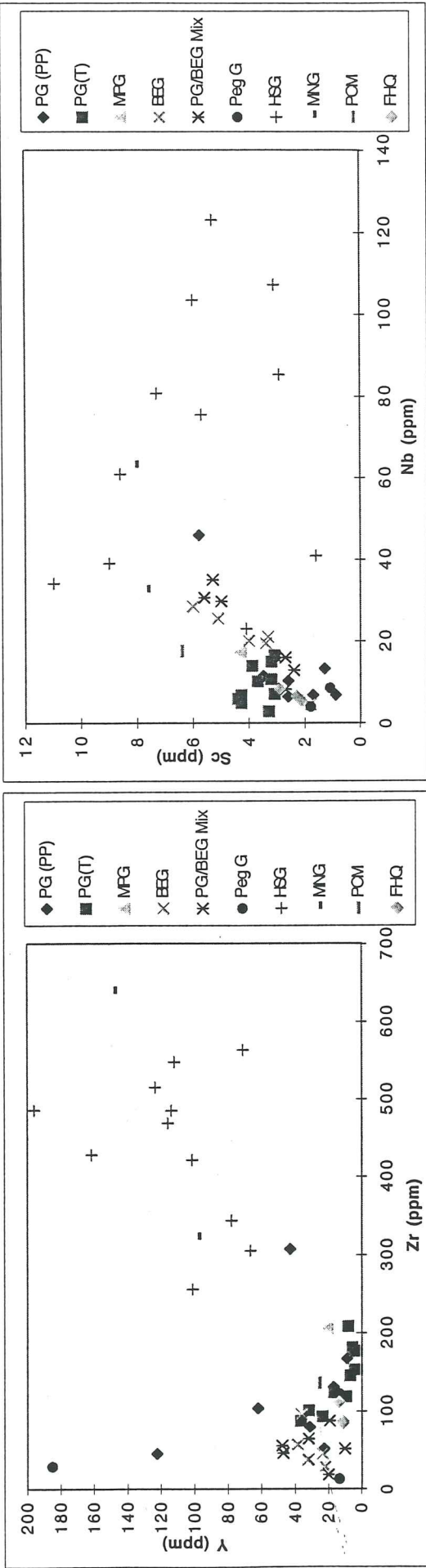
Paralana Granodiorite

This unit is characterised by low LREE, Rb, U, Th, Zr and Ti values (Figure 3.2) and elevated Sr and Pb concentrations. Samples from Paralana Plateau contain higher SiO₂% and lower Zr, V and Ti than the Tail lithologies (Figure 3.4) with a general fractionation trend observed between the two localities for most trace elements. As shown in Figure 3.5, there is a marked increase in Th and Y with decreasing Zr, suggesting early crystallisation of zircon with respect to monazite and apatite (J. Foden, *pers. comm.*, 1996). The I-type signature indicated by Aluminium Saturation Index values ranging from 1.04 to 1.1 (Figure 3.6) indicate derivation from melting of pre-existing igneous rocks within the crust, or fractionation of mafic magmas derived from the mantle or lower crust. Although tectonic discrimination plots suggest generation in a volcanic arc or syn-collisional setting (Figure 3.7), Pearce *et al.* (1984) suggests that post-collision granites can plot within the volcanic-arc granite and syn-collisional field due to difficulties in explaining granitic production within this setting in terms of a single, well-defined mantle or crustal source.

British Empire Granite

This unit contains high U, Rb and K values and low Ba, LREE, Sr, P, Zr, Ti and Sc concentrations (Figure 3.2). A narrow range in SiO₂% from 75 to 77% with particularly low MnO, MgO, CaO and TiO₂ values suggest a composition very close to that of a minimum melt (Teale, 1979; Schaefer, 1993). The strong S-type signature reflected by ASI values greater than 1.1 (Figure 3.6) indicates derivation from melting of metasedimentary crustal sources, with tectonic discrimination plots suggesting either within-plate, syn-collisional, volcanic arc or post-collisional setting (Figure 3.7). The Pegmatitic Granite contains elevated Rb, Ba, K and P values together with low LREE, Th, Zr, Ti Y and Sc concentrations also consistent with a minimum crustal melt (Figure 3.2). Indeed, trace element plots such as Zr against Th (Figure 3.5) suggest this unit may represent the crustal endmember of British Empire Granite fractionation.

Figure 3.5 : Trace element comparison diagrams for selected Mount Painter Inlier units



PG(PP)=Paralana Granodiorite (Paralana Plateau), PG(T)=Paralana Granodiorite (Tail), BEG=British Empire Granite, HSG=Hot Springs Gneiss, MNG=Mount Neill Granite, PCM=Paralana Creek Metasediments, FHQ=Freeling Heights Quartzite

Figure 3.6 : Granite suite discrimination diagrams

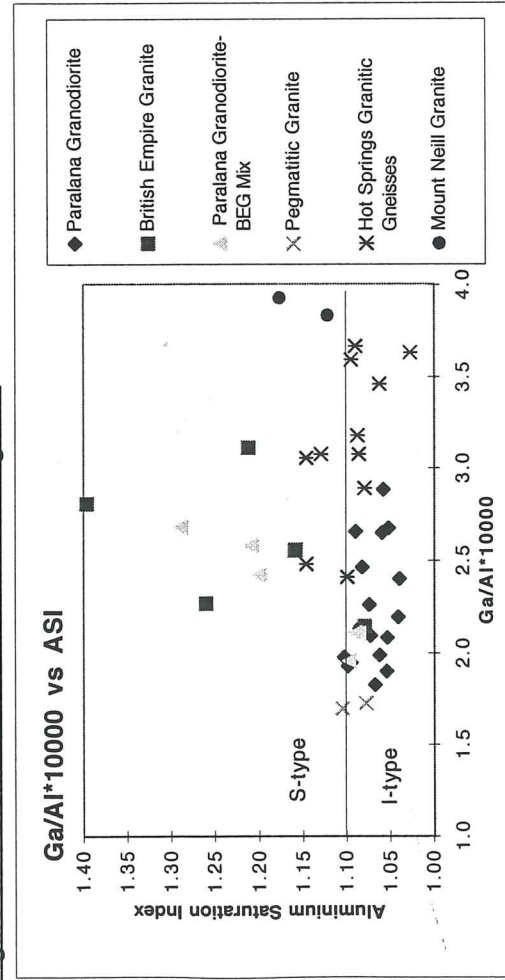
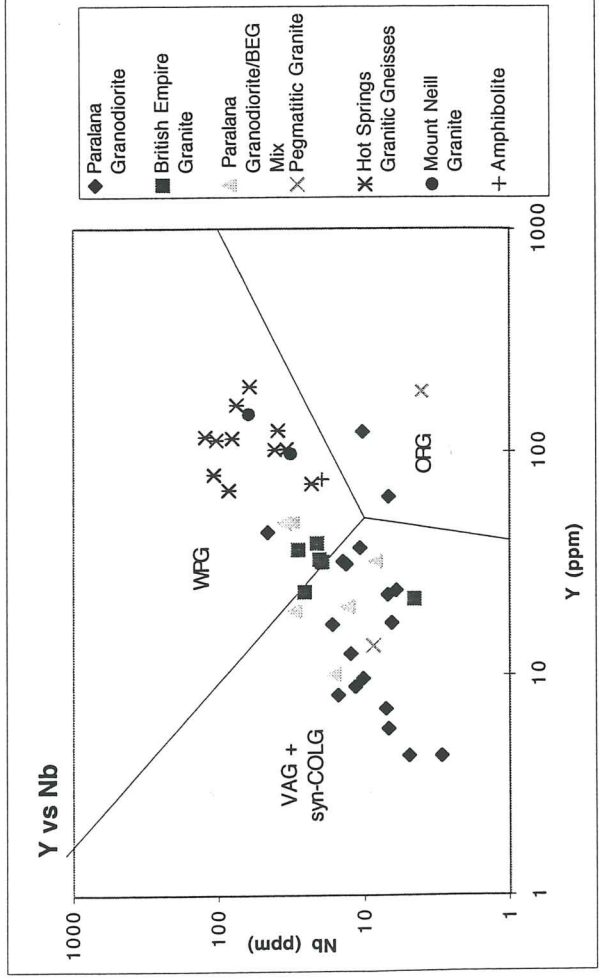
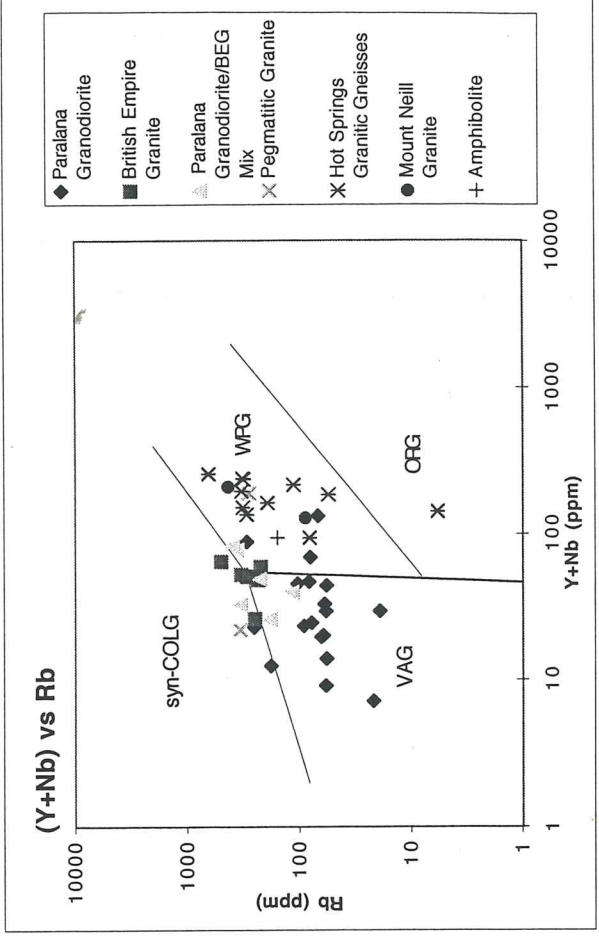
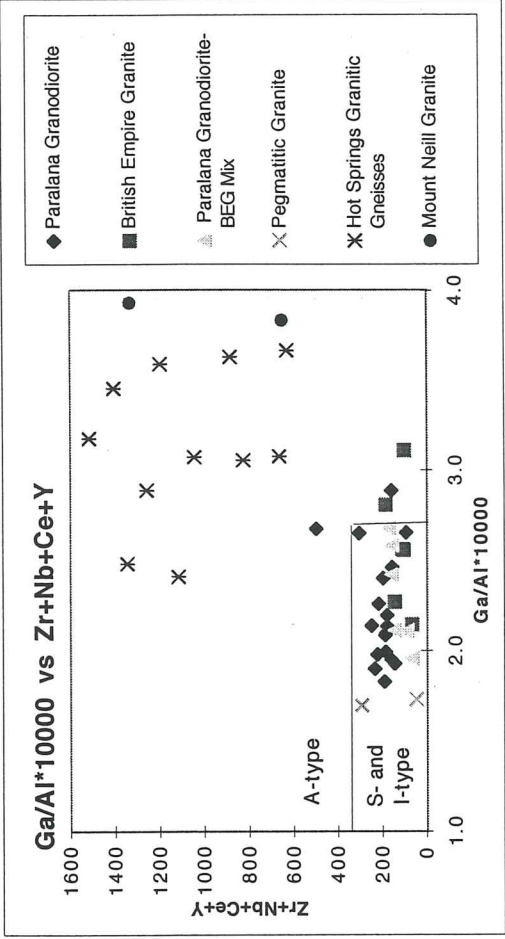


Figure 3.7 : Granite tectonic discrimination diagrams



VAG=volcanic-arc granites, syn-COLG=syn-collisional granites, WPG=within-plate granites, ORG=ocean-ridge granites



3.2 Geochemical relationships between Mount Painter Inlier Units

Hot Springs Gneisses analysed from both Paralana Plateau and Tail produce similar multi-element signatures, thus confirming that this suite is structurally repeated by the regional anticline. The geochemical characteristics of this suite also correspond to those of the Mount Neill Granite, suggesting either derivation from the same source region or significant incorporation of the gneissic material within the volcanics during genesis. Similar correlations for Paralana Granodiorite samples from Paralana Plateau and Tail further indicate the involvement of this unit in Delamerian folding. Minor variations in Ba, U, Th and Y between locations represents either secondary element mobilisation associated with the Paralana Fault Zone or fractionation variations within the granodiorite. Paralana Creek Metasediments and Freeling Heights Quartzite contain similar geochemical signatures, suggesting derivation from the same source region or sediments of similar characteristics.

The Paralana Granodiorite has a distinctly different multi-element trend compared to the Hot Springs Gneisses, with significant incompatible element depletion in the granodiorite indicated by low Rb, Ba, U, Th, Nb and LREE concentrations. The Paralana Granodiorite may therefore represent either melt derivation from source material different to the Proterozoic igneous suites or sampling of residual lower-crust/mantle material depleted in incompatible elements due to melt extraction associated with the Hot Springs Gneisses.

Although multi-element plots for the British Empire Granite correlate strongly to the Paralana Granodiorite trends, higher U, Th, Pb, K and Rb together with lower Sr and Zr values produce minor distinctions between the two units (Figure 3.2). Samples from the Tail-Body mixture zone plot between the Paralana Granodiorite and British Empire Granite signatures, reflecting either cogenetic generation of the two units or granodiorite incorporation within the granite magma during genesis. Incompatible element enrichment in the British Empire Granite relative to the Paralana Granodiorite suggests derivation from a different source material, small amounts of Paralana Granodiorite partial melting for British Empire Granite generation or a comagmatic fractionation trend between the two units. Indeed, the elevated concentration of incompatible elements within the British Empire Granite are precisely the elements that would be enriched with minimum melting of the granodiorite. This mixing or co-magmatic evolution curve is also observed in trace element plots (Figure 3.5), implying an intimate association between these two units during granite melting and crystallisation.

3.3 Geochemical characteristics of Neoproterozoic Adelaidean Cover Units

In order to investigate the likelihood of British Empire Granite derivation from Adelaidean sediments, multi-element plots of both suites were constructed to consider the possibility of the British Empire Granite inheriting its geochemical signature from the Neoproterozoic sequence. As shown in Figure 3.3, selected members from the cover sequence represent wide variations in geochemical concentration but generally have higher LREE, Zr, Ti and Sc, together with lower U, Th, Rb and Nb values.

3.4 Geochemical comparisons to other Australian Terrains

Multi-element plots for the Hot Springs Gneisses show striking similarities to the anorogenic I-type Sr depleted, Y undepleted granites identified by Wyborn *et al.* (1992) in many Australian Proterozoic terrains. However, elemental comparisons between Mount Painter Inlier units and Archaean Gawler Craton (Figure 3.8) and Proterozoic Gawler Range Volcanics (GRV) (Figure 3.9) show the Hot Springs Gneisses are enriched in Rb, U, Th, Nb, La, Ce and Y relative to GRV dacitic and rhyolitic units and marked by lower Ba, Sr and P values. Figure 3.10 indicates no geochemical correlation between the British Empire Granite and Delamerian granites and mafics from the Southern Adelaide Fold Belt, reflecting different source material and/or magmatic processes active within the fold belt during this deformational event.

3.5 Conclusions

A strong geochemical correlation between the A-type Massive K-feldspar Gneiss, Augen-textured Gneiss and S-type Felsic Volcanics within the Mount Painter Inlier suggest generation and incorporation from the same enriched source followed by similar magmatic evolutionary processes. In contrast, the Paralana Granodiorite represents derivation from the lower crust or mantle due to its I-type nature, with geochemical trends differing greatly from the other Proterozoic units. However the multi-element pattern of the granodiorite corresponds closely to that of the British Empire Granite, suggesting that granodiorite and granite are comagmatic or that the granite is derived from the granodiorite together with other units, with distinctly different sources and/or processes from those of the Southern Adelaide Fold Belt. Indeed, British Empire Granite enrichment in incompatible elements relative to Paralana Granodiorite suggests that minimum melting of granodiorite, together with metasediment incorporation, can create the geochemical signature of the granite.

Figure 3.8 : Multi-element comparison between Mount Painter Inlier and Gawler Craton units

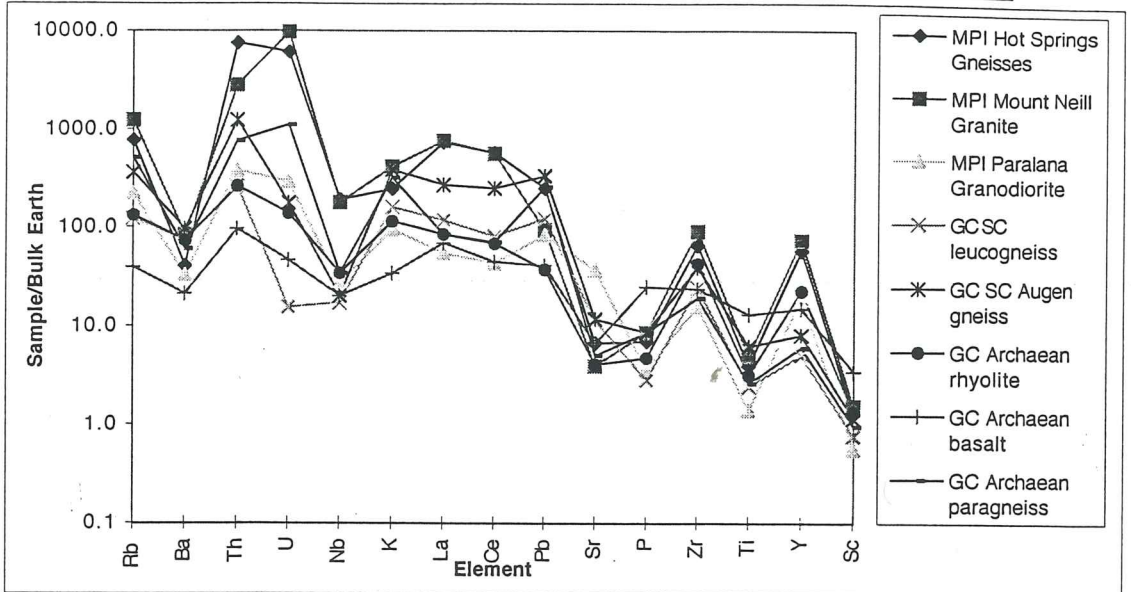


Figure 3.9 : Multi-element comparison between Mount Painter Inlier and Gawler Range Volcanics units

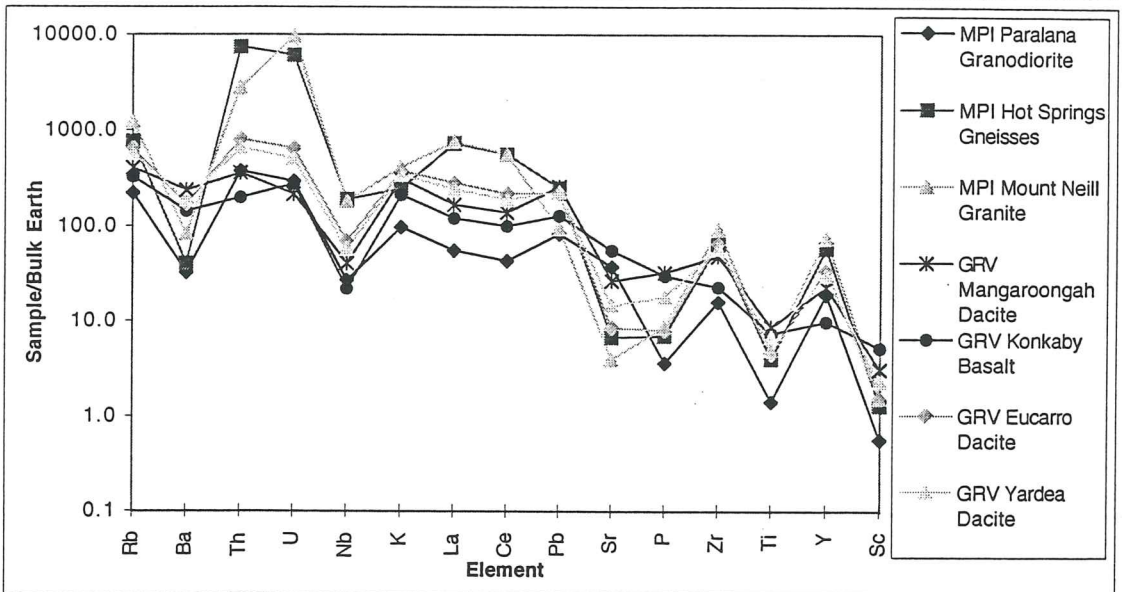
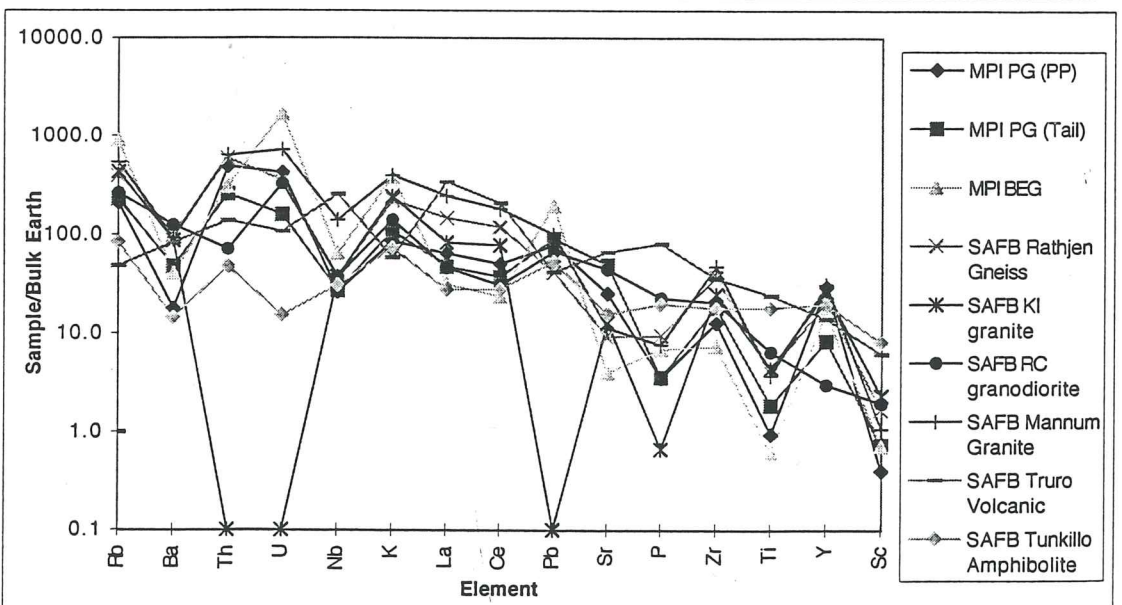


Figure 3.10 : Multi-element comparison between Mount Painter Inlier & Southern Adelaide Fold Belt



MPI=Mount Painter Inlier, GC=Gawler Craton, SC=Sleaford Complex, GRV=Gawler Range Volcanics, SAFB=Southern Adelaide Fold Belt, KI=Kangaroo Island, PP=Paralana Plateau, T=Tail, RC=Reedy Creek

Chapter Four

RADIOGENIC ISOTOPE GEOCHEMISTRY AND GEOCHRONOLOGY

The use of radiogenic isotopic signatures provides important constraints on the source regions of both igneous and sedimentary rocks. This process is based on the radioactive decay of isotopes to stable daughter products at a constant rate, with the relative proportion of parent and daughter products measured indicating the time taken for the accumulation of a certain amount of a particular isotope by radioactive decay (Nier, 1940). The isotopic systems rubidium and strontium (^{87}Rb and ^{86}Sr), samarium and neodymium (^{147}Sm and ^{143}Nd) and uranium and lead (^{235}U and ^{207}Pb and also ^{238}U and ^{206}Pb) are often used, providing information on geochronology and petrogenesis. When calculating and interpreting isotopic signatures it is assumed that the system has remained closed since the time of differentiation. This chapter presents radiogenic isotope data for the British Empire Granite, Paralana Granodiorite and Freeling Heights Quartzite in order to constrain magmatic crystallisation ages and mantle separation ages, and to identify possible melt provenance regions.

4.1 Zircon isotope systematics

U-Pb isotopic signatures preserved within zircons reflect the time of zircon crystallisation associated with magmatic or metamorphic events. Construction of concordia-discordia diagrams using $^{206}\text{Pb}/^{238}\text{U}$ vs $^{207}\text{Pb}/^{235}\text{U}$ concentrations can indicate primary magmatic events and re-opening of the system due to later secondary events (Rollinson, 1993). Due to their robust nature zircons survive weathering, erosion and transport well and their low solubility within most magmas together with extremely high closure temperature to the U-Pb system often results in inherited components within zircon populations. Thus analysis of smaller samples in order to recognise discrete age groups preserved within zircon populations and also strong trace element zonation within single crystals can assist in identification and age-determination of numerous events which may reset Pb ratio systematics (Williams, 1992). The procedures undertaken to extract the zircon fraction from bulk samples and calculate magmatic/metamorphic ages from Pb ratios obtained from mass spectrometry using the Pb-Pb evaporation technique are outlined in Appendix K and F, respectively.

4.1.1 Zircon Pb-Pb data and interpretations

Although previous studies (Teale, 1979; Schaefer, 1993) have proposed a post-Delamerian age for the British Empire Granite based on field observations, the crystallisation age of this body has not been calculated. Pb-Pb systematics were therefore used to constrain the British Empire Granite age and also calculate the age of the Paralana Granodiorite in order to determine whether the two units are comagmatic. In addition, internal characteristics of zircons and apatites were observed to identify different zoning textures using backscattered electron imaging on a SX-51 electron microprobe, where the zircon images obtained primarily reflect compositional contributions to electron backscattering (Paterson *et al.*, 1992).

The British Empire Granite sample from Mawson Plateau contain a limited population of zircons which display numerous distinct rims characterised by variations in grey-colour level around a small central core (Plate 3a) corresponding to variations in elemental composition. As these zircons contained no measurable radioactive Pb, a crystallisation age could not be calculated. This result suggests either Pb loss from metamict crystals due to high U values within the crystal or limited U radioactive-decay (dictated by large decay constants and possibly small radiogenic U concentrations) indicating a young age for the granite. Apatite crystals within this sample display distinct simple core-rim texture (Plate 3b).

A British Empire Granite-Paralana Granodiorite sample collected from the Body-Tail junction contained small zircon crystals exhibiting two different textures. A large percentage of zircons contained large core zones with extensive fractures surrounded by a minimal number of thick parallel rims (Plate 3c), with other zircons consisting of a number of zircons enclosed within a concentric rim (Plate 3d). Although the radiogenic Pb values within these zircons were too low to calculate a crystallisation age, the two distinct internal textures may represent mixing of two different magmas containing varying zircon populations which record different previous events.

A small number of zircons within a Paralana Granodiorite sample from Paralana Plateau display complex internal zoning (Plate 3g and Plate 3h). Core regions are surrounded by a large number of truncated non-continuous rims with minimal fracturing within the crystals.

The Paralana Granodiorite sample from the Tail contained small zircon crystals exhibiting more simple textures. Internal zoning is characterised by a dark-coloured large core region containing extensive fracturing surrounded by a lighter coloured rim zone with the boundary between the two zones ranging from distinct (Plate 3f) to gradual (Plate 3e). The Paralana

PLATE 3a

Microprobe image of a zircon crystal from the British Empire Granite (Sample A1086-MP1) displaying numerous rims around a small core zone, where rim growth is limited to two directions. Scale bar represents 100 microns.

PLATE 3b

Apatite crystals within the British Empire Granite (A1086-MP1) contain a distinct core region with one major surrounding rim zone, with a similar elongated crystal shape to the zircons. Scale bar represents 100 microns.

PLATE 3c

This zircon crystal from the Paralana Granodiorite-British Empire Granite mixture zone (Sample A1086-MP5) exhibits similar textural characteristics to Plate 3a, suggesting that they may both be a part of the same magmatic population. However unlike the Plate 3a sample, the rims within this zircon are concentric in all directions. Scale bar represents 50 microns.

PLATE 3d

The microprobe image of a zircon from the Paralana Granodiorite-British Empire Mixture zone (A1086-MP5) illustrates complex textural features, with a number of small zircon cores enclosed within a large rim zone. The cores contain numerous cracks which do not extend to the rim area. Scale bar represents 50 microns.

PLATE 3e

This zircon contained within Paralana Granodiorite from the Tail (Sample A1086-PCf) shows a more simple morphology than the other samples, with one distinct core surrounded by a lighter coloured core. Scale bar represents 100 microns.

PLATE 3f

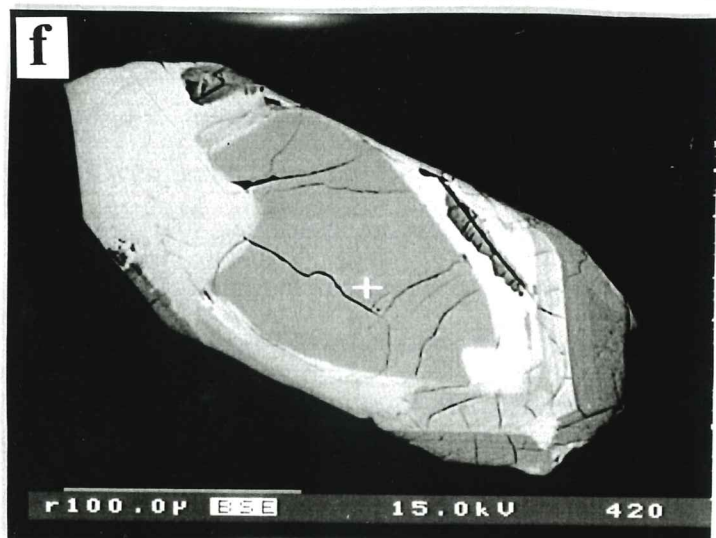
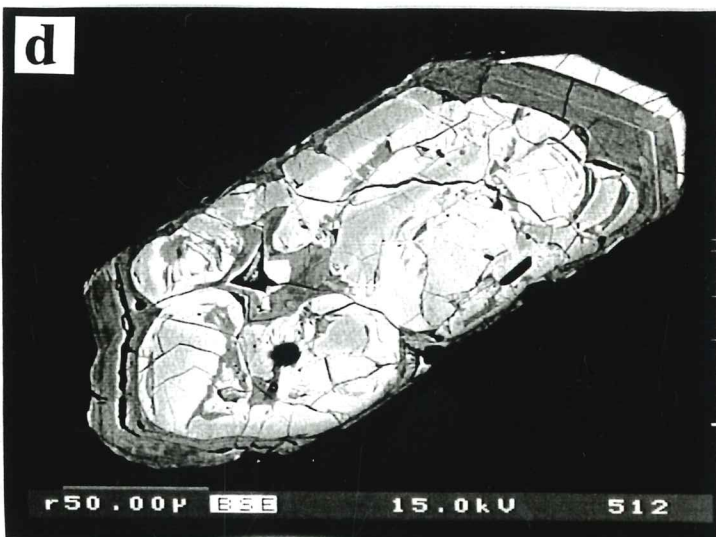
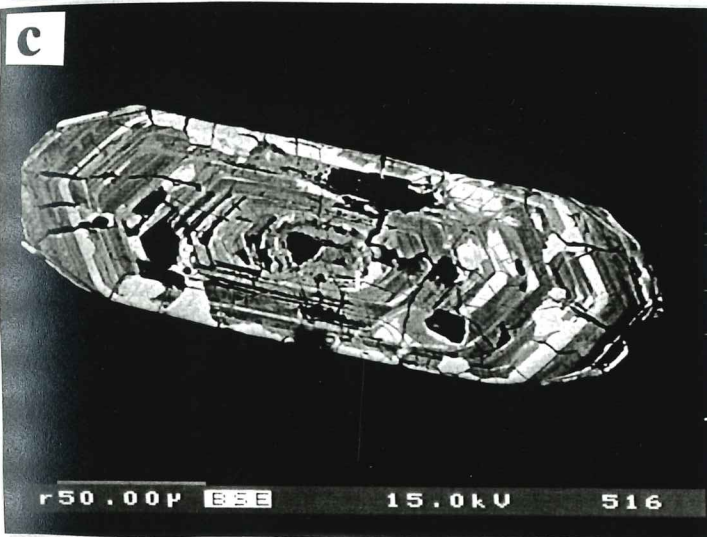
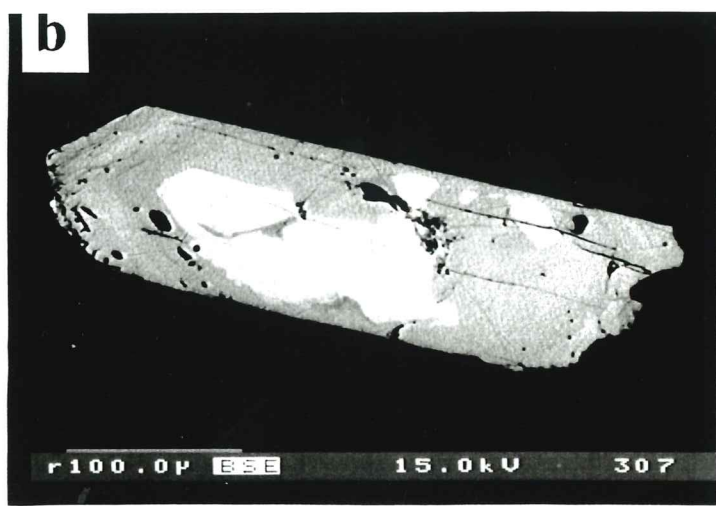
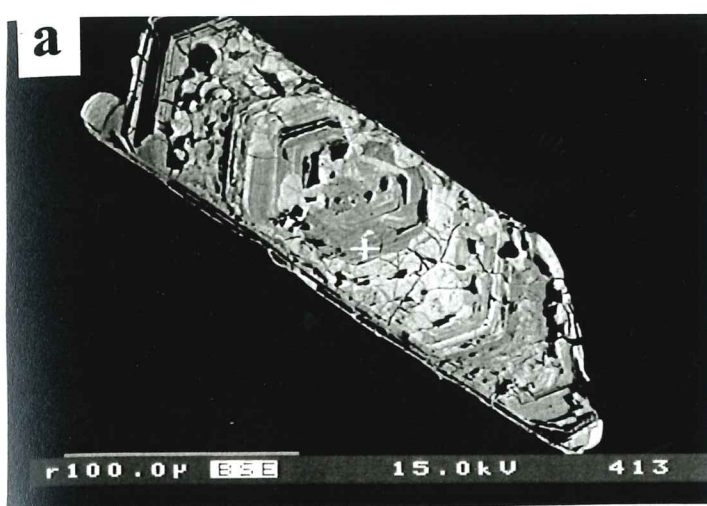
This microprobe image of a Paralana Granodiorite zircon (A1086-PCf) from the Tail (Paralana Creek) contains similar textural characteristics as Plate 3e. Significant cracking of the core region suggests higher concentrations of radioactive elements within this central region. Scale bar represents 100 microns.

PLATE 3g

The textural features of a Paralana Granodiorite zircon from Paralana Plateau (Sample A1096-HSE) are significantly different from those collected at the Tail. Core regions are surrounded by a number of truncated rims. Scale bar represents 100 microns.

PLATE 3h

This zircon also contained within Paralana Granodiorite from Paralana Plateau (A1086-HSE) also exhibits non-continuous rims which are truncated, suggesting minor amounts of repeated rim dissolution associated with a heating event. Scale bar represents 100 microns.



Granodiorite ages calculated in Table 4.1 indicate at least two distinct zones within the 5 zircons analysed, reflecting either inherited core, magmatic crystallisation or metamorphic rim growth (J. Dougherty-Page, *pers. comm.*, 1996). The primary minimum crystallisation age of 1543 ± 1 Ma (Figure 4.1) corresponds closely to igneous activity identified within the Mount Babbage Inlier, where crystallisation ages of 1551 ± 38 Ma for the Yerila Granite (Johnson, 1980) and 1556 ± 4 Ma for the Terrapinna Granite (Thornton 1980) have been calculated. This suggests either a magmatic crystallisation age of approximately 1550 Ma for the Paralana Granodiorite, or an inherited zircon age indicating Mesoproterozoic granite incorporation during granodiorite genesis. Furthermore, the 1086 ± 3 Ma age indicated in Figure 4.1 represents either the granodiorite magmatic crystallisation age (assuming the primary age is inherited), a metamorphic rim age, a 'mixing' age reflecting ratio measurements of an older and younger zone within the crystal or isotope ratio alteration due to element loss at some time after crystallisation. Therefore, although a crystallisation age could not be determined for the Paralana Granodiorite, it can be concluded that growth of the rims cannot be older than 1086 ± 3 Ma and as such represents a maximum magmatic age for the granodiorite.

4.1.2 Zircon Backscattered Electron Imagery and Microprobe Analysis

Zircons from the four lithological units were analysed to identify any changes in the element characteristics between the different populations and within crystals. As indicated in Table 4.2, electron microprobe analyses of zircons and apatites give significant variation in elemental composition, with U and Th values up to 2.902 and 0.141 weight %, respectively, measured in zircons and 0.618 and 18.182 weight % in apatites (Appendix G). Furthermore, the ratios and actual weight % values of these elements varies significantly between core and rim regions, providing important indicators for the distinction between metamorphic and magmatic crystallisation events.

4.2 Whole rock Rb-Sr and Sm-Nd isotopic systematics

Although the Rb-Sr isotopic system can be used for age discrimination of a range of rocks and rock forming minerals, Rb-Sr isochrons are rarely used in constraining crust formation ages as both Rb and Sr are readily mobilised by common crustal processes including weathering, melting, metamorphism and hydrothermal activity (McCulloch and Wasserburg,

Table 4.1 : Summary of $^{207}\text{Pb}/^{206}\text{Pb}$ Isotopic data for Paralana Granodiorite (Tail)

Sample	Number	Deposition	$^{204}\text{Pb}/^{206}\text{Pb}$	$^{204}\text{Pb}/^{206}\text{Pb}$ error	$^{207}\text{Pb}/^{206}\text{Pb}$	$^{207}\text{Pb}/^{206}\text{Pb}$ error	$^{204}\text{Pb}/^{206}\text{Pb}^*$	$^{207}\text{Pb}/^{206}\text{Pb}^*$	Age	Error
Zircon 1	1		0.000078	0.000010	0.077850	0.000766	0.076781	0.076644	1086.0	2.6
			0.000111	0.000015	0.075895	0.000118	0.074374	0.074169		
			0.000101	0.000022	0.075537	0.000058	0.074154	0.073852		
			0.000067	0.000017	0.075534	0.000043	0.074617	0.074384		
	2		0.000010	0.000010	0.092674	0.000035	0.092537	0.092400	1471.7	2.0
			0.000021	0.000010	0.092184	0.000083	0.091896	0.091759		
Zircon 1	1		0.000037	0.000004	0.094897	0.000042	0.094390	0.094336	1519.8	0.8
			0.000027	0.000006	0.095188	0.000068	0.094819	0.094737		
			0.000038	0.000012	0.095483	0.000072	0.094963	0.094799		
			0.000055	0.000009	0.095704	0.000056	0.094951	0.094828		
	2		0.000029	0.000003	0.096091	0.000065	0.095695	0.095654	1542.9	0.8
			0.000010	0.000010	0.096736	0.000226	0.096600	0.096463		
Zircon 3	1		0.000010	0.000010	0.089354	0.000188	0.089217	0.089080	1408.8	2.9
Zircon 4	1		0.000010	0.000010	0.081529	0.000129	0.081392	0.081255	1221.8	2.4
			0.000010	0.000010	0.080742	0.000127	0.080605	0.080468		
	2		0.000010	0.000010	0.091147	0.000119	0.091010	0.090873	1443.4	2.0
			0.000010	0.000010	0.090836	0.000096	0.090699	0.090562		
Zircon 5	1		0.000178	0.000072	0.087404	0.000628	0.084958	0.083965	1359.9	8.7
			0.000084	0.000031	0.088475	0.000120	0.087323	0.086897		
	2		0.000207	0.000050	0.094655	0.000131	0.091815	0.091126	1461.8	14.1
			0.000412	0.000279	0.094713	0.000356	0.089044	0.085165		

*= corrected for common Pb

Figure 4.1 Pb-Pb age discrimination Diagram for Paralana Granodiorite from the Tail

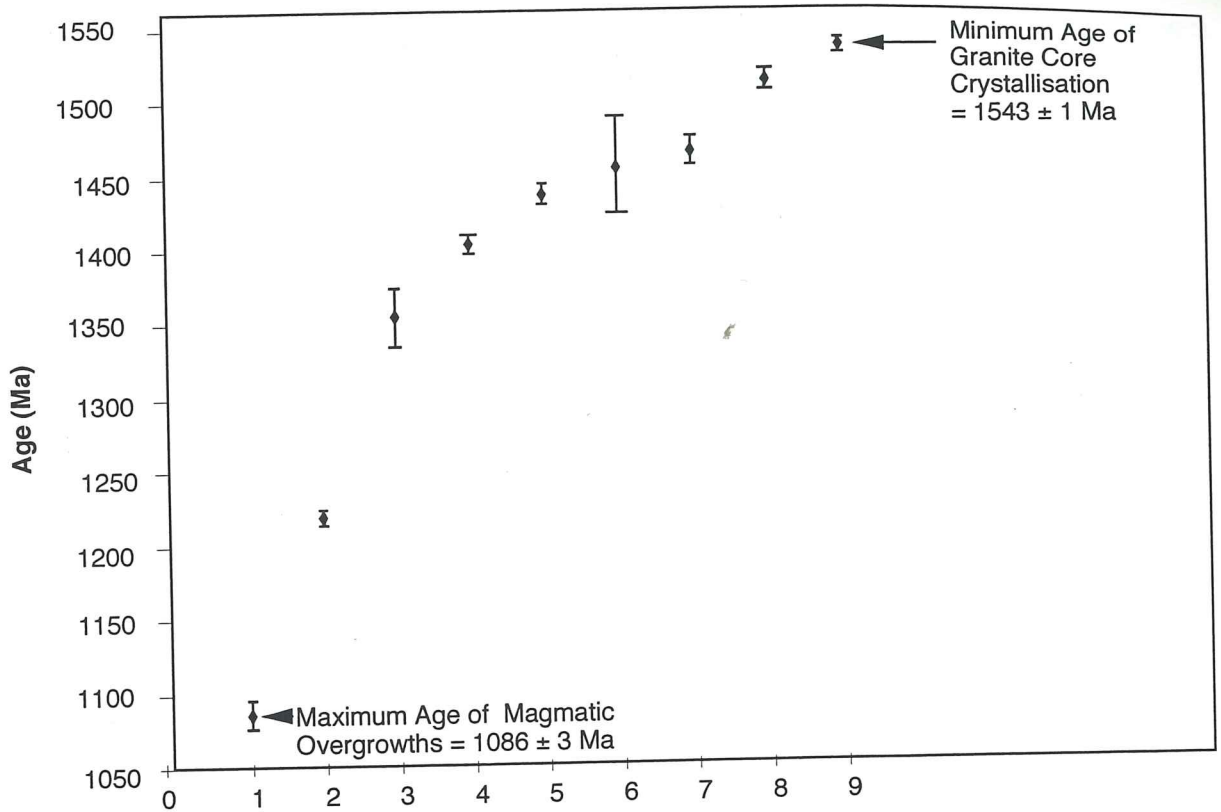


Figure 4.2 Rb-Sr isochron for selected British Empire Granite samples

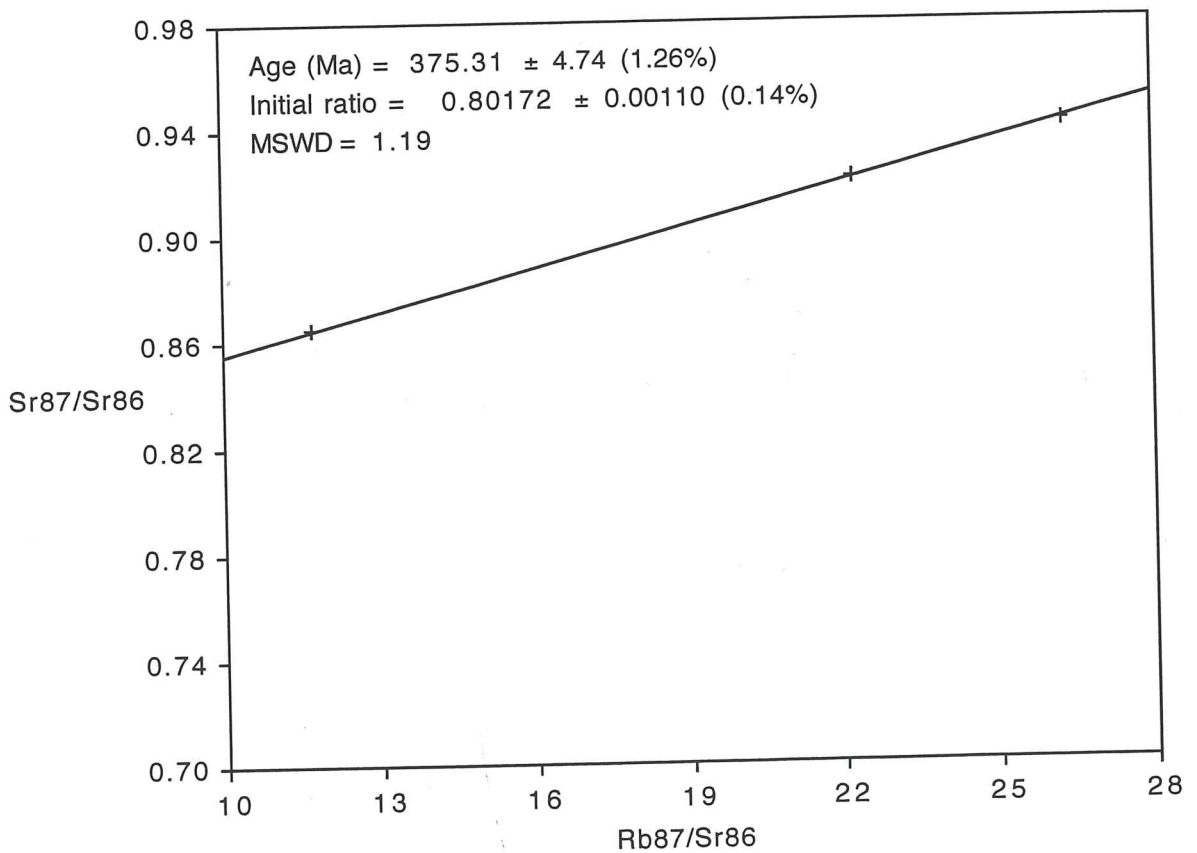


Table 4.2 : Microprobe element concentrations for zircon and apatite crystals

FOUR
PAGE

ZIRCON MICRPROBE

weight %	British Empire Granite (A1086-MP1)			Paralana Granodiorite-British Empire Granite (A1086-MP5)		
	Plate 3a-Core	Plate 3a-light	Plate 3a-med	Plate 3d-core	Plate 3d-core	Plate 3d-rim
Mg	0.007	0.000	0.000	0.000	0.011	0.028
Al	0.853	0.001	0.583	0.000	0.011	0.000
Si	9.754	14.831	10.684	13.130	12.889	12.767
P	3.449	0.000	2.793	0.000	0.020	0.000
Ca	0.820	0.000	0.695	0.010	0.000	0.018
Ti	0.126	0.000	0.140	0.000	0.002	0.000
Mn	0.028	0.040	0.079	0.000	0.000	0.026
Fe	0.841	0.000	1.031	0.040	0.015	0.018
Zr	38.169	48.495	39.526	40.590	39.806	39.344
Th	0.063	0.081	0.000	0.043	0.000	0.017
U	1.278	0.201	0.619	0.000	0.045	0.128
O	44.610	36.352	43.851	46.187	47.201	47.655
	99.998	100.001	100.001	100.000	100.000	100.001

Paralana Granodiorite from Tail (A1086-PCf)

	Plate 3e-Core	Plate 3e-rim	Plate 3f-light	Plate 3f-med	Plate 3f-dark	Other-med
Mg	0.019	0.012	0.009	0.007	0.055	0.015
Al	0.000	0.000	0.006	0.000	0.428	0.002
Si	14.727	14.775	14.970	14.518	11.536	14.589
P	0.020	0.004	0.000	0.000	0.803	0.013
Ca	0.000	0.000	0.000	0.022	0.940	0.008
Ti	0.000	0.024	0.014	0.020	0.168	0.009
Mn	0.000	0.015	0.000	0.010	0.000	0.002
Fe	0.000	0.023	0.000	0.060	0.562	0.000
Zr	48.838	49.473	47.819	46.999	41.384	46.397
Th	0.043	0.115	0.000	0.000	0.106	0.000
U	0.094	0.417	0.056	0.035	0.401	0.000
O	36.260	35.142	37.127	38.329	43.616	38.964
	100.000	100.000	100.001	100.000	99.999	99.999

Paralana Granodiorite from Paralana Plateau (A1086-HSE)

	Plate 3g-core	Plate 3g-core	Plate 3g-rim	Plate 3g-rim	Other-Core	Other-rim
Mg						
Al	0.011	0.000	0.000	0.016	0.008	0.009
Si	0.005	0.000	0.029	0.005	0.000	0.003
P	13.805	13.528	13.665	13.746	13.685	14.070
Ca	0.000	0.000	0.000	0.000	0.020	0.000
Ti	0.036	0.003	0.005	0.011	0.018	0.000
Mn	0.005	0.000	0.000	0.000	0.000	0.009
Fe	0.000	0.000	0.000	0.000	0.000	0.000
Zr	0.002	0.061	0.007	0.000	0.000	0.000
Th	42.605	42.241	42.573	42.943	42.292	43.864
U	0.000	0.051	0.090	0.043	0.000	0.000
O	0.000	0.086	0.030	0.095	0.000	0.252
	43.531	44.028	43.602	43.141	43.976	41.793
	100.000	99.998	100.001	100.000	99.999	100.000

APATITE MICROPROBES

	British Empire Granite				Paralana-British mix Paralana Granodiorite	
	Plate 3b-core	Plate 3b-rim	Other-Core	Other-rim	Other-core	Other core
Mg	0.000	0.000	0.000	0.005	0.000	0.000
Al	0.015	0.007	0.002	0.003	0.000	0.000
Si	0.707	0.206	0.114	0.189	0.244	0.086
P	11.603	12.683	12.686	12.474	11.878	18.664
Ca	2.253	1.732	1.855	1.981	0.624	39.506
Ti	0.023	0.010	0.000	0.024	0.034	0.000
Mn	0.000	0.000	0.000	0.000	0.000	0.052
Fe	0.000	0.000	0.000	0.000	0.000	0.040
Zr	0.000	0.000	0.000	0.000	0.000	0.000
Th	18.182	10.257	8.308	11.258	4.086	0.039
U	0.000	0.568	0.265	0.618	0.000	0.000
O	67.217	74.537	76.769	73.448	83.135	41.613
	100.000	100.000	99.999	100.000	100.001	100.000

Probe position codes : core=zircon core, rim=zircon rim, light=light coloured zone, med=medium coloured zone, dark=dark coloured zone
 Other=non-photographed zircons/apatites
 Complete zircon/apatite microprobe data set in Appendix G

1978; Goldstein, 1988). Nevertheless, if a Rb-Sr isochron is obtained it can often reflect a definite event such as metamorphism or the ages of diagenesis in sedimentary rocks.

Due to their robust nature through sediment and metamorphic cycles, Sm-Nd isotopic systematics are not substantially disrupted during sedimentation or diagenesis and so isochron diagrams constructed can indicate the initial $^{143}\text{Nd}/^{144}\text{Nd}$ ratio and age of the rock. Nd model ages calculated for an individual rock are commonly used for the Sm-Nd system, measuring the length of time a sample has been separated from the mantle from which it was derived (DePaolo and Wasserburg, 1976; McCulloch and Wasserburg, 1978; Rollinson, 1993). Thus calculated Nd model ages can be used to characterise and possibly identify the provenance region of sedimentary rocks (Goldstein, 1988; Turner *et al.*, 1992). Sm-Nd data is often expressed in terms of epsilon notation (ϵ) which is the proportional variation of the sample $^{143}\text{Nd}/^{144}\text{Nd}$ ratio from the Chondritic Uniform Reservoir (CHUR) at any one time. As the CHUR curve describes the Nd evolution of the mantle reservoir, any deviations from this curve suggests processes which are resulting in Sm-Nd ratios different from bulk earth (DePaolo and Wasserburg, 1976).

Samples of British Empire Granite from Mawson Plateau and the body/Tail junction, Paralana Granodiorite from the Tail and Paralana Plateau together with Freeling Heights Quartzite represent the widest lithological and locational range of these units. Procedures undertaken to obtain the isotopic data and calculated isotopic ratios and model ages discussed below are outlined in Appendix J. Values obtained were used together with data on potential British Empire Granite provenance units provided by O'Halloran (1992), Smith (1992) and Schaefer (1993) (Appendix H).

4.2.1 Rb-Sr and Sm-Nd results

Samples of the British Empire Granite (additional data from Schaefer 1993) show $^{87}\text{Sr}/^{86}\text{Sr}_{(470\text{Ma})}$ of 0.75607-0.78583 (Table 4.3) with the more extreme samples possibly representing later mobilisation of Rb and Sr. $\epsilon\text{Nd}_{\text{CHUR}}$ values at this time extend from -12.35 to -14.19 with Nd depleted mantle model ages (T_{DM}) ranging from 2.91 to 3.36 Ga.

The British Empire Granite-Paralana Granodiorite mix sample has a $^{87}\text{Sr}/^{86}\text{Sr}$ value at 470 Ma of 0.72325 with an ϵNd value of -11.52 at that time and (T_{DM}) of 2.43 Ga.

The Paralana Granodiorite sample from the Tail contains $^{87}\text{Sr}/^{86}\text{Sr}$ 0.70803 at 470 Ma, with an ϵNd value of -6.66 and (T_{DM}) of 1.56 Ga. In contrast the Paralana Plateau Paralana Granodiorite $^{87}\text{Sr}/^{86}\text{Sr}$ is 0.70809 with an ϵNd value of -1.52 at 470 Ma, and a Nd depleted mantle model age of 1.25 Ga. The high Sr content of these two samples minimises variations

Table 4.3 : Summary of isotopic data for selected lithologies within the mapped area

Lithology	British Empire Granite				BEG-PG Mixture			Paralana Granodiorite			Paralana Creek Metasediments		Freeling Heights Quartzite	
	948-92-BE1	948-92-BE2	948-92-BE3	948-92-BE4	MP1	NC7	HSE (P Plat)	HSE (P Plat)	HV-60 (P Plat)	948-92-FHQ1	948-92-FHQ3	NC4	A1015-HV-55	
Sample Number	10.217	6.441	7.5345	5.649	10.312	4.443	14.653	8.145	3.797	19.686	20.146	18.863	16.881	
Nd ppm	2.403	1.664	1.8803	1.37	2.603	1.015	2.696	1.62	0.773	3.467	3.467	3.34	2.995	
Sm ppm	0.511826	0.511787	0.511865	0.511781	0.511858	0.51187	0.512034	0.512325	0.1231	0.51142	0.511509	0.511435	0.511493	
143/144 Nd	0.1423	0.1563	0.1510	0.1467	0.1527	0.1382	0.1130	0.1203	0.511407519	0.1065	0.1041	0.1071	0.1073	
147Sm/144Nd	0.511388	0.511306	0.511400	0.511329	0.511388	0.511443	0.511691	0.511955	-	0.511092	0.511189	0.511105	0.511163	
T mod:chur	2.26	3.19	2.56	2.60	2.69	2.00	1.08	0.63	-	2.05	1.85	2.04	1.95	
T mod:dep	2.65	3.36	2.91	2.91	3.00	2.43	1.56	1.25	-	2.35	2.18	2.34	2.26	
eps Nd (0)	-15.8396	-16.6004	-15.0789	-16.7174	-15.2154	-15.0203	-11.7822	-6.1057	-	-23.7595	-22.0233	-23.4669	-22.3354	
Sr ppm	35.36	38.603	47.744	61.706	52.5	178	883	609.2	539.5	5.366	6.93439	5.5	19.60018	
Rb ppm	489.545	290.114	320.898	245.989	220.2	180.4	177.4	90.9	77.1	272.984	1056.15	137.5	102.306	
Sr87/86	0.979981	0.921056	0.901534	0.864247	0.838366	0.74295	0.711922	0.709979	0.72	2.317549	4.429876	1.578829	0.967251	
Rb/Sr	13.84460	7.51532	6.72122	3.98647	4.19429	1.01348	0.20091	0.14921	0.1428	50.87290	152.30611	25.00000	5.21965	
87Rb/86Sr	41.12289	22.19757	19.81495	11.71050	12.29025	2.94238	0.58151	0.43180	0.413904307	170.36849	601.11803	78.49544	15.48521	
87/86Sr (470 Ma)	0.70460893	0.772413924	0.768846769	0.785829727	0.756067	0.72325	0.708028	0.7070875	0.721235364	1.176706975	0.404596863	1.05319834	0.863557045	

All samples prefixed A1086- except A1015- (Schaefer 1993) and 948- (Foden unpublished data in Schaefer 1993)

in the isotopic signature with the low $^{87}\text{Sr}/^{86}\text{Sr}$ values at 470 Ma suggesting unrealistically low ratios at the Mesoproterozoic (J. Foden, *pers. comm.*, 1996).

The large variation of $^{87}\text{Sr}/^{86}\text{Sr}$ at 470Ma in Paralana Creek Metasediments (Schaefer 1993) and Freeling Heights Quartzite from 0.40460 to 1.7670 at 470 Ma suggests significant mobilisation of Rb and Sr. ϵ_{Nd} values extend from -16.33 to -18.37 at this time with (T_{DM}) values more restricted, ranging from 2.26 to 2.35.

4.2.2 Rb-Sr isotopic analysis and interpretations

An isochron plot of $^{87}\text{Rb}/^{86}\text{Sr}$ against $^{87}\text{Sr}/^{86}\text{Sr}$ utilising ratios of three closely associated samples calculated in Table 4.3 produces a British Empire Granite age of 375 ± 5 Ma (Figure 4.2) with initial $^{87}\text{Sr}/^{86}\text{Sr}$ of 0.80172. The Mean Squares of Weighted Deviates (MSWD) value, defined as a measure of the fit of the line to the data within the limits of analytical error by Rollison (1993), is within the accepted value of 2.5 and thus supports the credibility of this isochron age. Indeed, this age corresponds well to the Rb-Sr isochron age of 384 Ma calculated for the British Empire Granite by Schaefer (1993). Therefore, this age may represent resetting of the isotopic signature associated with a later metamorphic or hydrothermal fluid event, or alternatively could constrain the British Empire Granite crystallisation age as other post-Delamerian granitoids within the Inlier range in age from 450 ± 4 to 372 ± 2 Ma (Farrand and Preiss, 1995).

4.2.3 Sm-Nd isotopic analysis and interpretations

As the isotopic characteristic of a source region and derived magma will be the same at the time of magma genesis, the intersection of British Empire Granite isotopic ratios with potential melt sources suggest times that the magma could inherit the signature it now contains. The ultimate magma source is the depleted mantle, with isotopic values for Paralana Granodiorite equating to this primitive source at approximately 1.6 and 1.35 Ga for the Tail and Paralana Plateau samples respectively (Figure 4.3a and b). In contrast, the British Empire Granite samples form a tight envelope which intersects the depleted mantle at a minimum age of 2.5 Ga (Figure 4.3b), reflecting its parental provenance's extensive crustal history.

Figure 4.3a : MPI Granitic-gneissic Nd evolution through time

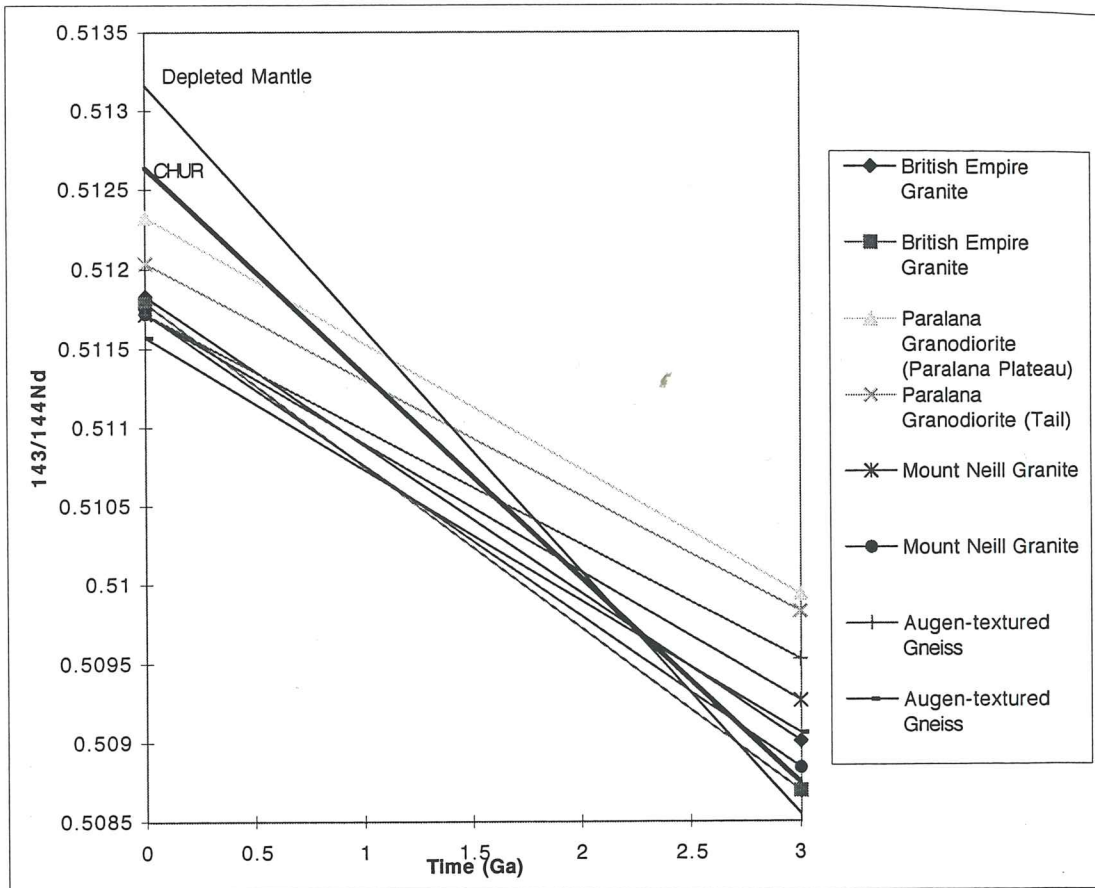
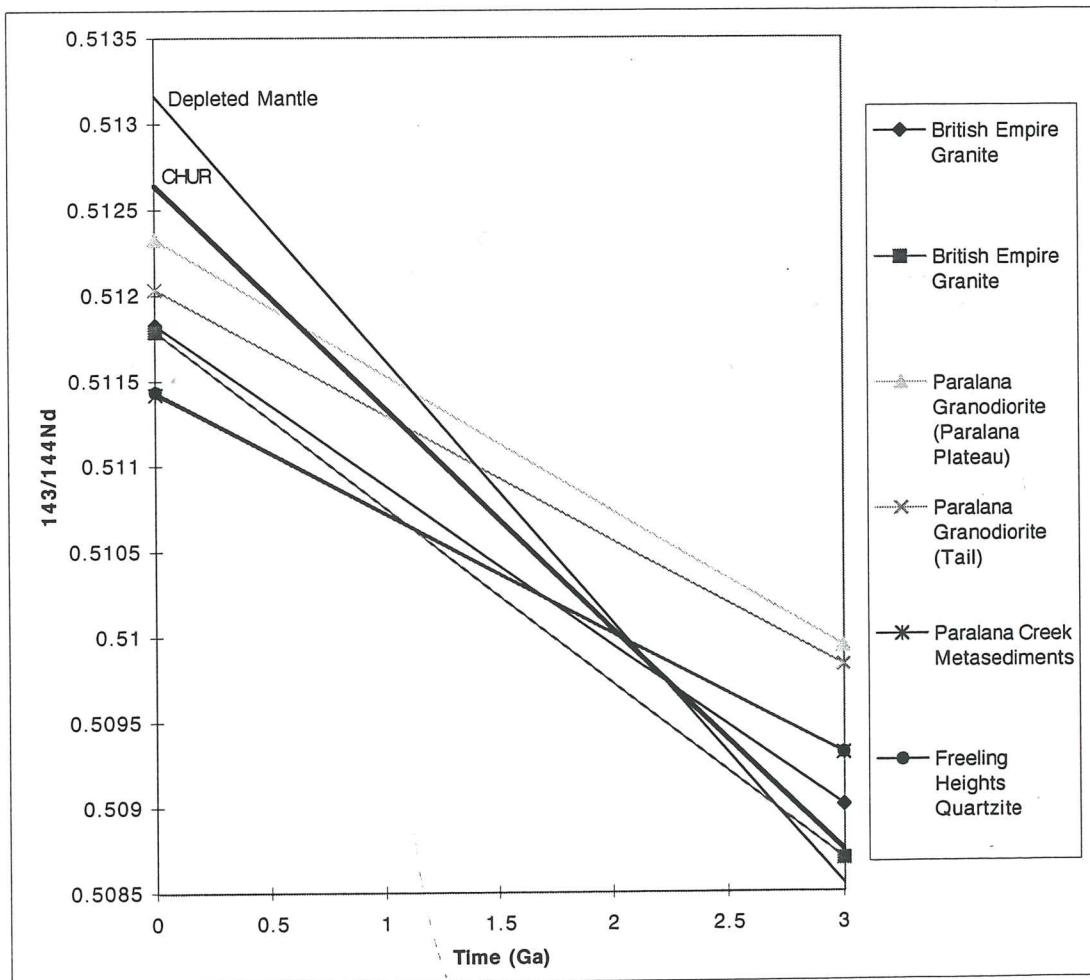


Figure 4.3b : MPI Tail-Body and metasediment Nd evolution through time



Similar time-trajectories can be established using CHUR values, indicating potential derivation of units or their provenance from a chondritic reservoir. Figure 4.3a shows that the Paralana Granodiorite isotopic signature of the tail and Paralana Plateau have similar slopes, with CHUR intersections at 1.1 and 0.6 Ga respectively. Furthermore the Paralana Granodiorite Tail isotopic evolution strongly correlates to the trajectory of the Palaeoproterozoic gneiss suite possibly reflecting a similar magmatic evolution. Again the British Empire Granite samples produce a different trajectory to the granodiorite, with intersection of the CHUR evolution curve at approximately 2 Ga (Figure 4.3b) again suggesting the granites source region evolved from the mantle during the Palaeoproterozoic.

This same system can assist provenance identification if the granites of interest were derived from crustal material alone. $^{143}/^{144}\text{Nd}_{\text{CHUR}}$ time-trajectories for British Empire Granite suite intersect units of the Palaeo- and Mesoproterozoic metasediments between 1.5 and 0.8 Ga (Figure 4.3b) indicating the time at which the granite would evolve from this source to acquire the isotopic signature it now contains. However, as British Empire Granite generation may be Delamerian, another source containing a lower Nd_{CHUR} ratio (such as Paralana Granodiorite) is required produce the isotopic signature calculated. As shown in Figure 4.3b, the British Empire Granite trajectory lies between Paralana Granodiorite (representing a mantle source) and crustal metasediments at Delamerian times, suggesting a mixing scenario of these two units for granite genesis. Furthermore, the Epsilon Nd values of Adelaidean sedimentary units intersect British Empire Granite at 0.8 to 0.2 Ga, which corresponds strongly to the Palaeozoic age proposed for this granite (Figure 4.4a). The Willouran Wooltana Volcanics, a basaltic suite within the Mount Painter Inlier which intersect Paralana Granodiorite between 1 Ga and 0.5 Ga (Figure 4.4b) may represent a mafic endmember for granodiorite and British Empire Granite co-genesis.

Of special interest is the Depleted Mantle model age of Tail Paralana Granodiorite, which is equivalent to the inherited zircon age of approximately 1.56 Ga obtained from Pb-Pb analysis. Depleted Mantle and Chondritic Uniform Reservoir Model Ages calculated for the British Empire Granite present some difficulty, indicating this unit's original source material separated from the mantle at approximately 2.9 and 2.6 Ga respectively. As calculated in Table 4.3, these values are greater than ages calculated for all other potential British Empire Granite sources except the Mount Neill Granite. Therefore British Empire Granite generation involving Mount Neill Granite incorporation would be required to produce the age calculated, especially if melt generation involved mixing with the younger model ages of units identified. Assuming British Empire Granite generation at 470 Ma, the $^{87}\text{Sr}/^{86}\text{Sr}$ vs $\epsilon\text{Nd}_{\text{CHUR}}$ values calculated for surrounding lithologies at that time indicate that the British Empire Granite

Figure 4.4a : Selected granitic and Adelaidean Nd evolution through time

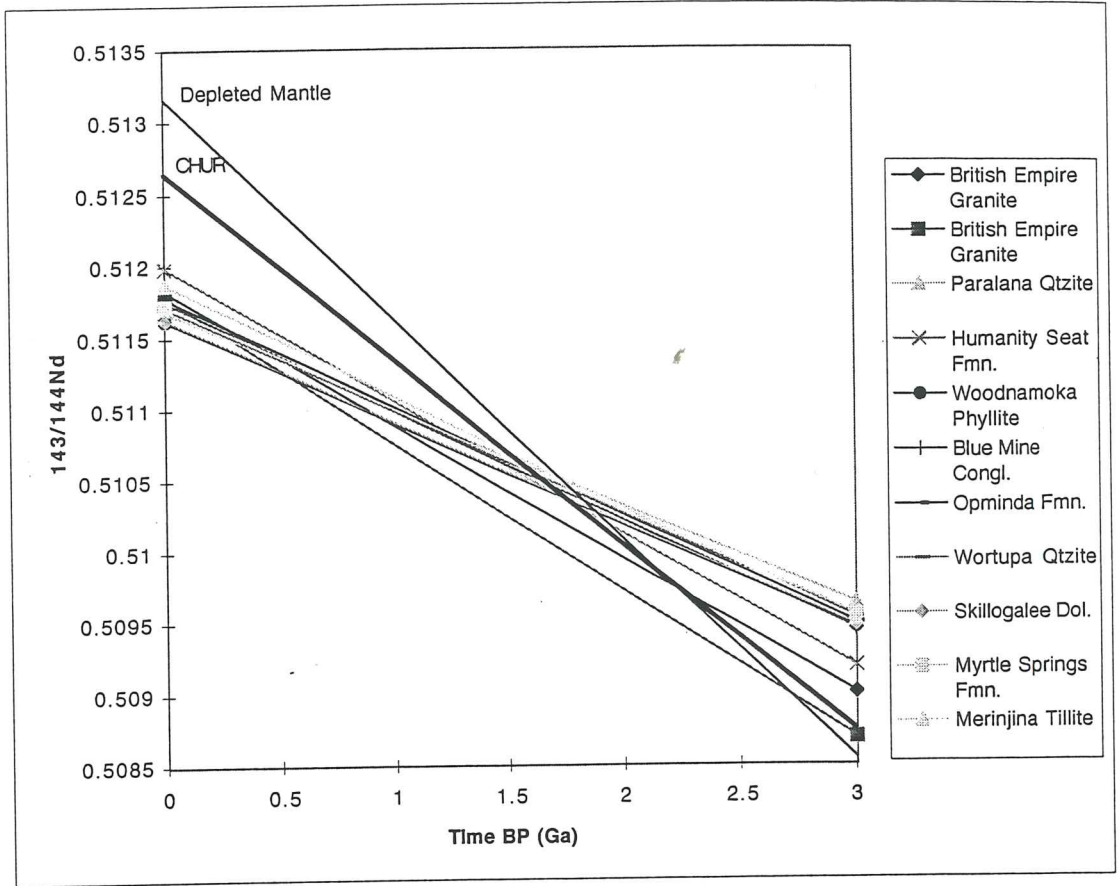
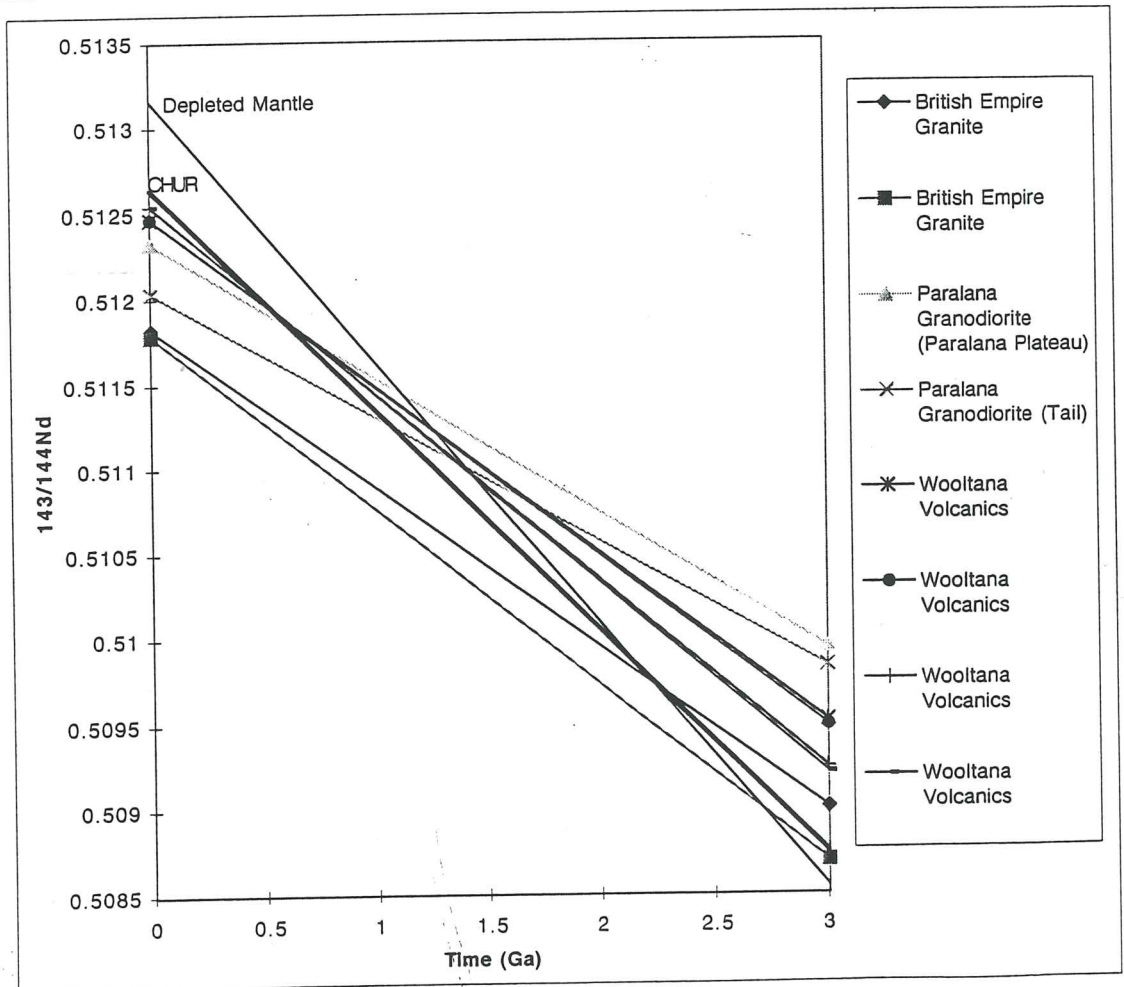


Figure 4.4b : Selected MPI granitic and Wootana Volcanic Nd through time



could inherit the ratios now measured from a number of provenances. The British Empire Granite values equate strongly to Adelaidean sedimentary units at this time, but also lie directly between a mixing combination of Paralana Granodiorite and Freeling Heights Quartzite (Figure 4.5a). The isotopic signature of the Mount Neill Granite is also closely associated to the British Empire Granite at 470 Ma and could therefore also be involved in the melt evolution.

In contrast, the Paralana Granodiorite ratios do not correlate spatially to any other lithologies identified within the local region and would therefore require the inclusion of a more primitive magmatic endmember to acquire the isotopic ratios observed if it was also of this age. Plots of the same ratios at 800 Ma (equivalent to the Wooltana Volcanics genesis age) indicate the British Empire Granite could not inherit the signature it contains from melting and mixing of surrounding units. The potential for Wooltana Volcanics as an intrusive endmember is therefore rejected, with the close isotopic correlation of British Empire Granite with surrounding lithologies strongly favouring Palaeozoic granite generation (Figure 4.5b).

Consideration of the geochemistry required to produce the characteristics observed in the generated granite can further assist provenance identification (Figure 4.5a and b) with both two-unit mixing or direct derivation from Adelaidean sediments will produce the Y and Zr distribution observed in British Empire Granite.

4.3 Conclusions

Radiogenic isotopic signatures together with lithological and geochemical characteristics clearly indicate distinct variations between the Paralana Granodiorite and British Empire Granite, with these magmas derived from different source material at different times within the Mount Painter Inlier. Together, Sm-Nd and Pb-Pb isotopic ratios imply Paralana Granodiorite derivation from the mantle or material sourcing the mantle during the Mesoproterozoic, with no crustal source(s) identified providing the isotopic signature required during genesis. Internal variations between the Tail and Paralana Plateau samples reflect isotopic re-setting associated with Delamerian activity concentrated at the Paralana Fault Zone. In contrast, the British Empire Granite isotopic signature must be derived from a crustal source involving melting of Freeling Heights Quartzite, Paralana Granodiorite or Adelaidean sediments during the Palaeozoic, with Mount Neill Granite incorporation required to attain the Nd Model Ages calculated for the British Empire Granite.

Figure 4.5a : $87/86\text{Sr}$ vs $\text{E}(\text{Nd})$ at 470 Ma

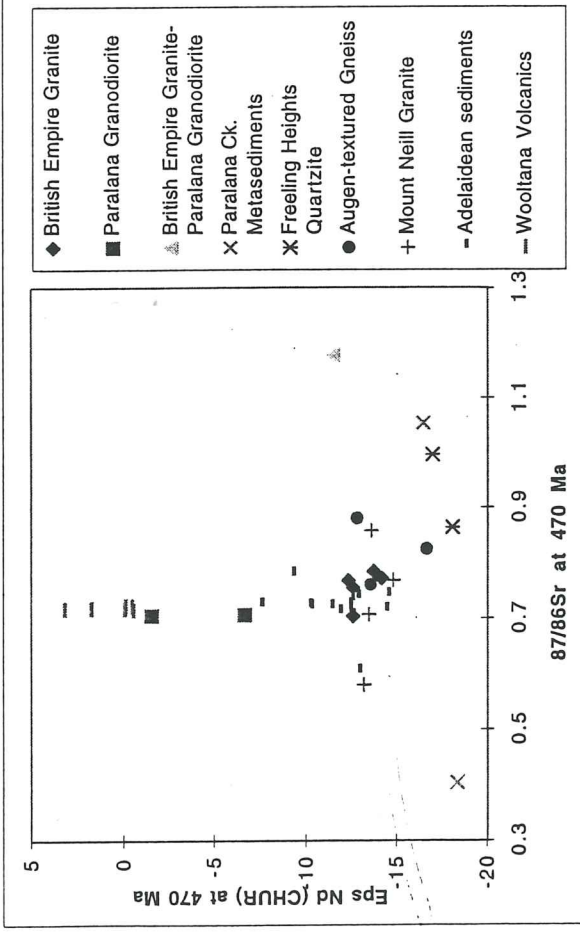


Figure 4.5b : $87/86\text{Sr}$ vs Eps Nd at 800Ma

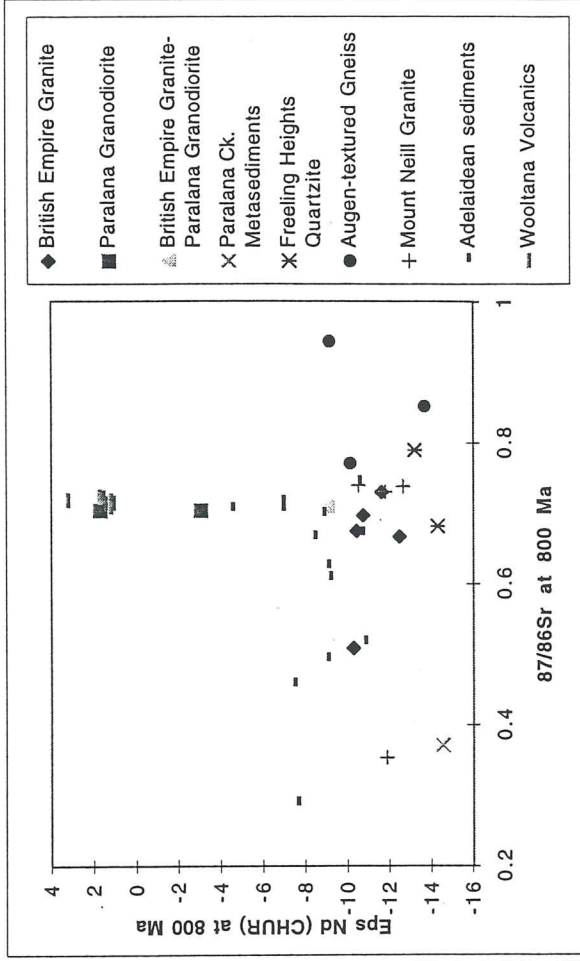


Figure 4.6a : Eps Nd vs Y at 470Ma

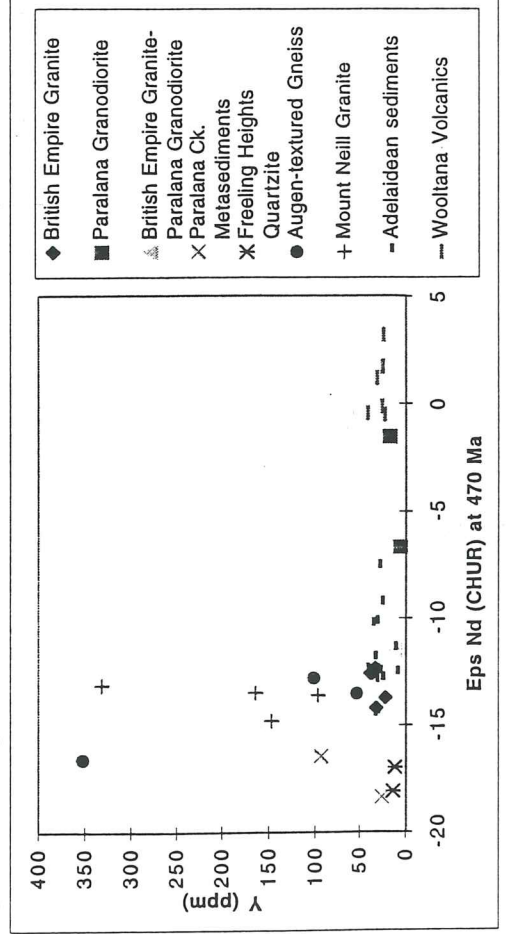
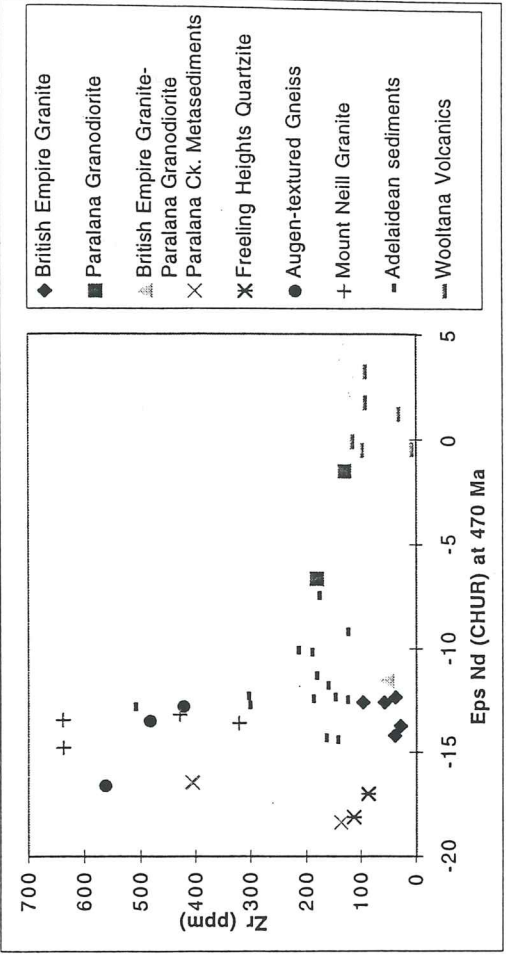


Figure 4.6b : Eps Nd vs Zr at 470Ma



Chapter Five

RADIOACTIVE ELEMENT CONCENTRATIONS IN THE MOUNT PAINTER INLIER

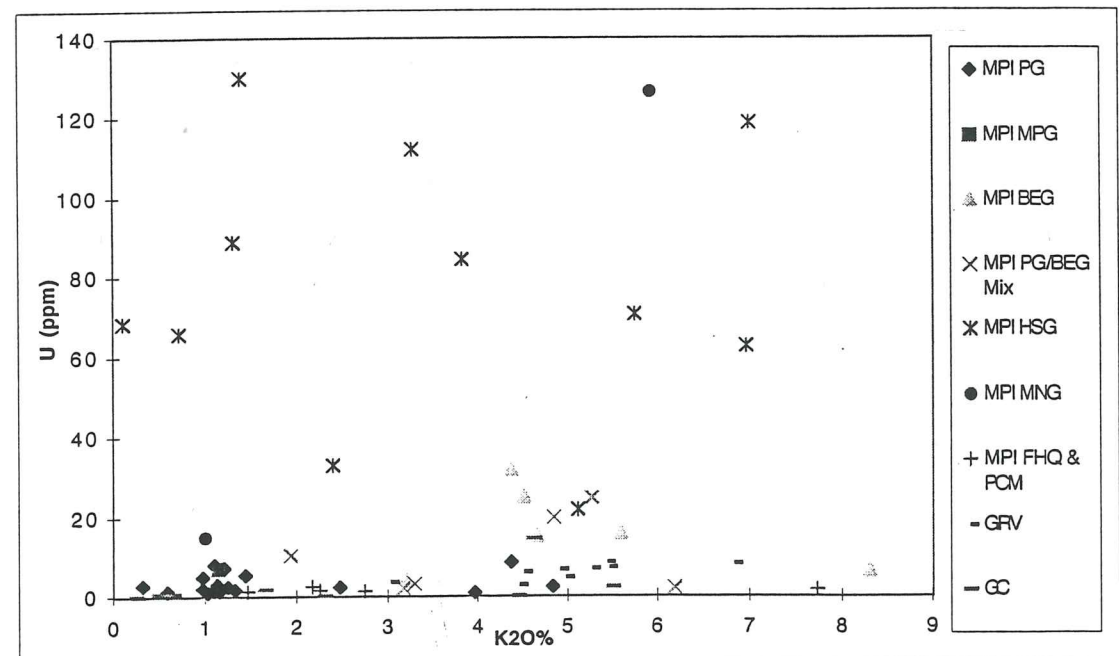
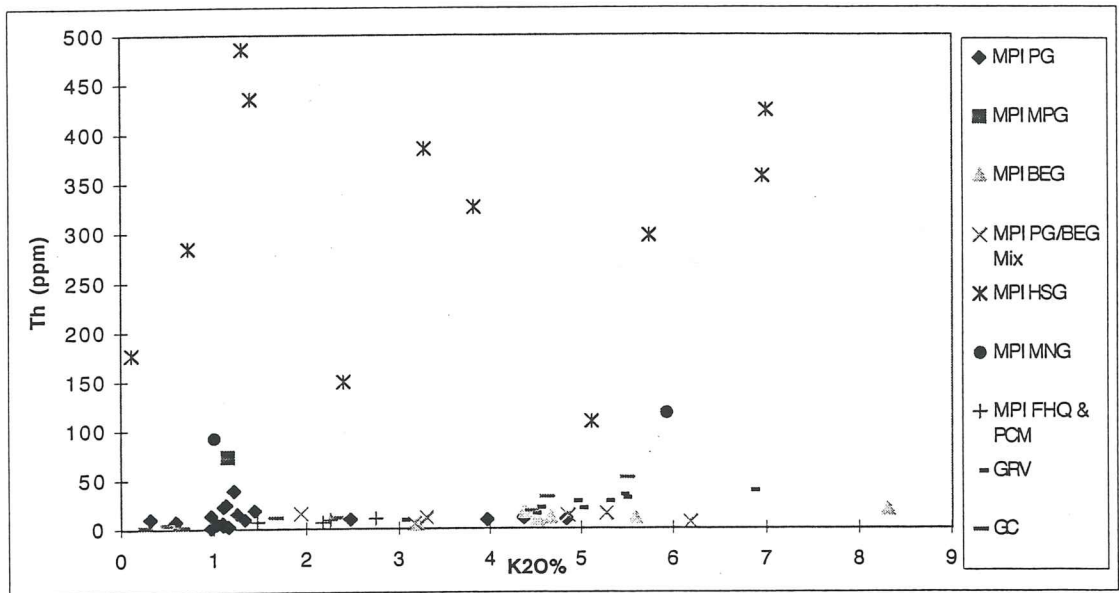
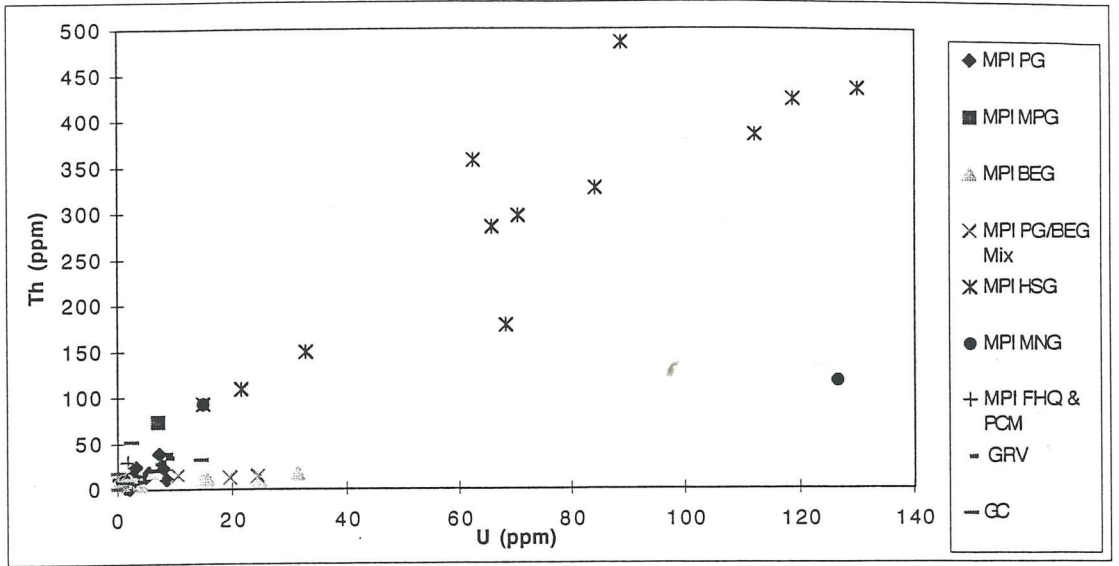
Geochemical and radiometric measurements indicate extreme enrichment in U, Th and K in Proterozoic granites of the Mount Painter Inlier relative to other contemporary magmas and many Australian Proterozoic terrains. Because such anomalous concentrations are likely to have a significant impact on the thermal budget within the crust during the Delamerian Orogeny, it is important to understand the processes which control such anomalous elemental concentration. It is shown that the enrichment is likely to be magmatic in origin and controlled by melt source composition and magmatic differentiation, as illustrated by the concentration of accessory minerals within the magma product relative to its source residual material.

5.1 Anomalous U, Th and K enrichment in the Mount Painter Inlier

Previous studies by Wall (1995) showed that Mesoproterozoic granites of the Mount Painter Block contain anomalous concentrations of heat-producing elements, with the Yerila Granite, Wattleowie Granite and Terrapinna Granite containing elevated U, Th and K concentrations as indicated by geochemical assay and radiometric survey.

Similar enrichments of high heat-producing elements are identified for Proterozoic granites and gneisses within the mapped area as reflected by a radiometric survey of the Inlier (M. Sandiford, *pers. comm.*, 1996), with the light colour of the Mount Painter Block indicating elevated concentrations of U, Th and K (Appendix L). In particular, the Hot Springs Gneisses appear white indicating extreme enrichment in U, Th and K, with these units clearly folded by the south-southwest plunging anticline and therefore appearing at both the Paralana Plateau and eastern Tail boundary. The colour signature of these gneisses corresponds strongly to those of the Mesoproterozoic Yerila Granite, Wattleowie Granite and Terrapinna Granite of the Mount Painter Block, suggesting that these enriched granites may be part of the same magmatic suite. The Tail Paralana Granodiorite appears brown, reflecting low values for all three elements whereas the pink-coloured British Empire Granite body is clearly differentiated by its high K values, as indicated in Figure 5.1. Other areas within the Mount Painter Inlier including the northwestern boundary of the British Empire Granite, also suggest significant enrichment of U, Th and K but are not presently correlated to any igneous bodies identified in the area.

Figure 5.1 : U, Th and K for Mount Painter Inlier, Gawler Range Volcanics & Gawler Craton Units



MPI=Mount Painter Inlier, BEG = British Empire Granite, MPG = Migmatitic Parana Granodiorite, PG=Parana Granodiorite, HSG = Hot Springs Gneiss, MNG = Mount Neill Granite, FHQ = Freeing Heights Quartzite, PCM = Parana Creek Metasediments, GC = Gawler Craton, GRV = Gawler Range Volcanics

Whole rock trace element analyses of lithologies within the Paralana Hot Springs area show that Proterozoic units also contain elevated U, Th and K concentrations (Table 5.1). In particular, the Massive K-feldspar Gneiss and Augen-textured Gneiss units of the Hot Springs Gneiss Suite are extremely enriched, with average concentrations of 3.2% K, 330 ppm Th and 76 ppm U. The Mount Neill Granite also has elevated U, Th and K concentrations with an average of 4.9% K, 69 ppm Th and 16 ppm U, whereas the Paralana Granodiorite concentrations of 1.7% K, 15 ppm Th and 3 ppm U are similar to the average crustal values. As indicated by the radiometric survey and trace element analyses, both the Paralana Creek Metasediments and Freeling Heights Quartzite contain low concentrations of heat-producing elements.

Comparisons of the Mount Painter Inlier Proterozoic gneisses and volcanics with other Australian terrains (Figure 5.1) show these units contain anomalous U and Th values compared to the Gawler Craton, Gawler Range Volcanics. Enrichment is also significantly higher than in the Palaeozoic Lachlan Fold Belt granites (Chappell and White, 1992), thus suggesting that the anomalous U, Th and K values of the Mount Painter Inlier are extraordinary on both a spatial and temporal scale.

5.2 Origin and processes controlling heat-producing element distribution and concentration

Igneous rocks contain primary magmatic Th/U ratios of about 3.5 to 4.0 (Durrance, 1986). Due to variations in U and Th mobility, any secondary alteration will change this ratio and therefore indicate whether U and Th concentrations are a primary igneous characteristic developed during magmatic crystallisation or a later secondary feature. As the Proterozoic units within the Mount Painter Inlier contain Th/U ratios of approximately 4.4 (Table 5.1), it can be concluded that enrichment in these units is a primary magmatic feature that has been characteristic since magmatic crystallisation. In comparison, the Th/U ratio of 0.7 measured within the British Empire Granite suggests later secondary processes have altered element concentrations.

Although granite batholiths are relatively enriched in the heat producing elements U, Th and K in comparison to other magmatic lithologies, the anomalous concentrations observed within the basement suite of Proterozoic granites, gneisses and volcanics within the Mount Painter Inlier are extraordinary. Because it has been shown that the high heat producing element (HPE) concentrations are a primary magmatic feature, they must reflect the chemistry of the source regions together with magmatic differentiation processes (Tilling *et al.*, 1970; Morgan *et al.*, 1987).

Most anorogenic I-type Proterozoic granites within Australia are characterised by depleted Sr, normal Y concentrations and significant K, Th and U enrichment (Wyborn *et al.* 1992). For example, these characteristics are observed in the Gawler Range Volcanics, Hiltaba and Charleston Granites and Olympic Dam Suite. Wyborn *et al.* (1992) noted that granites from this igneous suite are always coeval with major extensional events and are always preceded by I-type granites which are less enriched in incompatible elements. The source of these K, U, Th and incompatible element enriched Proterozoic granites is enigmatic as their geochemical and isotopic signatures preclude direct derivation from the mantle, from the subduction environment or from remelting of Archaean granites and gneisses which are characterised by Y-depletion (Wyborn *et al.*, 1992). The source of I-type Proterozoic granites is therefore suggested to be a fractionated mantle-derived mafic forming an underplate, where this source probably accumulated to the crust base during major tectothermal events (Etheridge *et al.*, 1987; L. Wyborn *et al.*, 1987; Wyborn *et al.*, 1992).

However, as U, Th and K concentrations within the Mount Painter Block are significantly more elevated than other so-called “enriched” I-type Proterozoic granites additional processes acting to produce the extreme enrichment observed are implied. Wall (1995) suggested that Proterozoic granites within the Mount Babbage Inlier containing geochemical signatures similar to those of the enriched Mount Painter Inlier granites are a highly fractionated version of the Hiltaba Suite granites of the Gawler Craton, with the most fractionated radiogenic units occurring in the Mount Painter Inlier and tapering off to the west and east.

Clearly source composition and processes of magmatic differentiation must play an important role in radioactive-element enrichment. It is accessory minerals such as apatite, zircon, sphene, allanite and monazite that contain the significant proportion of radioactive elements (Webb *et al.*, 1987; Bea, 1996). Therefore, U and Th enrichment is primarily controlled by magmatic fractionation together with the abundance of radioactive elements in earlier

crystallising products and initial concentrations in the source material (Webb *et al.*, 1987). Furthermore, the order of accessory mineral precipitation will be determined by parental and melt composition parameters and will therefore also influence the partitioning of radioactive elements between early crystallising minerals and the residual melt. The rate of melt segregation from a source during melting also plays an important role, with rapid segregation limiting dissolution of accessory phases and resulting in accessory enrichment in the residual (Watt *et al.*, 1996). Anatectic temperature controls the proportion of melting, with the low solubilities of many accessories including zircon implying minimal dissolution during low temperature melting (Watt *et al.*, 1996). In addition, as accessories are too small to settle within convecting magmas, they are often separated from the melt as inclusions within larger minerals; biotite commonly exhibits this and thus controls the concentration of REE, Y, U and Th (Bea, 1996). Large radioactive halos around zircons included within biotite of the Hot Springs Gneisses (Appendix D) clearly show that the zircons have significant radioactive element concentrations. Furthermore, microprobe analyses of zircons and apatites indicate high U and Th concentrations within these accessories for British Empire Granite and some Parana Granodiorite crystals (Appendix G).

Bea (1996) showed that increases in Aluminium Saturation Index (ASI) are coupled with decreases in REE (except Eu), Y, Th and U due to the progressive replacement of allanite and sphene by monazite and xenotime with increasing ASI and decreasing CaO. Metaluminous I-type granites therefore display downward decreases in heat-producing elements within plutons. In contrast, fractionation trends of peraluminous S-type granites indicate no significant change in heat-producing element concentrations with associated U and Th enrichment in the residual sources due to low accessory mineral solubilities in such melts (Sawka and Chappell, 1986). The vertical level of a pluton exposed in outcrop may thus result in significant U and Th variations.

Therefore, high concentrations of U, Th and K in Proterozoic granite and gneisses of the Mount Painter Inlier may represent derivation from an enriched mantle-derived mafic source, where repeated rapid segregation of melts has led to a residual source enriched in these high heat producing elements within accessory minerals.

5.3 Absolute Crustal Heat Production within the Mount Painter Inlier

In the Mount Painter Block, thermal energy produced by the decay of radioactive elements within the crust have resulted in decreases in crustal strength and thus basement-cover coupling during Delamerian deformation (Wall, 1995). Calculations of crustal heat production for units within the study area can therefore indicate the extent to which thermal energy produced by the observed anomalous U, Th and K concentrations can impact on the regional geothermal regime of the Mount Painter Inlier.

As current crustal heat production for a given terrain from natural decay of radioactive elements including ^{40}K , ^{232}Th , ^{235}U and ^{238}U is less than at any time in the past, it is possible to back calculate productivity for such exponential element decay (Fowler, 1990). Current surface average heat production values are 2-4 μWm^{-3} (Mildren and Sandiford, 1995). Calculated present surficial heat production for units within the Mount Painter Inlier from concentrations of U (ppm), Th (ppm) and K (%) indicate significant variations between lithologies (Table 5.1 and Appendix M).

TABLE 5.1 - Average Heat Production values for Mount Painter Inlier Units

Lithology	Average Concentration					Ave Heat Production (μWm^{-3})			
	No of samples	U (ppm)	Th (ppm)	K (wt %)	Th/U	At 0 Ma	At 470 Ma	At 1540 Ma	At 1670 Ma
Hot Springs Gneiss	14	76.4	330.1	3.2	4.4	44.3±16	46.5±17	52.1±19	52.9±19
Mount Neill Granite	6	15.8	69.3	4.9	4.8	9.6±2	10.1±2	11.3±2	11.4±2
Paralana Granodiorite	19	3.4	15.0	1.7	4.4	2.1±2	2.2±2	2.5±2	2.5±2
Paralana Granodiorite-British Empire Granite	6	10.2	10.8	4.1	1.1	3.9±3	4.1±3	4.7±4	4.8±4
British Empire Granite	6	16.2	11.6	5.1	0.7	5.6±3	5.9±3	6.9±4	7.0±4
Paralana Creek Metasediments	3	1.8	6.1	2.0	3.5	1.1±0.1	1.1±0.1	1.3±0.2	1.3±0.2
Freeling Heights Quartzite	3	1.5	16.3	4.4	11	2±1	2.1±1	2.2±1	2.2±1

The anomalous U, Th and K values for Proterozoic units produces an average present heat production value of approximately $40\mu\text{Wm}^{-3}$, with lower values calculated for the Mount Neill Granite still significantly higher than average granite heat production values of about $5\mu\text{Wm}^{-3}$ (Durrance, 1986). In contrast, the Paralana Granodiorite has surface heat production values of $2\mu\text{Wm}^{-3}$ and the metasediments contain heat production values of $1.1\mu\text{Wm}^{-3}$. If the Hot Springs Gneisses are of Mesoproterozoic age, the initial heat production values for this suite would be in excess of $45\mu\text{Wm}^{-3}$, with similar values during the Delamerian Orogeny also listed in order to identify the crustal thermal gradient of the inlier at time of folding and British Empire Granite genesis.

5.4 Conclusions

Although elevated concentrations of radioactive U, Th and K are characteristic of anorogenic I-type Proterozoic granites in many Australian terrains, the magmatic concentrations identified in Proterozoic granites, gneisses and volcanics of the Mount Painter Inlier are extremely anomalous. Therefore derivation from fractionated mantle-derived underplates added to the crust during Proterozoic thermal events is unlikely to produce the extreme radioactive element concentrations alone. It is thus concluded that other magmatic processes and the composition and solubility of accessory minerals in source regions and magmas must also control their distribution and enrichment. An important result of anomalous U, Th and K concentrations is the elevated surface heat production values calculated for units in both the Mount Painter and Mount Babbage Inliers, with heat production values of up to $40\mu\text{Wm}^{-3}$ for the Proterozoic units likely to have significant implications for the magmatic and structural evolution of these terrains.

Chapter Six

BRITISH EMPIRE GRANITE PROVENANCE AND IMPLICATIONS FOR MAGMATIC PROCESSES WITHIN THE MOUNT PAINTER INLIER

This chapter combines field observations together with geochemical and geochronological attributes to identify all potential provenance units for the British Empire Granite. These proposed models are then explored with respect to the magmatic, metamorphic and structural evolution of the Mount Painter Inlier in order to identify the origin of the thermal perturbation required to initiate melting and generate the resulting British Empire Granite.

6.1 Potential British Empire Granite Sources

The geochemical and isotopic characteristics of the British Empire Granite could be inherited from a number of nearby lithologies. Isotopic signatures of the British Empire Granite strongly correlate to Adelaidean sediments during the Delamerian, suggesting the granite may represent melting of these sediments. However, as major and trace element characteristics of the British Empire Granite do not correspond to the Adelaidean sediments, the isotopic similarities may indicate derivation of both granite and sediments from the same basement source.

Isotopic signatures at 470 Ma indicate the Granite can represent part of a mixing curve between a primitive mantle intrusive similar to the Wooltana Volcanics and a crustal component such as the Freeling Heights Quartzite. Furthermore, the British Empire Granite can also be modelled as a mixing curve between the Paralana Granodiorite and Freeling Heights Quartzite. Simple bulk mixing curves using Paralana Granodiorite (mantle component) and Freeling Heights Quartzite (crustal component) as endmembers cannot produce the Nd signature of the British Empire Granite (Appendix I). Assimilation and fractional crystallisation (AFC) calculations (DePaolo, 1981) with the same endmembers can produce the required British Empire Granite isotopic signature, as can modelling with Wooltana Volcanics as the basaltic endmember (Appendix I). Therefore, to further constrain British Empire Granite provenance, it is essential to clarify the relationship between the British Empire Granite and Paralana Granodiorite, with geochemical characteristics and

isotopic signatures of these two units indicating two potential scenarios. Either the Paralana Granodiorite and British Empire Granite represent part of a mixing curve between a “contemporary” mantle component and an ancient crustal component, or the British Empire Granite evolved from the re-melting of Paralana Granodiorite together with a crustal source. As incorporation of the Paralana Granodiorite within the regional anticline of probable Delamerian age implies it is a pre-Delamerian intrusive, a co-magmatic relationship between the two units therefore requires the British Empire Granite to also be pre-Delamerian. Therefore, as both scenarios are possible, it is essential to determine which of the models proposed above is thermally plausible to further constrain the potential source(s) of the British Empire Granite.

6.2 Origins and potential thermal perturbations initiating crustal anatexis and British Empire Granite production

Although crustal rocks may begin melting at temperatures as low as 600-650°C given appropriate compositions, higher temperatures are often required to produce the melt proportions and scale of melting appropriate to segregation of granite melts (Wickham, 1987). The minimum critical temperature required for granite formation by crustal melting was estimated to be 800°C by Wickham (1987), which is well in excess of the steady-state geotherm characteristic of normal continental crust. Therefore, the production of significant volumes of granitic melt due to melting of crustal material requires the addition of thermal energy values in excess of that associated with the normal steady-state crustal geotherm. Previous studies have identified a number of thermal source(s) which may initiate such perturbations during continental collision, including crustal thickening (England and Thompson, 1984; Sandiford *et al.*, 1992), magmatic intrusions (Lux *et al.*, 1986) and anomalously high radioactive heat production (Chamberlain and Sonder, 1990; Lathrop *et al.*, 1994).

If crustal thickening produced by thrust sheets occurs, melting can be initiated at 50 to 60 km depths with thermal energy transferred to shallower mid-crustal levels through upward advection of these melts (Lathrop *et al.*, 1994). Even though British Empire Granite generation may be associated with Delamerian folding and deformation, total crustal thickening associated with this event is estimated to be only 40 to 50 km (M. Sandiford, *pers. comm.*, 1996) and will therefore not attain the temperatures essential for melting. Indeed, the

metasedimentary pile hosting the British Empire Granite records sillimanite-grade metamorphism indicating maximum burial depths of only 15 km during Delamerian folding. Furthermore, Lathrop *et al.* (1994) emphasise that melts produced at shallow to mid-crustal levels due to the upward advection of lower crustal or mantle melts generated by extensive crustal thickening must contain a proportion of the intrusive magma. However, isotopic analyses of this study show that surrounding lithologies can provide the British Empire Granite isotopic ratios and thus lower crustal material is not required to produce the observed signature, although it should be noted that the lower crust material may have an isotopic signature similar to the proposed British Empire Granite sources. In addition, as significant volumes of granite are not identified in adjacent terrains that were buried to similar depths during Delamerian folding, simple burial, heating and melting cannot explain the limited lateral extent of the British Empire Granite. It is therefore concluded that crustal thickening associated with Delamerian folding alone cannot account for British Empire Granite genesis.

The addition of thermal energy from upward advection of lower crust or mantle-derived melts can produce mid-crustal partial melts without leaving their lower-crustal isotopic signatures in the mid-crustal product (Lathrop *et al.*, 1994). If a co-magmatic relationship between Parana Granodiorite and British Empire Granite exists, the granodiorite may represent a middle-member of a mafic mantle-derived magma which would provide the required thermal energy to the crust to produce near *insitu* partial melting of the overlying crustal units. Therefore, intrusion of a mafic melt and associated Parana Granodiorite into Freeling Heights Quartzite and Palaeoproterozoic metasediments would result in melting of these units and thus fractionation from the granodiorite to granite as observed in geochemical and isotopic trends. However, as field observations indicate that the Parana Granodiorite is associated with Delamerian folding and thus must represent a pre-Delamerian intrusive, this co-magmatic model would also require a pre-Delamerian age for the British Empire Granite. This model is plausible as the British Empire Granite body does dip gently to the west on the western limb of the regional anticline and may therefore not be structurally repeated on the eastern limb due to the Parana Fault. However, large volumes of lower-crustal material would be required to initiate British Empire Granite generation and no such intrusive has been identified. Therefore, although this model cannot be rejected, the British Empire Granite isotopic signature does not demand lower crustal or mantle- primitive values as shallow-level meta-igneous and metasedimentary units can provide the isotopic ratios required.

If neither crustal thickening nor lower-crust or mantle-derived intrusives can initiate shallow-level crustal melting, another source of thermal energy is required to produce the British Empire Granite at less than 20 km depths. Recent studies (Chamberlain and Sonder, 1990; Lathrop *et al.*, 1994; Lathrop *et al.*, 1996) have acknowledged that radioactive decay of U, Th and K may lead to anomalously high heat production within crustal sources, potentially initiating metamorphism and anatexis at mid-crustal levels especially if coupled with crustal thickening. As indicated in Chapter 5, Proterozoic gneisses within the Mount Painter Inlier have extreme radioactive element concentrations resulting in heat production values of up to $40 \mu\text{Wm}^{-3}$ and an average crustal heat production for the Mount Painter Block during the Delamerian Orogeny estimated at $14 \mu\text{Wm}^{-3}$ (Wall, 1995).

Thermal models of the Mount Painter Inlier can be generated through a vertical section of sequence in order to evaluate the impact of a high heat producing layer on the geothermal regime. The Hot Springs Gneisses, together with other Mesoproterozoic igneous members identified by Wall (1995), represent a high-heat producing layer approximately 5 km in vertical thickness and containing internal heat production values of $15 \mu\text{Wm}^{-3}$. Using an estimated Freeling Heights Quartzite vertical thickness of 3 km together with 7 km of Adelaidean sediment lithologies (E. Paul, *pers. comm.*, 1996) provides a 10 km thick sedimentary cover over the high heat producing layer, with a background heat production value of $1 \mu\text{Wm}^{-3}$. As wet sediments generally have much lower conductivity values than crystalline basement, burial of the high heat-producing basement by this thermally insulating sedimentary cover will have further impacts on the thermal regime (McLaren 1996, M. Sandiford, *pers. comm.*, 1996). As shown in Figure 6.1, for a proposed gneissic layer 20 km in horizontal length, temperatures of up to 500°C can be generated above and 600°C below this heat-producing layer. Potential temperatures increase to 600°C for a heat producing layer of 50km lateral length, with temperatures greater than 700°C attained below the layer, thus providing the thermal energy required to produce the minimal temperate melting represented by the near *insitu* British Empire Granite. This model produces a present surface heat flow value of 129mWm^{-2} which corresponds to the value of 126mWm^{-2} measured by Sass, Jaeger and Munroe (1976).

Figure 6.1

Images on the adjacent page show thermal modelling of the Mount Painter Inlier, using the Partial Differential Toolbox application from the MATLAB® program (see McLaren, 1996 for more details).

The parameters used in these models are:

$$k \text{ Mesoproterozoic igneous members} = 3 \text{ Wm}^{-1}\text{K}^{-1}$$

$$Q \text{ Mesoproterozoic igneous members} = 15 \mu\text{Wm}^{-3}$$

$$k \text{ Upper sedimentary sequence} = 2 \text{ Wm}^{-1}\text{K}^{-1}$$

$$Q \text{ Upper sedimentary sequence} = 3 \mu\text{Wm}^{-3}$$

$$k \text{ Background lithologies} = 3 \text{ Wm}^{-1}\text{K}^{-1}$$

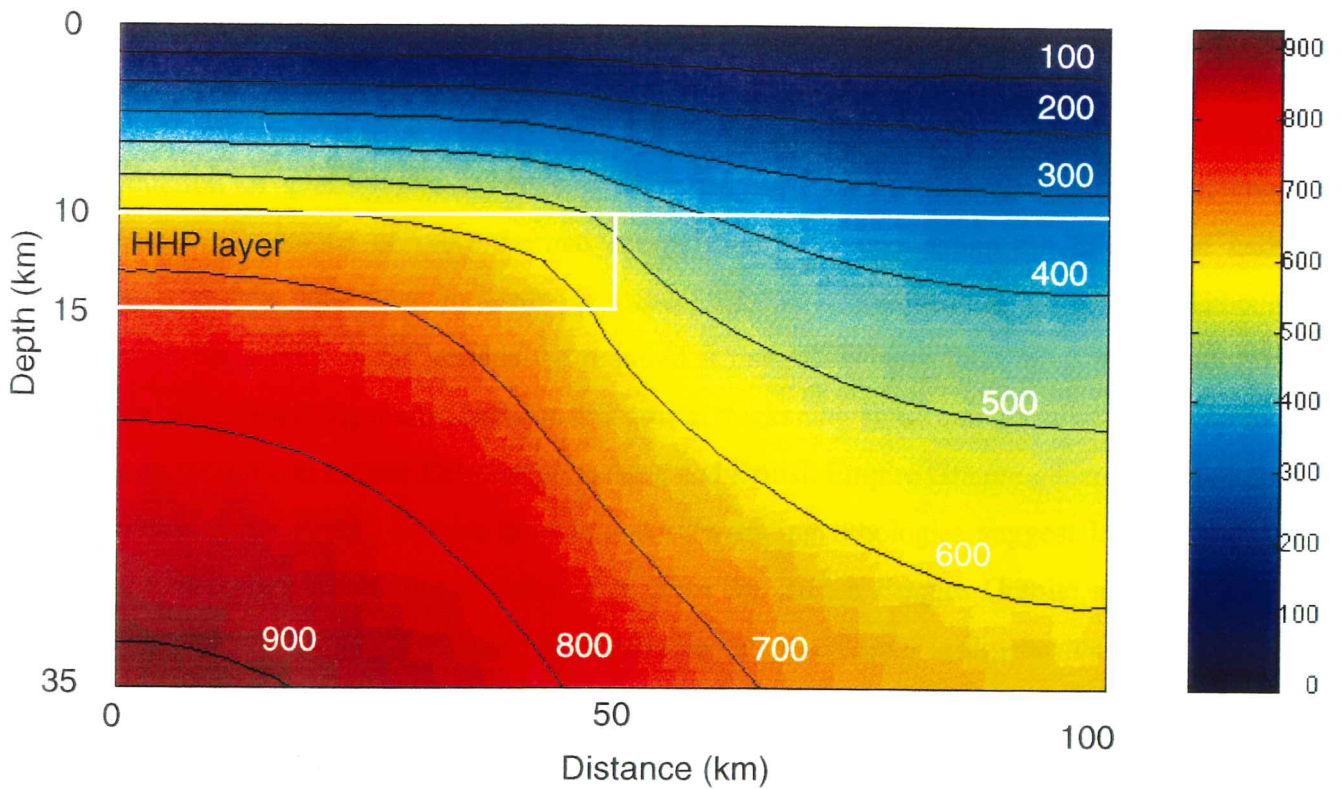
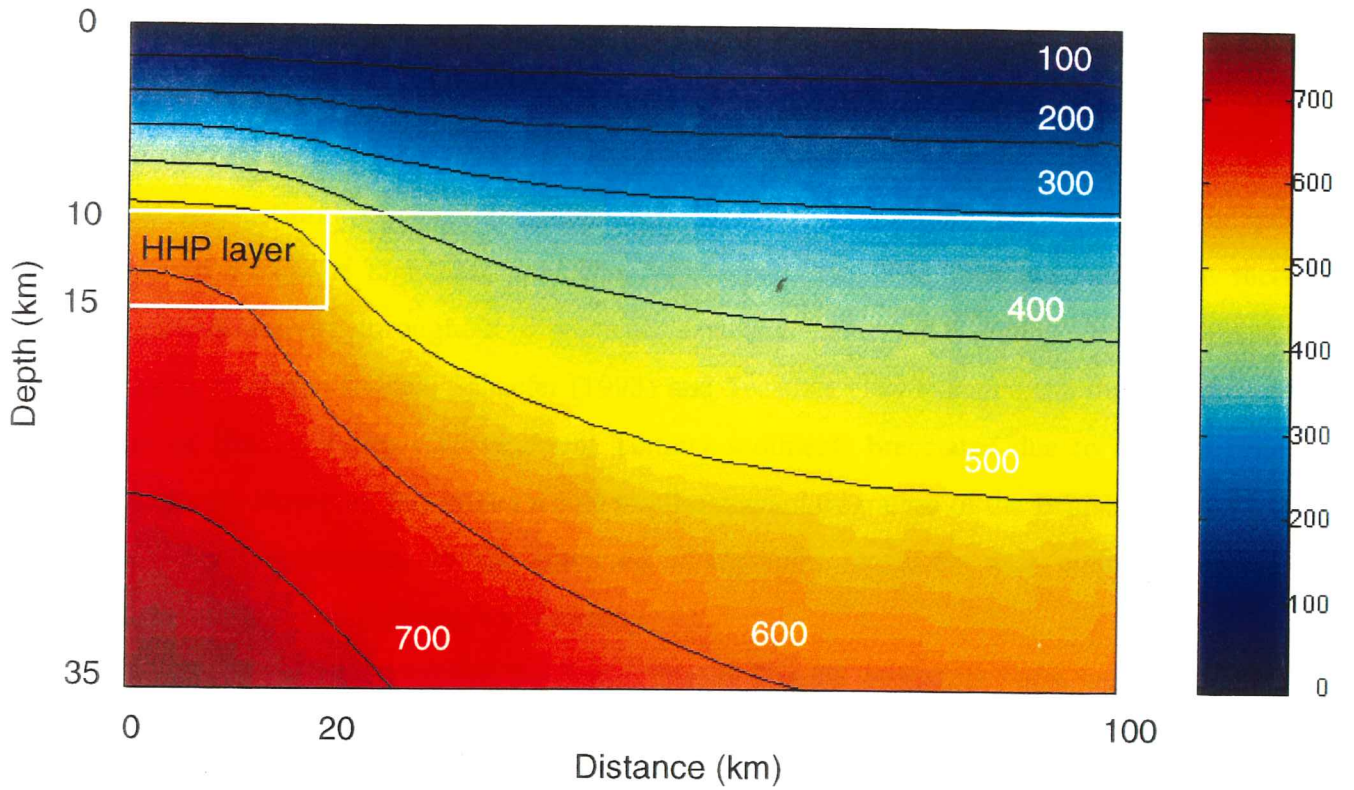
$$Q \text{ Background lithologies} = 1 \mu\text{Wm}^{-3}$$

$$q_m \text{ (mantle heat flow)} = 20 \text{ mWm}^{-2}$$

Figure 6.1a shows variations in temperature ($^{\circ}\text{C}$) with depth for a section through the Mount Painter Inlier, where the horizontal length of the high heat-producing igneous layer is limited to a half width of 20 km. Temperatures of 500°C can be achieved above this layer, corresponding to depths of 10 km. Figure 6.1b indicates the significant influence of the horizontal dimension of the high heat-producing layer on the geothermal gradient (M. Sandiford, *pers. comm.*, 1996). As shown, temperatures of 600°C can be achieved at the same depth when the lateral length of the layer is extended to 50 km.

The temperatures generated in these models indicate that minimal melting can be initiated either above, below or within a high heat-producing layer, especially when coupled with an upper sedimentary thermally-insulating layer. Therefore, these thermal models suggest that the generation of the British Empire Granite from near *insitu* melting of surrounding lithologies due to elevated heat productivity of Mesoproterozoic igneous units is thermally plausible.

Figure 6.1 Mount Painter Inlier thermal model - temperature with depth



6.2 Implications for British Empire Granite Provenance

Radioactive heat production as the driving thermal perturbation which initiates shallow to mid-crustal melting has significant implications for British Empire Granite provenance. If the British Empire Granite represents melting of Adelaidean sediments as a result of anomalous heat production, considerable Delamerian thrusting is essential to juxtapose Adelaidean material under the high heat producing basement layer. The Paralana Fault Zone records extensive activity throughout time, with extensive detached thrusting during Delamerian folding possible. Indeed, Schaefer (1993) and Teasdale (1993) suggested that a sedimentary unit of Hidden Valley may represent Tertiary sediments brecciated due to overthrusting of basement. However, this model would require upward migration of the British Empire Granite melt for emplacement in the observed stratigraphic position, thus contradicting field observations which indicate *insitu* melting.

Therefore, it is concluded that the British Empire Granite represents *insitu* melting of Freeling Heights Quartzite and Paralana Creek Metasediments, together with Paralana Granodiorite, as a response to anomalous radioactive heat production associated with extreme U, Th and K concentrations in underlying Proterozoic gneisses.

6.3 Conclusions

Production of granites due to melting of crustal material at shallow to mid-crustal levels requires the addition of more thermal energy than is present within the lithosphere under normal mantle heat flow and average concentrations of radioactive elements. Although Delamerian activity could provide the required structural deformation, observed metamorphic grade and isotopic signatures indicate that crustal thickening alone cannot produce the thermal energy required to initiate Delamerian melting and British Empire Granite generation. Isotopic analyses of the British Empire Granite and surrounding lithologies suggest lower-crustal or mantle-derived material is not required to form the British Empire Granite, as the Freeling Heights Quartzite and Paralana Granodiorite or Adelaidean sediments can produce the observed isotopic signature. Furthermore, no major mafic lower-crustal bodies have been identified within the inlier. If the additional thermal energy required for melting at mid-crustal levels is provided by radioactive decay of U, Th and K enriched in Proterozoic units, the stratigraphic locations of the two potential sources and the heat-

producing layer play a crucial role in identifying the provenance of the British Empire Granite. As the required juxtaposition of Adelaidean sediments under the enriched basement rocks implies that the resulting British Empire Granite melt must be an intrusive, this source is unlikely to provide the British Empire Granite source material. Therefore it is concluded that anomalous crustal heat production associated with radioactive-elemental enrichment in Proterozoic units can provide the additional thermal energy required to initiate the *in situ* melting of Freeling Heights Quartzite, Paralana Creek Metasediments and Paralana Granodiorite represented as the British Empire Granite.

REFERENCES

- Bea, F., 1996. Residence of REE, Y Th and U in granites and crustal protoliths; Implications for the chemistry of crustal melts. *J. Petrology*, **37**, p. 521-552.
- Blight, P.G., 1977. Uraniferous Metamorphics and "Younger" Granites of the Parana area, Mount Painter Province, South Australia: A Petrographical and geochemical study. Honours Thesis, University of Adelaide (unpublished).
- Bowes, D.R., 1953. The genesis of some granitic and associated rocks in the north-eastern Flinders Ranges, South Australia. *Trans. Royal Soc. S. Aust.*, **76**, 85-107.
- Chamberlain, C.P. and Sonder, L.J., 1990. Heat-producing elements and the thermal and baric patterns of metamorphic belts. *Science*, **250**, p.763-769.
- Chappell, B.W. and White, A.J.R., 1992. I- and S-type granites in the Lachlan Fold Belt. *Trans. Royal Soc. Edinburgh: Earth Sciences*, **83**, p. 1-26.
- Coats, R.P. and Blissett, A.H., 1971. Regional and economic geology of the Mount Painter Province. *Bull. geol. Surv. S. Aust.*, **43**, p. 1-426.
- Coats, R.P., Horwitz, R.C., Crawford, A.R., Campana, B. and Thatcher, D., 1969. Mount Painter Province map sheet, Geol. Atlas. Spec. Series, 1:125,000. (Geol. Surv. S. Aust., Adelaide.)
- DePaolo, D.J., 1981. Trace element and isotopic effects of combined wallrock assimilation and fractional crystallisation. *Earth Planet. Sci. Lett.*, **53**, p. 189-202.
- DePaolo, D.J. and Wasserburg, G.J., 1976. Inferences about magma sources and mantle structure from variations of $^{143}\text{Nd}/^{144}\text{Nd}$. *Geophys. Res. Lett.* **3**, p. 743-746.
- Dougherty-Page, J.S. and Foden, J., 1996. Pb-Pb zircon evaporation date for the Charleston Granite, South Australia: comparisons with other zircon geochronology techniques. *Aust. J. of Earth Sciences* **43**, p. 133-137.
- Durrance, E.M., 1986. Radioactivity in Geology: Principles and applications. Ellis Horwood Limited, West Sussex, 441 p.
- England, P.C. and Thompson, A.B., 1984. Pressure-temperature-timepaths of regional metamorphism I, Heat transfer during the evolution of regions of thickened continental crust. *J. Petrol.*, **25**, p. 894-928.
- Etheridge, M.A., Rutland, R.W.R. and Wyborn, L.A.I, 1987. Orogenesis and tectonic process in the early and middle Proterozoic of northern Australia. *Am Geophys. Union, Geodynamic Series* **17**, p. 131-147.

- Farrand, M.G. and Preiss, W., 1995. Delamerian Igneous Rocks. In: Drexel, J.F., Preiss, W.V. and Parker, A.J. (Eds) *The Geology of South Australia, Volume 2. South Australia. Geological Survey, Bulletin* **54**, P. 54-57.
- Flint, R.B., 1993. Introduction to The Mesoproterozoic. In: Drexel, J.F., Preiss, W.V. and Parker, A.J. (Eds) *The Geology of South Australia, Volume 1: The Precambrian. South Australia. Geological Survey, Bulletin* **54**, p. 107.
- Fowler, C. M. R., 1990. *The Solid Earth: an introduction to global geophysics*. Cambridge University Press, Cambridge, 472 p.
- Goldstein, S.L., 1988. Decoupled evolution of Nd and Sr isotopes in the continental crust and the mantle. *Nature*, **336**, p. 733-738.
- Huston, M.B., 1995. A kinematic analysis of the northern Mount Painter Inlier, South Australia. Honours Thesis, University of Adelaide (unpublished).
- Johnson, G.I., 1980. The geology of the Mount Babbage Inlier, northern Mount Painter Province, South Australia - a petrological, geochemical and geochronological study. Honours Thesis, University of Adelaide (unpublished).
- Kober, B., 1987. Single zircon evaporation combined with Pb⁺ emitter bedding for ²⁰⁷Pb/²⁰⁶Pb age investigations using thermal ion mass spectroscopy, and implications for zirconology. *Contrib. Mineral. Petrol.*, **93**, p. 482-490.
- Lathrop, A.S., Blum, J.D. and Chamberlain, C.P., 1994. Isotopic evidence for closed-system anatexis at mid-crustal levels: An example from the Acedian Appalachians of New England. *J. Geophys Res.*, **99**, p. 9453-9468.
- Lathrop, A.S., Blum, J.D. and Chamberlain, C.P., 1996. Nd, Sr and O isotopic study of the petrogenesis of two syntectonic members of the New Hampshire Plutonic Series. *Contrib. Mineral Petrol.*, **124**, p. 126-138.
- Lux, D.R., De Yoreo, J.J., Guidotti, C.V. and Decker, E.R., 1986. The role of plutonism in low-pressure metamorphic belt formation. *Nature*, **323**, p.794-797.
- McCulloch, M.T. and Wasserburg, G.J., 1978. Sm-Nd and Rb-Sr Chronology of Continental Crust Formation. *Science*, **200**, p. 1003-1011.
- McLaren, S., 1996. The role of internal heat production during metamorphism of the Eastern Arunta Complex, central Australia, and the Mount Isa Inlier, Queensland. Honours Thesis, University of Adelaide (unpublished).
- Mildren, S.D. and Sandiford, M., 1995. Heat refraction and low-pressure metamorphism in the northern Flinders Ranges, South Australia. *Aust. J. of Earth Sciences* **42**, p. 241-247.
- Morgan, P., Sawka, W.N. and Furlong, K.P., 1987. Background and implications of the linear heatflow-heat production relationship. *Geophys. Res. Lett.*, **14**, p.248-251.
- Nier, A.O., 1940. A mass spectrometer for routine isotope abundance measurements. *Rev. Sci. Instrum.*, **11**, p. 212-216.

- O'Halloran, G., 1992. The evolution of provenance and depositional processes during early Adelaidean sedimentation. A sedimentational and Nd isotope investigation. Honours Thesis, University of Adelaide (unpublished).
- Paterson, B.A., Stephens, W.E., Rogers, G., Williams, I.S., Hinton, R.W. and Herd, D.A., 1992. The nature of zircon inheritance in two granite plutons. *Trans. Royal Soc. Edinburgh: Earth Sciences*, **83**, p.459-471.
- Pearce, J.A., Harris, N.B.W. and Tindle, A.G., 1984. Trace element discrimination diagrams for the tectonic interpretation of granitic rocks. *Jl. of Petrology*, **25 part 4**, p. 956-983.
- Preiss, W.V., 1987. Tectonics of the Adelaide Geosyncline. In: The Adelaide Geosyncline: Late Proterozoic stratigraphy, sedimentation, palaeontology and tectonics. Geological Survey of South Australia Bulletin 53, p. 255-281.
- Preiss, W.V., 1995. Early and Middle Palaeozoic Orogenesis: Delamerian Orogeny. In Drexel, J.F. and Preiss, W.V. (eds) The Geology of South Australia, Volume 2 : The Precambrian. *South Australia. Geological Survey. Bulletin* **54**, p. 45-53.
- Roberts, R.H., 1976. Structure and Petrology of Basement Metasediments and Granites in the Mount Painter Inlier. Honours Thesis, University of Adelaide (unpublished).
- Rollinson, H., (1993). Using radiogenic isotope data. In: Using geochemical data: evaluation, presentation, interpretation. Longman Scientific and Technical, Essex, p. 215-265.
- Sandiford, M., Foden, J., Zhou, S. and Turner, S., 1992. Granite genesis and the mechanics of convergent orogenic belts with application to the southern Adelaide Fold Belt. *Trans. Royal Soc. Edinburgh: Earth Sciences*, **83**, p. 83-93.
- Sass, J.H., Jaeger, J.C. and Munroe, R.J., 1976. Heat flow and near surface radioactivity in the Australian continental crust. United States Geological Survey, Open File Report, 76-250.
- Sawka, W.N. and Chappell, B.W., 1986. The distribution of radioactive heat production in I- and S-type granites and residual source regions: implications to high heat flow areas in the Lachlan Fold Belt, Australia. *Aust J. Earth Sciences*, **33**, p. 107-118.
- Schaefer, B., 1993. Isotopic and geochemical constraints on Proterozoic crustal growth of the Mount Painter Inlier. Honours Thesis, University of Adelaide (unpublished).
- Sheard, M.J., Fanning, C.M. and Flint, R.B., 1992. Geochronology and Definition of Mesoproterozoic volcanics and granitoids of the Mount Babbage Inlier, northern Flinders Ranges. Quarterly Geological Notes issued by the Geological Survey of South Australia, 123, p. 18-32.
- Slade, J.V., 1995. Metamorphic Evolution of northern Mount Painter Inlier, South Australia. Honours Thesis, University of Adelaide (unpublished).
- Smith, P.B., 1992. The Alteration History of Late Proterozoic Wooltana Volcanics, Mount Painter Province, South Australia. Honours Thesis, University of Adelaide (unpublished).

- Teale, G.S., 1979. Revision of Nomenclature for Palaeozoic Intrusives of the Mount Painter Province, South Australia. *Trans. Royal Soc. S.A.* **103**, 119-131.
- Teale, G.S., 1993a. Palaeoproterozoic of the Mount Babbage and Mount Painter Inliers. In: J.F. Drexel, W.V. Priess, and Parker, A.J. (Ed.), *The Geology of South Australia. South Australia. Geological Survey. Bulletin* **54**, p. 93-100.
- Teale, G.S., 1993b. Mesoproterozoic Geology of the Mount Painter and Mount Babbage Inliers. In: J.F. Drexel, W.V. Preiss and Parker, A.J. (Ed.), *The Geology of South Australia. South Australia. Geological Survey. Bulletin* **54**, p.149-156.
- Teale, G.S., 1995. Highly deformed alkaline granites from the southern Mount Painter Inlier, northern Flinders Ranges. *South Australia. Geological Survey. Quarterly Geological Notes*, **127**, p. 19-28.
- Teasdale, J., 1993. Proterozoic tectonic models with application to the Mount Painter Inlier. Honours Thesis, University of Adelaide (unpublished.).
- Teasdale, J., Schaefer, B.F., and Sandiford, M., 1995. Post-Delamerian thrusting along the Paralana Fault, Northern Flinder Ranges, South Australia. Abstracts No. 40, Clare Valley Conference, Specialist Group in Tectonics and Structural Geology, Geological Society of Australia, 161.
- Thorton, G.D., 1980. Geology, geochemistry and geochronology of the eastern Babbage Block, Mount Painter Province, South Australia. Honours Thesis, University of Adelaide (unpublished).
- Tilling, R.I., Gottfried, D.G. and Dodge, F.C.W., 1970. Radiogenic heat production and contrasting magma series: Bearing on the interpretation of heat flow, *Geol. Soc. Am. Bull.*, **81**, p. 1447-1462.
- Turner, S.P., Foden, J.D., Sandiford, M. and Bruce, D., 1992. Sm-Nd isotopic evidence for the provenance of sediments from the Adelaide Fold Belt and southeastern Australia with implications for episodic crustal addition. *Geochim. et Cosmochim. Acta.*, **57**, p. 1837-1856.
- Wall, N.M., 1995. Observations on the role of thermal regime on basement-cover deformation: Mount Painter Block v Broken Hill Block. Honours Thesis, University of Adelaide (unpublished.).
- Watt, G.R., Burns, I.M. and Graham, G.A., 1996. Chemical characteristics of migmatites: accessory phase distribution and evidence for fast melt segregation rates. *Contrib. Mineral. Petrol.*, **125**, p. 100-111.
- Webb, P.C., Lee, M.K. and Brown, G.C., 1987. Heat flow - heat production relationships in the UK and the vertical distribution of heat production in granite batholiths. *Geophys. Res. Lett.*, **14**, p. 279-282.
- Webb, P.C., Tindle, A.G. and Barritt, S.D., 1987. Factors controlling the distribution of heat production in selected UK granites. *Geophys. Res. Lett.*, **14**, p. 299-302.

- Whalen, J.B., Currie, K.L., and Chappell, B.W., 1987. A-type granites: geochemical characteristics, discrimination and petrogenesis. *Contrib. Mineral. Petrol.*, **95**, p. 407-419.
- Wickham, S.M., 1987. The segregation and emplacement of granitic magmas. *J. Geol. Soc. London*, **144**, p. 281-297.
- Williams, I.S., 1992. Some observations on the use of zircon U-Pb geochronology in the study of granitic rocks. *Trans. Royal Soc. Edinburgh: Earth Sciences*, **83**, p. 447-458.
- Wilson, M., 1989. Processes which modify the composition of primary magmas. In: *Igneous Petrogenesis: a global tectonic approach*. Unwin Hyman, London, p.73-98.
- Wyborn, L.A.I., Page, R.W. and Parker, A.J., 1987. Geochemical and geochronological signatures in Australian Proterozoic igneous rocks. *Geol. Soc. London Spec. Publ.* **33**, p. 377-394.
- Wyborn, L.A.I., Wyborn, D., Warren, R.G. and Drummond, B.J., 1992. Proterozoic granite types in Australia: Implications for lower crust composition, structure and evolution. *Trans. Royal Soc. Edinburgh: Earth Sciences*, **83**, p. 201-209.

ACKNOWLEDGMENTS

Firstly I would like to thank my supervisors, Dr. Mike Sandiford and Dr. John Foden for their supervision, support and enthusiasm throughout the year. Field work for this project was undertaken with Eike Paul and he is thanked for much assistance, friendship and entertainment throughout the six weeks at Yudnamautana, and later advice and discussions. Special thanks to the Sprigg family for permission to undertake research in this spectacular and beautiful part of Australia, and the Arkaroola crew for the help and good times during our weekly visits. The Mines and Energy Department are also thanked for their financial support during the field component of this study.

The technical staff of the Department of Geology and Geophysics are thanked for their advice and assistance with the laboratory part of this work and encouragement throughout the year. Special thanks to John Stanley for teaching me the fine art of making pressed pellets and fused discs, David Bruce for continually helping with the isotopes and John Dougherty-Page for patience with difficult zircons that didn't want to work. Special thanks also to Martin Hand, Bruce Schaefer and Kathy Stewart for their helpful discussions and assistance with data analysis.

Many thanks also to my fellow Honours students for enduring Honours 1996 with me, and always joking and helping out when times were grim. Special thanks to Sandra McLaren for helping with the computer problems, putting up with my continual silly questions and going mad with me on a daily basis. Thank also to my friends for their continual interest and encouragement, and for helping taking my mind off rocks.

My sisters were fantastic housemates throughout the year; putting up with the stresses, transporting me around at strange times of the day and night, and keeping food in the fridge. Finally I would like to thank my parents for their continual love, interest and support throughout the years, and for encouraging my appreciation and of the outdoors and desire to learn, for which I am truly grateful.

APPENDIX A

GEOLOGICAL MAP

PARALANA HOT SPRINGS- MAWSON PLATEAU AREA

MOUNT PAINTER INLIER

PARALANA HOT SPRINGS - MAWSON PLATEAU AREA

Geological mapping by Eike Paul and Narelle Neumann

6666000

6664000

6662000

6660000

342000

6658000

344000

346000



















348000

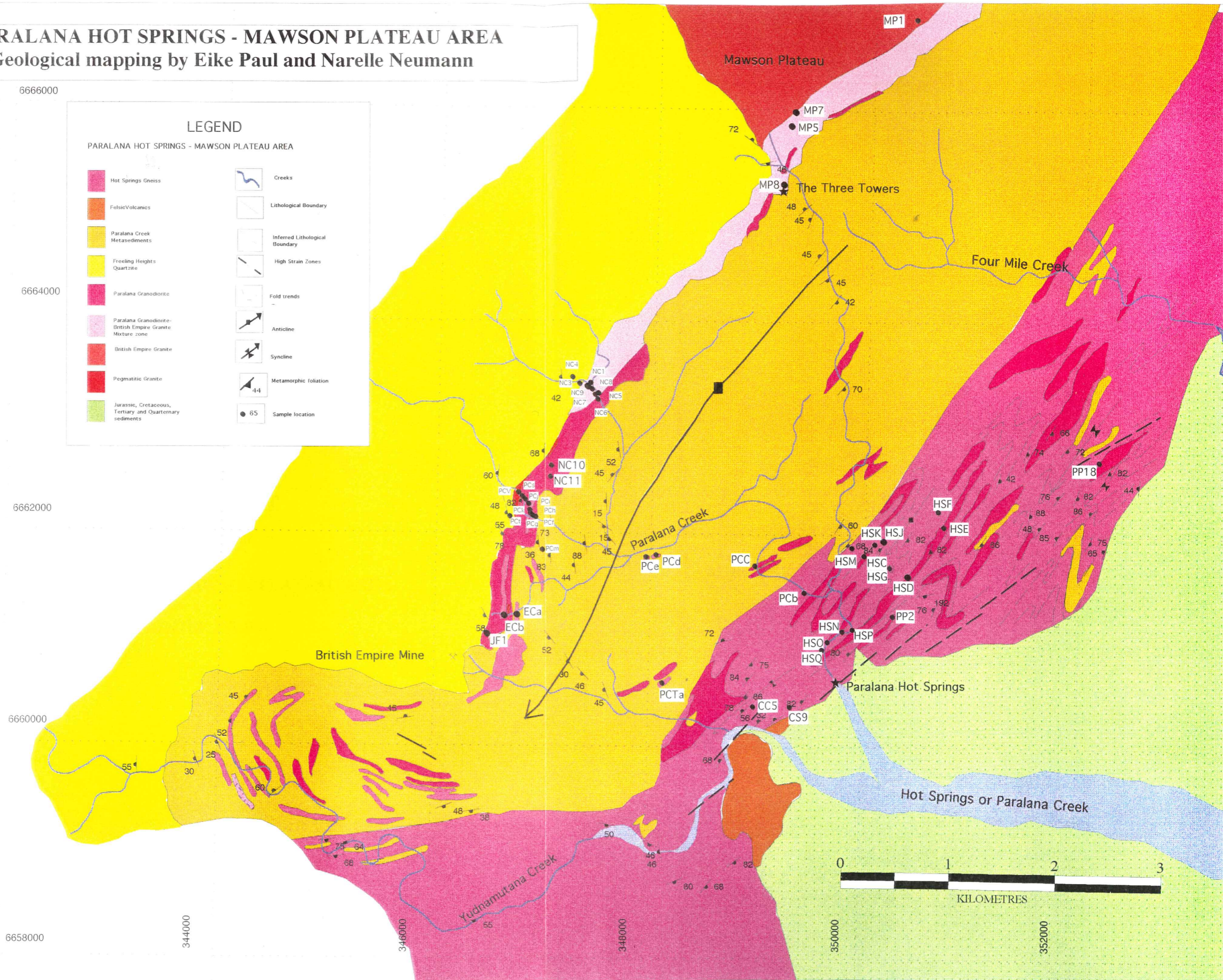
350000

352000

LEGEND

PARALANA HOT SPRINGS - MAWSON PLATEAU AREA

	Hot Springs Gneiss		Creeks
	Felsic Volcanics		Lithological Boundary
	Paralana Creek Metasediments		Inferred Lithological Boundary
	Freeling Heights Quartzite		High Strain Zones
	Paralana Granodiorite		Fold trends
	Paralana Granodiorite-British Empire Granite Mixture zone		Anticline
	British Empire Granite		Syncline
	Pegmatitic Granite		Metamorphic foliation
	Jurassic, Cretaceous, Tertiary and Quaternary sediments		Sample location



APPENDIX B

SAMPLE LOCATION MAP

PARALANA HOT SPRINGS - MAWSON PLATEAU AREA

MOUNT PAINTER INLIER

PARALANA HOT SPRINGS - MAWSON PLATEAU AREA
Sample Locations

6666000

6664000

6662000

6660000

342000

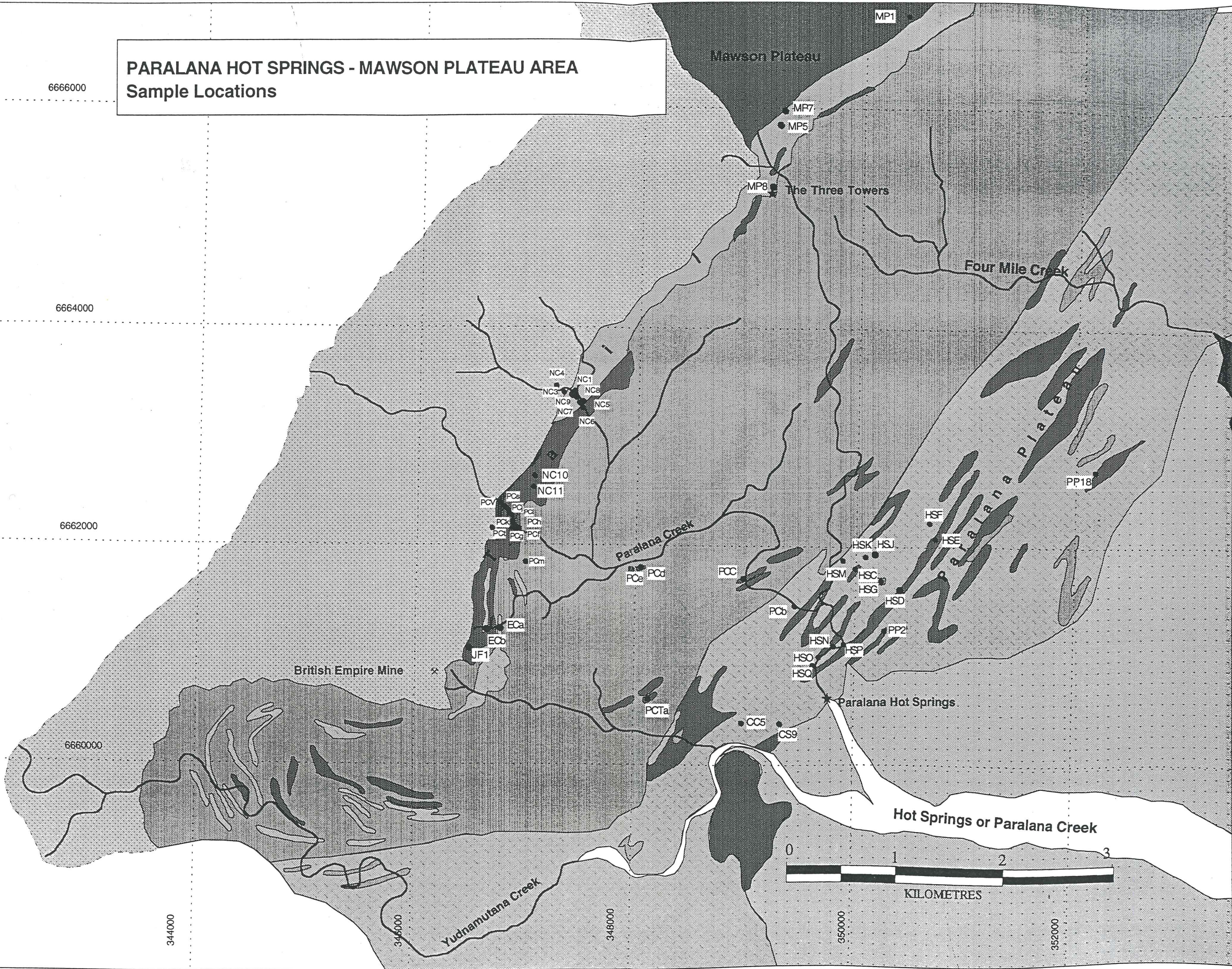
344000

346000

348000

350000

352000



APPENDIX C

THIN SECTION DESCRIPTIONS

APPENDIX C : THIN SECTION DESCRIPTIONS FOR SELECTED MOUNT PAINTER INLIER UNITS

SLIDE NO	LOCATION	ROCK LITHOLOGY	MINERALOGY	PETROLOGICAL TEXTURES
A1086 - HSE	Western Paralana Plateau	Paralana Granodiorite	qtz+fdsp+bte	also minor opaques and musc as cores within plag, qtz inclusions and matrix
A1096 - PCf	Southern Tail : Paralana Creek Gorge	Paralana Granodiorite	plag+qtz+bte+hnbld+ musc	symplectites, radio-damage within bte, minor musc within qtz, hnbld-bte & bte-musc replacement, musc cores within plag
A1086 - PCi	Southern Tail : Paralana Creek Gorge	Coarse Paralana Granodiorite	qtz+plag+bte+minor musc	plag+qtz coarse-grained, mus-plag reactions ('musc cores') and rafts in plag, minor bte-musc replacment
A1086 - JF2	Eastern Mawson Plateau	Quartzitic Paralana Granodiorite	qtz+plag_bte+musc	dominant musc cores within plag and also as matrix, minor hnbld, symplectites
A1086 - HSC	Western Paralana Plateau	Quartzitic Paralana Granodiorite	qtz+plag+kfdsp+bte	musc cores, symplectites
A1086 - NC11	Western Central Tail	Quartzitic Paralana Granodiorite	plag+qtz+bte+musc	musc cores within plagicolase, plag&qtz coarse-grained, fdsp contain bte and qtz inclusions.
A1086 - NC10	Western Central Tail	Biotite/Muscovite Granodiorite	plag+bte+musc+qtz	plag very coarse-grained with musc cores, musc also as matrix, bte contains radioactive damage, minor x-hatched fdsp
A1086 - MP1	Eastern Mawson Plateau	British Empire Granite	coarse-grained plag+musc+qtz+ microcline	musc contains qtz inclusions, mus core minerals in plag, X-hatched microcline, no bte
A1086 - MP5	Northern Tail	Paralana Granodiorite - British Empire Granite	plag+bte+musc+qtz	fdsp exsolution textures, bte-musc replacement, musc>bte
A1086 - NC1	Eastern Central Plateau	Paralana Granodiorite - British Empire Granite Mix	qtz+fdsp+plag+musc+bte	minor bte, dominant musc matrix, exsolution textures within fdsp
A1096 - NC7	Western Central Plateau	British Empire Granite with feldspar megacrysts	plag+fdsp+bte+musc+ qtz	bte-musc replacement, qtz inclusions & musc reactions in coarse plag, symplectites and exsolution in fdsp
A1086 - MP7	Northern Tail	Fine-grained British Empire Granite	plag+kfdsp+qtz+musc +minor bte	bte cores within musc, plag strongly twinned, minor x-hatched fdsp with rims
A1086 - PCV	Southern Tail : Paralana Creek Gorge	Pegmatitic Granite	kfdsp+plag+qtz+bte+ musc	bte with musc rims, fdsp exsolution textures, musc cores in plag
A1086 - ECb	Cairn at Southern Tail	Pegmatitic Granite	qtz + fdsp + plag +	Yellow accessories as minerals/matrix with

			allunite + zircon	radioactive damage, x-hatched fdsp with musc cores & plag inclusions
A1086 - HSO	Hot Springs Gorge	Massive K-feldspar Gneiss (Hot Springs Gneiss)	kfdsp + plag + qtz + bte + accessories	musc cores within plag, yellow/orange accessories associated with radio-damaged bte, opaques, microcline inclusions in qtz
A1086 - CC5	Eastern Yudnamutna Gorge	Massive K-feldspar Gneiss (Hot Springs Gneiss)	qtz+kfdsp+opaques+plag+zr+U-minerals	Zr & apatites contain radio-active rims, extensive mag, musc cores in fdsp, yellow-coloured accessories
A1086 - HSF	Western Paralana Plateau	Massive K-feldspar Gneiss (Hot Springs Gneiss)	fdsp+qtz+plag+bte+musc+opaques+zr	musc cores and rims within fdsp, radio-damaged bte, large zircons, yellow accessories within plag, x-hatched fdsp
A1086 - HSJ	Western Paralana Plateau	Augen-textured Gneiss (magnetitic)	bte+qtz+fdsp+opaques	magnetite dominant with minor yellow accessories associated with bte, symplectites
A1086 - PCS	Southern Tail : Paralana Creek Gorge	Migmatitic Paralana Granodiorite	qtz+plag+fdsp+bte+musc+opaques+zr	plag displays exsolution, primary and secondary qtz, musc before bte and also as matrix, symplectites, opaques very coarse-grained
A1086 - PCTa	West of Hot Springs Gorge	White- Black Granitic Gneiss (Hot Springs Gneiss)	fdsp+qtz+bte+accessories	zircons within bte contain radioactive rims, bte foliated, significant yellow accessories, x-hatched fdsp
A1086 - PCd	Paralana Creek	Pink-Black Granitic Gneiss (Hot Springs Gneiss)	qtz+plag+bte+musc+accessories+opaques	Foliated Bte with zircon inclusions containing radio-damaged rims, x-hatched fdsp contains qtz inclusions, speckled and fibrous musc within plag
A1086 - NC4	West of Central Tail	Freeling Heights Quartzite	qtz+bte+musc+opaques	Bte foliated, musc inclusions within qtz represent different orientation, minor x-hatched fdsp
A1086 - PCT	West of Southern tail:Paralana Ck Gorge	Amphibolite	qtz + hblende + bte + opaques	fine-grained qtz, strongly bte foliation, hblende as blades and megacrysts with qtz inclusions, minor plag

APPENDIX D

THIN SECTION PHOTOMICROGRAPHS

PLATE a and b

Photomicrograph of strong radioactive halos around zircons within biotite of the Hot Springs Gneiss Suite. Plate a is under plane polarised light, with Plate b showing haloes under cross polars. Scale: approximately 2.5 mm wide field of view.

PLATE c and d

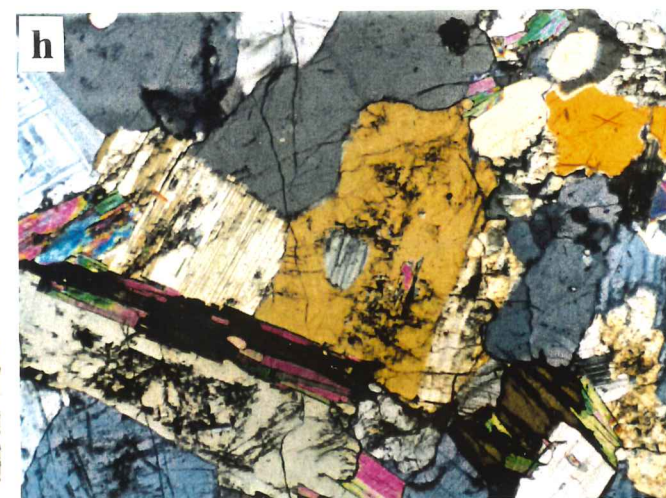
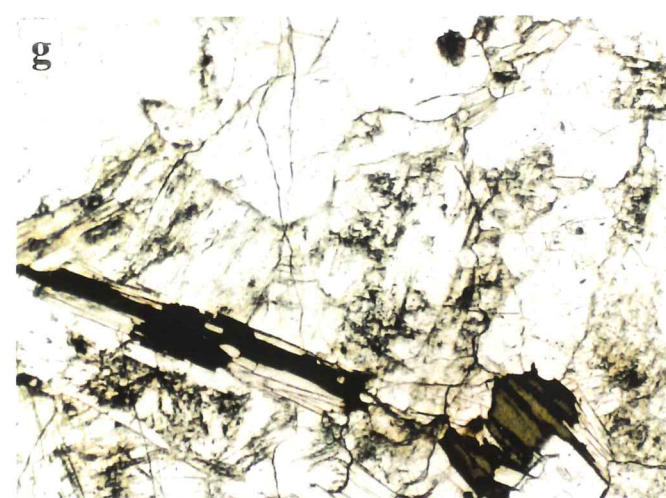
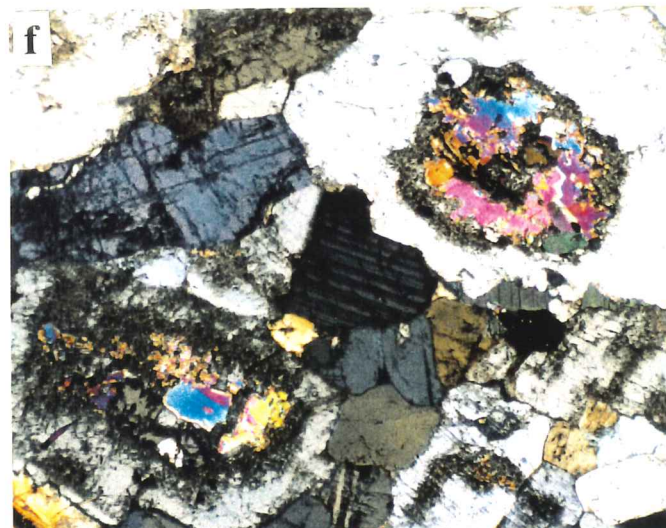
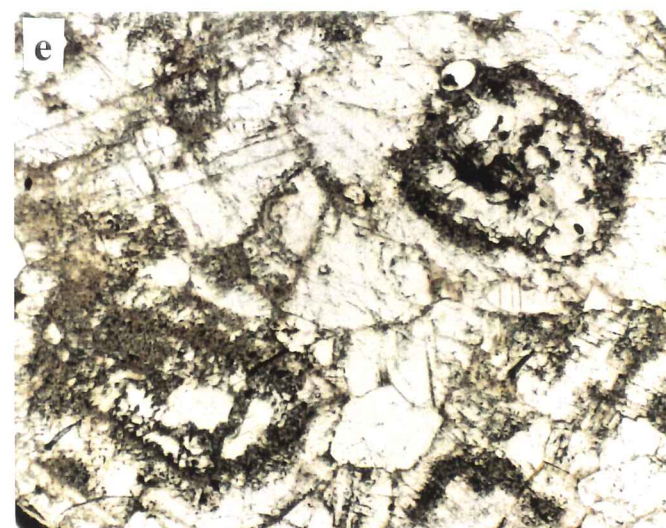
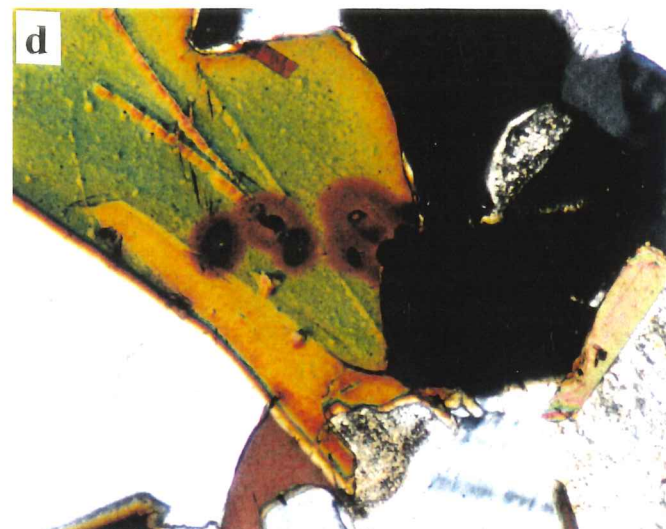
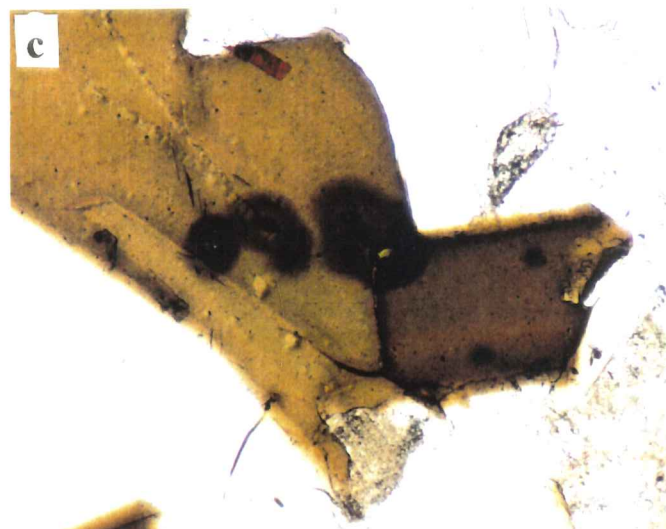
Zircons surrounded by large radioactive halos due to high U content clutter in groups within biotite of the Hot Springs Gneiss. Plain polarised light image in Plate c, and cross polars in Plate d. Scale: approximately 2.5 mm wide field of view.

PLATE e and f

Core-rim reactions between muscovite and plagioclase within Paralana Granodiorite. Plate e is under plain polarised light, Plate f is under cross polars. Scale : 4 mm of view

PLATE g and h

Both muscovite and biotite are contained within this sample from the Paralana Granodiorite-British Empire Granite mixture zone. Note feldspar inclusions within quartz. Plain polarised light image is displayed in Plate g, with Plate h illustrating the same image under cross polars. Scale: photo is 4mm wide.



APPENDIX E

MAJOR AND TRACE ELEMENT GEOCHEMICAL DATA

	Paralana Granodiorite										Qtz Paralana Granodiorite																
	Paralana Plateau					Tail					Paralana Plateau					Paralana Plateau											
	HSD	HSE	HSK	A1015-HV-60	PP2	PCa	PCI	PCj	PCk	PCl	PCm	PP1B	HSP	A1015-HV-59	HSD	HSE	HSK	A1015-HV-60	PP2	PCa	PCI	PCj	PCk	PCl	PCm	PP1B	HSP
SiO2%	75.70	71.38	72.39	67.87	67.29	75.03	69.64	71.95	69.52	71.32	73.93	73.50	77.96	75.70	71.38	72.39	67.87	67.29	75.03	69.64	71.95	69.52	71.32	73.93	73.50	77.96	
Al2O3%	13.96	16.10	15.26	17.09	16.18	14.40	16.11	16.03	17.38	16.32	15.42	15.94	13.16	13.96	16.10	15.26	17.09	16.18	14.40	16.11	16.03	17.38	16.32	15.42	15.94	13.16	
Fe2O3%	0.48	1.48	1.88	1.71	2.77	0.77	2.02	1.31	1.25	1.74	0.61	0.55	0.41	0.48	1.48	1.88	1.71	2.77	0.77	2.02	1.31	1.25	1.74	0.61	0.55	0.41	
MnO%	0.01	0.01	0.02	0.01	0.02	0.01	0.02	0.02	0.01	0.01	0.00	0.01	0.00	0.01	0.01	0.02	0.01	0.02	0.01	0.02	0.02	0.01	0.01	0.00	0.01	0.00	
MgO%	0.42	0.68	0.62	0.57	1.12	0.41	0.89	0.65	0.77	0.74	0.17	0.39	0.06	0.42	0.68	0.62	0.57	1.12	0.41	0.89	0.65	0.77	0.74	0.17	0.39	0.06	
CaO%	1.28	2.66	3.00	3.24	1.84	1.75	3.31	2.76	2.98	3.58	1.14	1.85	0.19	1.28	2.66	3.00	3.24	1.84	1.75	3.31	2.76	2.98	3.58	1.14	1.85	0.19	
Na2O%	5.54	5.74	4.97	5.48	4.44	4.41	3.02	5.36	5.91	6.68	6.93	6.33	5.19	5.54	5.74	4.97	5.48	4.44	4.41	3.02	5.36	5.91	6.68	6.93	6.33	5.19	
K2O%	1.44	1.10	0.97	1.16	4.37	2.47	3.97	1.09	1.13	5.08	1.10	1.21	0.31	1.44	1.10	0.97	1.16	4.37	2.47	3.97	1.09	1.13	5.08	1.10	1.21	0.31	
Ti2O%	0.06	0.20	0.21	0.18	0.55	0.09	0.29	0.18	0.15	0.58	0.06	0.07	0.05	0.06	0.20	0.21	0.18	0.55	0.09	0.29	0.18	0.15	0.58	0.06	0.07	0.05	
P2O5%	0.02	0.06	0.06	0.09	0.17	0.03	0.04	0.04	0.04	0.04	0.02	0.05	0.02	0.02	0.06	0.06	0.09	0.17	0.03	0.04	0.04	0.04	0.04	0.02	0.05	0.02	
SO3%	0.00	0.00	0.00	0.00	0.00	0.00	0.00	0.00	0.00	0.00	0.00	0.00	0.00	0.00	0.00	0.00	0.00	0.00	0.00	0.00	0.00	0.00	0.00	0.00	0.00	0.00	
LOI%	0.41	0.31	0.39	0.33	0.56	0.32	0.42	0.33	0.47	0.23	0.38	0.43	0.36	0.41	0.31	0.39	0.33	0.56	0.32	0.42	0.33	0.47	0.23	0.38	0.43	0.36	
TOTAL%	99.31	99.72	99.76	97.72	99.30	99.70	99.74	99.72	99.63	99.88	99.51	99.61	99.44	99.31	99.72	99.76	97.72	99.30	99.70	99.74	99.72	99.63	99.88	99.51	99.61	99.44	
ASI	1.07	1.04	1.04	1.06	1.05	1.10	1.05	1.07	1.06	1.05	1.08	1.08	1.09	1.07	1.04	1.04	1.06	1.05	1.10	1.05	1.07	1.06	1.05	1.08	1.08	1.08	
K2O/Na2O	0.260	0.192	0.195	0.212	0.984	0.560	1.315	0.203	0.191	0.114	0.165	0.204	0.045	0.260	0.192	0.195	0.212	0.984	0.560	1.315	0.203	0.191	0.114	0.165	0.204	0.045	
Ga/Al*1000	2.261	2.195	2.403	2.886	2.675	1.929	1.900	1.827	1.990	2.084	2.463	2.139	2.657	2.261	2.195	2.403	2.886	2.675	1.929	1.900	1.827	1.990	2.084	2.463	2.139	2.657	
Zr+Nb+Ce+Y	216.900	178.200	197.700	158.600	497.000	145.600	233.400	190.900	185.800	188.300	155.900	249.500	93.000	216.900	178.200	197.700	158.600	497.000	145.600	233.400	190.900	185.800	188.300	155.900	249.500	93.000	
K2O+Na2O	6.980	6.840	5.940	6.640	8.810	6.880	6.990	6.450	7.040	5.660	7.780	7.140	7.240	6.980	6.840	5.940	6.640	8.810	6.880	6.990	6.450	7.040	5.660	7.780	7.140	7.240	
(K2O+Na2O)/Cl	5.453	2.571	1.980	2.049	4.788	3.931	2.112	2.337	2.362	1.581	6.825	3.859	38.105	5.453	2.571	1.980	2.049	4.788	3.931	2.112	2.337	2.362	1.581	6.825	3.859	38.105	
K2O/MgO	3.429	1.618	1.565	2.035	3.902	6.024	4.461	1.677	1.468	0.784	6.471	3.103	5.167	3.429	1.618	1.565	2.035	3.902	6.024	4.461	1.677	1.468	0.784	6.471	3.103	5.167	
K/Rb	150.556	100.458	132.224	124.415	124.794	355.984	185.777	159.027	114.819	220.865	161.336	148.153	134.736	150.556	100.458	132.224	124.415	124.794	355.984	185.777	159.027	114.819	220.865	161.336	148.153	134.736	
Rb ppm	79.4	90.9	60.9	77.4	290.7	57.6	177.4	56.9	81.7	21.8	56.6	67.8	19.1	79.4	90.9	60.9	77.4	290.7	57.6	177.4	56.9	81.7	21.8	56.6	67.8	19.1	
Ba	113	176	106	146	1202	565	534	179	234	202	134	71	39	113	176	106	146	1202	565	534	179	234	202	134	71	39	
Th	18.3	3.3	18.3	2.1	10.8	0.8	8.2	5.7	24.3	6.9	22.4	38.6	9.7	18.3	3.3	18.3	2.1	10.8	0.8	8.2	5.7	24.3	6.9	22.4	38.6	9.7	
U	5.4	1.5	1.9	1.3	8.4	2.2	0.8	1.4	4.8	1.3	7.9	7.2	2.8	5.4	1.5	1.9	1.3	8.4	2.2	0.8	1.4	4.8	1.3	7.9	7.2	2.8	
Nb	6.8	6.5	11.5	12.3	45.9	6	6.8	7.1	10.7	2.9	13.3	10.3	6.9	6.8	6.5	11.5	12.3	45.9	6	6.8	7.1	10.7	2.9	13.3	10.3	6.9	
K	11954.1	9131.6	8052.4	9629.7	36277.5	20504.7	32956.9	9048.6	9380.7	4814.9	9131.6	10044.8	2573.5	11954.1	9131.6	8052.4	9629.7	36277.5	20504.7	32956.9	9048.6	9380.7	4814.9	9131.6	10044.8	2573.5	
La	19	12	8	12	66	11	19	14	26	15	17	35	7	19	12	8	12	66	11	19	14	26	15	17	35	7	
Ce	44	24	10	13	100	23	39	31	51	28	32	71	12	44	24	10	13	100	23	39	31	51	28	32	71	12	
Pb	9	6.2	13.8	17.3	5.6	19.1	6.2	11.5	7.1	8.3	8.9	12.7	2.8	9	6.2	13.8	17.3	5.6	19.1	6.2	11.5	7.1	8.3	8.9	12.7	2.8	
Sr	190.4	609.2	509.6	534.8	268.9	283.9	883	622	513.9	803.9	184.8	207	41	190.4	609.2	509.6	534.8	268.9	283.9	883	622	513.9	803.9	184.8	207	41	
P	87.3	261.9	261.9	392.8	741.9	130.9	174.6	174.6	174.6	174.6	87.3	218.2	87.3	87.3	261.9	261.9	392.8	741.9	130.9	174.6	174.6	174.6	174.6	87.3	218.2	87.3	
Nd	103.7	130.7	167.4	120.9	308.1	92.8	181.9	145.8	87.3	153.1	79.4	45.7	51.3	103.7	130.7	167.4	120.9	308.1	92.8	181.9	145.8	87.3	153.1	79.4	45.7	51.3	
Zr	359.7	1199.0	1258.9	1079.1	3297.2	539.5	1738.5	1079.1	899.2	1438.8	359.7	419.6	299.7	359.7	1199.0	1258.9	1079.1	3297.2	539.5	1738.5	1079.1	899.2	1438.8	359.7	419.6	299.7	
Ti	62.4	17	8.8	12.4	43	23.8	5.7	7	36.8	4.3	31.2	122.5	22.8	62.4	17	8.8	12.4	43	23.8	5.7	7	36.8	4.3	31.2	122.5	22.8	
Y	1.7	2.6	3.5	5.6	5.8	4.4	4.3	3.1	3.2	3.3	1.3	2.6	0.9	1.7	2.6	3.5	5.6	5.8	4.4	4.3	3.1	3.2	3.3	1.3	2.6	0.9	
Sc	2	2	2	8	16	2	1	2	3	2	0	0	3	2	2	2	8	16	2	1	2	3	2	0	0	3	
Cr*	5	16	17	18.8	31	12	21	19	15	20	6	6	5.3	5	16	17	18.8	31	12	21	19	15	20	6	6	5.3	
V	71	65	62	33.4	63	81	64	54	81	64	67	72	83.1	71	65	62	33.4	63	81	64	54	81	64	67	72	83.1	
Co	16.7	18.7	19.4	26.1	22.9	14.7	16.2	15.5	18.3	18	20.1	17.7	18.5	16.7	18.7	19.4	26.1	22.9	14.7	16.2	15.5	18.3	18	20.1	17.7	18.5	
Ga	1.4	1.4	1.2	1.0	9	11	17	10	10	15	13	6	11	1.4	1.4	1.2	1.0	9	11	17	10	10	15	13	6	11	
Cu	5	30	16	19	11	7	25	15	7	31	14	5	8	5	30	16	19	11	7	25	15	7	31	14	5	8	
Zn	0	0	0	10	4	0	0	0	0	0	0	0	4	0	0	0	10	4	0	0	0	0	0	0	0	4	
Ni	73867.2	85190.7	80746.0	90429.1	85614.0	76195.4	85243.6	84820.3	91963.6	86354.8	81592.6	82756.7	69634.1	73867.2	85190.7	80746.0	90429.1	85614.0									

Qtz Paralana Granodiorite

British Empire Granite

Paralana Granodiorite/British Empire Granite
Southern Region

Tail	JF1	JF2	JF3	PCg	NC8	Migmatite HSN	MP1	948-92-BE1	948-92-BE2	948-92-BE3	948-92-BE4	A1015-HV-56	NC5	NC7	NC8	NC9
SiO2%	71.59	71.71	70.33	71.81	69.80	75.17	75.25	77.10	77.10	76.56	77.20	77.20	73.54	74.90	73.51	80.40
Al2O3%	16.30	14.76	16.53	15.95	16.52	14.33	13.19	12.84	13.30	13.04	14.03	14.03	14.30	14.16	15.03	10.22
Fe2O3%	1.39	1.91	2.14	1.47	2.39	0.52	1.18	0.49	0.57	0.19	0.47	0.47	0.65	0.01	1.05	1.71
MnO%	0.63	0.57	0.92	0.77	0.90	0.18	0.23	0.14	0.02	0.00	0.01	0.01	0.01	0.01	0.01	0.01
MgO%	2.44	1.76	3.33	2.52	2.81	0.48	0.04	0.50	0.08	0.56	0.14	0.60	0.33	0.34	0.43	0.59
CaO%	5.68	3.35	4.56	5.33	5.64	3.50	0.23	3.21	3.29	3.14	4.27	4.27	3.31	4.57	5.33	2.11
Na2O%	1.03	4.83	1.33	1.25	1.15	4.38	8.31	4.52	4.66	5.59	3.20	3.17	6.18	3.20	1.94	3.30
TiO2%	0.32	0.13	0.30	0.19	0.23	0.05	0.12	0.05	0.06	0.03	0.04	0.04	0.06	0.11	0.12	0.19
P2O5%	0.05	0.10	0.04	0.03	0.05	0.05	0.05	0.10	0.09	0.07	0.04	0.04	0.07	0.06	0.06	0.05
SO3%	0.00	0.00	0.00	0.00	0.00	0.00	0.00	0.00	0.00	0.00	0.00	0.00	0.00	0.00	0.00	0.00
LOI%	0.44	0.45	0.56	0.41	0.33	0.74	0.85	0.47	0.49	0.26	0.52	0.52	0.41	0.35	0.41	0.66
TOTAL%	99.71	99.79	100.07	99.75	99.83	99.41	99.46	99.44	99.44	99.37	99.44	100.49	99.36	99.72	99.48	99.72
ASI	1.09	1.06	1.10	1.09	1.06	1.26	1.40	1.16	1.16	1.16	1.08	1.21	1.10	1.09	1.09	1.29
K2O/Na2O	0.181	1.442	0.292	0.235	0.204	1.251	36.130	1.408	1.408	1.416	1.780	0.749	1.867	0.694	0.364	1.564
Ga/Al*1000	1.948	2.650	1.978	2.133	2.345	2.268	2.808	2.561	2.558	2.145	1.956	3.112	1.956	2.109	2.112	2.681
Zr+Nb+Ce+Y	158.300	302.900	223.300	178.000	390.900	143.800	186.000	110.400	105.200	67.900	101.300	101.300	63.300	89.600	144.500	166.800
K2O+Na2O	6.710	8.180	5.890	6.580	6.790	7.880	8.540	7.730	7.950	7.950	7.470	7.470	7.740	7.470	7.270	5.410
(K2O+Na2O)/ K2O/MgO	2.750	4.648	1.769	2.611	2.416	16.417	213.500	15.460	14.196	18.188	18.188	12.450	18.980	6.730	4.516	11.041
	1.635	8.474	1.446	1.278	1.278	24.333	36.130	32.286	33.286	69.875	69.875	26.667	18.727	9.324	4.512	5.593
K/Rb	135.938	158.546	192.352	100.356	98.015	165.125	138.247	127.715	118.086	185.399	185.399	114.306	155.088	145.874	139.195	121.755
Rb ppm	62.9	252.9	57.4	103.4	97.4	220.2	499	293.8	327.6	250.3	232.4	232.4	330.8	180.4	115.7	225
Ba	198	967	404	327	111	209	460	152	317	241	92	92	680	404	543	741
Th	4.6	9.3	8.9	15.1	73.1	16.6	19	8.8	10.2	10.4	4.8	4.8	6.6	5.2	15	10.2
U	1	2.3	1.7	2.4	6.9	31.5	6.3	24.8	4	15.7	4	4	2	1.9	10.3	3
Nb	10.2	15	4.9	14	17.3	21.1	28.5	19.4	20.2	4.5	25.6	25.6	12.9	16	8.3	29.8
K	8550.5	40096.2	11041.0	10376.9	9546.7	36360.5	68985.4	37522.7	38684.9	46405.3	26564.8	26564.8	51303.2	26315.7	16104.9	27394.9
La	12	42	18	13	75	13	13	10	8	7	3	3	5	5	21	15
Ce	20	71	37	31	146	27	25	21	15	13	7	7	12	12	40	30
Pb	10.9	21.8	7.4	12.1	14.3	20.5	22.2	22.7	24.3	27.2	18.9	18.9	24.5	18	15.8	11.5
Sr	447.6	186.5	810.1	486.6	352.5	52.5	35.1	38.3	47.6	61.5	26.8	26.8	161.8	178	219.2	58.6
P	218.2	436.4	174.6	130.9	218.2	218.2	218.2	436.4	392.8	305.5	174.6	174.6	305.5	261.9	261.9	218.2
Nd	8	21	17	10	52	11	9	8	5	5	6	6	3	4	14	11
Zr	118.5	208.8	177.1	101.1	207.2	57.2	96.4	38.3	37.4	28.6	45.4	45.4	18.4	51.6	64.2	87.8
Ti	779.3	1918.4	1798.5	1139.0	1378.8	299.7	719.4	299.7	359.7	179.8	239.8	239.8	359.7	659.4	719.4	1139.0
Y	9.6	8.1	4.3	31.9	20.4	38.5	36.1	31.7	32.6	21.8	23.3	23.3	20	10	32	19.2
Sc	3.7	3.2	4.3	3.9	4.3	3.3	6	3.4	4	1.8	5.1	5.1	2.4	2.7	2.7	5
Cr	3	4	4	5	2	0	29	31	29	29	4	4	0	1	1	6
V	12	18	28	20	28	5	8.2	4.4	5.1	3.8	5.2	5.2	7	8	10	15
Co	75	52	61	55	73	73	35.2	30.1	44.4	35.9	57	57	75	74	64	71
Ga	16.8	20.7	17.3	18	20.5	17.2	19.6	17.4	18	14.8	23.1	23.1	14.8	15.8	16.8	14.5
Cu	16	14	8	14	11	8	13	0	2	-	7	7	10	4	7	11
Zn	11	33	26	15	23	4	8	11	10	4	12	12	4	5	11	6
Ni	0	0	0	0	0	0	3	4	2	2	5	5	0	0	0	0
Al	86249.0	78100.3	87466.0	84397.0	87413.1	75825.0	69792.9	67940.9	70374.9	68999.2	74237.6	74237.6	75666.3	74925.5	79529.0	54077.6

All samples prefixed A1096- except A1015- (Schaefer 1993) and 948- (Foden unpubl. data in Schaefer 1993)

Pegmatitic Granite

Northern Region	Hot Springs Granitic Gneisses										Augen-textured Gneiss				A1015-HV-80 A1015-HV-87
	MP8	MP5	HSQ	FCV	HSO	CS9	HSQ	HSF	PCn	POK	HSM	ECa	PCTa		
	74.73	74.65	71.35	74.22	71.04	74.62	72.45	71.33	72.29	71.28	72.10	73.49	70.33	71.34	
SiO2%	14.19	13.89	14.92	13.66	13.33	13.66	13.01	13.53	14.08	13.32	13.33	14.09	13.32	13.16	
Fe2O3%	0.77	0.76	1.39	0.48	4.82	2.31	3.62	4.88	2.51	2.16	3.68	1.35	2.03	4.66	
MnO%	0.01	0.02	0.01	0.01	0.03	0.00	0.01	0.03	0.02	0.03	0.02	0.01	0.05	0.05	
MgO%	0.22	0.23	0.33	0.21	0.43	0.25	0.43	0.63	1.18	1.70	1.08	1.21	2.38	0.42	
CaO%	0.60	0.65	0.36	0.34	0.95	0.13	0.58	1.71	1.32	0.38	1.37	0.92	0.50	1.61	
Na2O%	3.06	3.08	3.37	2.75	4.42	6.63	2.58	4.87	5.09	2.37	4.37	4.29	2.29	2.65	
K2O%	5.27	4.85	6.75	6.96	3.28	0.72	5.75	1.31	1.40	6.96	2.40	3.83	7.00	5.11	
Ti2O%	0.08	0.07	0.07	0.05	0.35	0.28	0.23	0.50	0.50	0.33	0.50	0.36	0.43	0.48	
P2O5%	0.06	0.08	0.07	0.06	0.06	0.05	0.04	0.09	0.09	0.09	0.08	0.08	0.09	0.07	
SO3%	0.00	0.00	0.00	0.00	0.00	0.00	0.00	0.00	0.00	0.00	0.00	0.00	0.00	0.00	
LOI%	0.61	0.61	0.46	0.29	0.52	0.60	0.61	0.39	0.77	0.41	0.54	0.43	0.44	0.16	
TOTAL%	99.59	98.88	99.08	99.02	99.22	99.26	99.13	99.28	99.25	99.03	99.48	100.06	98.85	99.71	

Hot Springs Granitic Gneisses

Northern Region	Hot Springs Granitic Gneisses										Augen-textured Gneiss				A1015-HV-80 A1015-HV-87
	MP8	MP5	HSQ	FCV	HSO	CS9	HSQ	HSF	PCn	POK	HSM	ECa	PCTa		
	74.73	74.65	71.35	74.22	71.04	74.62	72.45	71.33	72.29	71.28	72.10	73.49	70.33	71.34	
SiO2%	14.19	13.89	14.92	13.66	13.33	13.66	13.01	13.53	14.08	13.32	13.33	14.09	13.32	13.16	
Fe2O3%	0.77	0.76	1.39	0.48	4.82	2.31	3.62	4.88	2.51	2.16	3.68	1.35	2.03	4.66	
MnO%	0.01	0.02	0.01	0.01	0.03	0.00	0.01	0.03	0.02	0.03	0.02	0.01	0.05	0.05	
MgO%	0.22	0.23	0.33	0.21	0.43	0.25	0.43	0.63	1.18	1.70	1.08	1.21	2.38	0.42	
CaO%	0.60	0.65	0.36	0.34	0.95	0.13	0.58	1.71	1.32	0.38	1.37	0.92	0.50	1.61	
Na2O%	3.06	3.08	3.37	2.75	4.42	6.63	2.58	4.87	5.09	2.37	4.37	4.29	2.29	2.65	
K2O%	5.27	4.85	6.75	6.96	3.28	0.72	5.75	1.31	1.40	6.96	2.40	3.83	7.00	5.11	
Ti2O%	0.08	0.07	0.07	0.05	0.35	0.28	0.23	0.50	0.50	0.33	0.50	0.36	0.43	0.48	
P2O5%	0.06	0.08	0.07	0.06	0.06	0.05	0.04	0.09	0.09	0.09	0.08	0.08	0.09	0.07	
SO3%	0.00	0.00	0.00	0.00	0.00	0.00	0.00	0.00	0.00	0.00	0.00	0.00	0.00	0.00	
LOI%	0.61	0.61	0.46	0.29	0.52	0.60	0.61	0.39	0.77	0.41	0.54	0.43	0.44	0.16	
TOTAL%	99.59	98.88	99.08	99.02	99.22	99.26	99.13	99.28	99.25	99.03	99.48	100.06	98.85	99.71	

All samples prefixed A1086- except A1015- (Schaefer 1993) and 948- (Foden unpubl. data in Schaefer 1993)

	Mount Neill Granite				Freeling Heights Quartzite				Paralana Creek Metasediments			
	A1015-HV-57	HV-48	NC3	NC4	A1015-HV-55	948-FHO1	948-FHQ3	PCI	Quartzite	Mica Schist	Amphibolite	PCI
SiO2%	70.52	75.86	89.98	87.79	78.71	84.10	31.50	50.87				
Al2O3%	14.28	13.35	4.63	5.72	4.95	7.42	24.91	14.23				
Fe2O3%	3.77	0.82	2.78	2.34	2.25	2.16	14.28	15.14				
MnO%	0.01	0.01	0.01	0.01	0.03	0.03	0.07	0.20				
MgO%	0.32	1.31	0.21	0.44	0.17	1.87	16.59	5.42				
CaO%	0.23	0.27	0.01	0.02	0.02	0.01	0.23	7.59				
Na2O%	3.22	6.28	0.06	0.16	0.11	0.14	0.35	1.03				
K2O%	5.93	1.00	1.47	2.26	2.17	2.75	7.73	1.37				
Ti2O%	0.51	0.37	0.17	0.22	0.16	0.27	0.72	2.57				
P2O5%	0.09	0.06	0.01	0.02	0.01	0.01	0.19	0.55				
SO3%	0.00	0.00	0.00	0.00	-0.01	0.00	0.00	0.00				
LOI%	0.86	0.47	0.68	0.74	0.57	0.91	2.77	0.91				
TOTAL%	99.76	99.79	100.02	99.71	89.16	99.67	99.34	99.88				
ASI	1.18	1.12	2.71	2.08	1.93	2.30	2.66	0.84				
K2O/Na2O	1.842	0.159	24.500	14.125	19.727	19.643	22.086	1.330				
Ga/Al*1000	3.931	3.836	2.163	1.784	4.314	3.362	2.929	3.214				
Zr+Nb+Ce+Y	1332.600	650.500	130.200	177.000	133.900	186.300	657.800	518.000				
K2O+Na2O	9.150	7.280	1.530	2.420	2.280	2.890	8.080	2.400				
(K2O+Na2O)/K2O/MgO	39.783	26.963	153.000	121.000	114.000	289.000	35.130	0.316				
K/Rb	18.531	0.763	7.000	5.136	12.765	1.471	0.466	0.253				
	114.537	94.121	149.183	136.446	177.830	83.045	60.000	72.811				
Rb ppm	429.8	88.2	81.8	137.5	101.3	274.9	1069.5	156.2				
Ba	574	148	448	443	623	181	375	863				
Th	117.2	92.1	6.5	8.7	6.2	9.7	29.5	12				
U	126.5	14.9	1.3	1.5	2.5	1.3	1.7	4.3				
Nb	62.7	32.2	5.5	8.4	6.6	17.6	18.4	19.4				
K	49227.8	8301.5	12203.2	18761.4	18014.2	22829.1	64170.5	11373.0				
La	248	101	14	22	13	4	75	61				
Ce	485	200	30	43	29	7	141	116				
Pb	11.3	9	1	2	6.6	3.8	8.4	2.1				
Sr	46.7	56.4	6.5	5.5	19.4	6.2	5.7	107.5				
P	392.8	261.9	43.6	87.3	43.6	43.6	829.2	2400.3				
Nd	136.9	34.2	10	16	14	2	50	63				
Zr	637.7	321.2	84	112	87.1	136.3	405.2	307.8				
Ti	3057.4	2218.1	1019.1	1318.9	959.2	1618.6	4316.4	15407.1				
Y	147.2	97.1	10.7	13.6	11.2	25.4	93.2	74.8				
Sc	8	7.6	2.1	2.9	2.3	6.4	10.1	47.6				
Cr*	2	8	11	12	18	50	39	70				
V	7.2	22.5	25	17	24.5	28.1	76	330				
Co	81.9	67.1	84	91	60.6	53.3	59.2	57				
Ga	29.7	27.1	5.3	5.4	11.3	13.2	38.6	24.2				
Cu	19	10	7	3	4	0	0	5				
Zn	25	7	1	2	23	50	168	75				
Ni	5	5	0	0	10	8	39	10				
Al	75560.4	70639.5	24498.9	30266.5	26192.2	39261.8	131807.5	75295.9				

All samples prefixed A1086- except A1015- (Schaefer 1993) and 948- (Foden unpubl. data in Schaefer 1993)

APPENDIX F

ZIRCON Pb-Pb DATA

APPENDIX F: SUMMARY OF 207Pb/206Pb ISOTOPIC DATA FOR PARALANA GRANODIORITE (TAIL)

Sample Number	Deposition Number	204Pb/206Pb	204Pb/206Pb error	207Pb/206Pb	207Pb/206Pb error	204Pb/206Pb*	207Pb/206Pb*	Age	Error
Zircon 1	1	0.000078	0.000010	0.077850	0.000766	0.076781	0.076644	1086.0	2.6
		0.000111	0.000015	0.075895	0.000118	0.074374	0.074169		
		0.000101	0.000022	0.075537	0.000058	0.074154	0.073852		
		0.000067	0.000017	0.075534	0.000043	0.074617	0.074384		
Zircon 2	2	0.000010	0.000010	0.092674	0.000035	0.092537	0.092400	1471.7	2.0
		0.000021	0.000010	0.092184	0.000083	0.091896	0.091759		
Zircon 1	1	0.000037	0.000004	0.094897	0.000042	0.094390	0.094336	1519.8	0.8
		0.000027	0.000006	0.095188	0.000068	0.094819	0.094737		
		0.000038	0.000012	0.095483	0.000072	0.094963	0.094799		
Zircon 2	2	0.000055	0.000009	0.095704	0.000056	0.094951	0.094828	1542.9	0.8
		0.000029	0.000003	0.096091	0.000065	0.095695	0.095654		
		0.000010	0.000010	0.096736	0.000226	0.096600	0.096463		
Zircon 3	1	0.000010	0.000010	0.089354	0.000188	0.089217	0.089080	1408.8	2.9
Zircon 4	1	0.000010	0.000010	0.081529	0.000129	0.081392	0.081255	1221.8	2.4
		0.000010	0.000010	0.080742	0.000127	0.080605	0.080468		
Zircon 2	2	0.000010	0.000010	0.091147	0.000119	0.091010	0.090873	1443.4	2.0
		0.000010	0.000010	0.090836	0.000096	0.090699	0.090562		
Zircon 5	1	0.000178	0.000072	0.087404	0.000628	0.084958	0.083965	1359.9	8.7
		0.000084	0.000031	0.088475	0.000120	0.087323	0.086897		
Zircon 2	2	0.000207	0.000050	0.094655	0.000131	0.091815	0.091126	1461.8	14.1
		0.000412	0.000279	0.094713	0.000356	0.089044	0.085165		

*= corrected for common Pb

APPENDIX G

ZIRCON MICROPROBE DATA

APPENDIX G : ELEMENT CONCENTRATIONS OF ZIRCON AND APATITE CRYSTALS FROM PARALANA GRANODIORITE & BRITISH EMPIRE GRANITE

ZIRCON MICROPROBE

weight %	PCJ_Zr1-Core1	PCJ_Zr1-rim1	PCJ_Zr3-Rim1	PCJ_Zr3-Rim2	PCJ_Zr6-Dark1	PCJ_Zr6-Lght1	PCJ_Zr6-med1	PCJ_Zr6-ight2	PCJ_Zr7-ight1	PCJ_Zr7-med1	PCJ_Zr7-dark1	MP1_Zr11-Core1
Mg	0.019	0.012	0.144	0.009	0.022	0.000	0.015	0.007	0.009	0.007	0.055	0.007
Al	0.000	0.000	0.393	0.000	0.425	0.013	0.000	0.000	0.006	0.000	0.428	0.853
Si	14.727	14.775	13.201	14.909	12.635	14.571	14.589	14.179	14.970	14.518	11.536	9.754
P	0.020	0.004	1.207	0.057	0.538	0.000	0.013	0.082	0.000	0.000	0.803	3.449
Ca	0.000	0.000	1.413	0.000	0.556	0.000	0.008	0.026	0.000	0.022	0.940	0.820
Ti	0.000	0.024	0.069	0.013	0.030	0.002	0.009	0.015	0.014	0.020	0.168	0.126
Mn	0.000	0.015	0.000	0.000	0.015	0.000	0.002	0.017	0.000	0.010	0.000	0.028
Fe	0.000	0.023	0.722	0.000	0.623	0.024	0.000	0.000	0.000	0.060	0.562	0.841
Zr	48.838	49.473	43.693	49.269	41.901	46.409	46.397	47.819	47.819	46.999	41.384	38.169
Th	0.043	0.115	0.110	0.047	0.059	0.141	0.000	0.034	0.000	0.000	0.106	0.063
U	0.094	0.417	1.288	0.279	0.472	0.212	0.000	0.288	0.056	0.035	0.401	1.278
O	36.260	35.142	37.762	35.416	42.723	38.629	38.964	39.353	37.127	38.329	43.616	44.610
	100.000	100.000	100.002	99.999	99.999	100.001	99.999	100.000	100.001	100.000	99.999	99.998

	MP1_Zr11-ight1	MP1_Zr11-med1	HSE_Zr2-Core	HSE_Zr2-Core2	HSE_Zr2-rim1	HSE_Zr5-core1	HSE_Zr5-core2	HSE_Zr5-rim1	HSE_Zr5-rim2	MP5_Zr1-core1	MP5_Zr1-core3	MP5_Zr1-rim2
Mg	0.000	0.000	0.008	0.009	0.009	0.011	0.000	0.000	0.016	0.000	0.011	0.028
Al	0.001	0.583	0.000	0.000	0.003	0.005	0.000	0.029	0.005	0.000	0.011	0.000
Si	14.831	10.684	13.685	13.888	14.070	13.805	13.528	13.665	13.746	13.130	12.889	12.767
P	0.000	2.793	0.020	0.000	0.000	0.000	0.000	0.000	0.000	0.000	0.020	0.000
Ca	0.000	0.695	0.018	0.000	0.000	0.036	0.003	0.005	0.011	0.010	0.000	0.018
Ti	0.000	0.140	0.000	0.007	0.009	0.005	0.000	0.000	0.000	0.000	0.002	0.000
Mn	0.040	0.079	0.000	0.008	0.000	0.000	0.000	0.000	0.000	0.000	0.000	0.026
Fe	0.000	1.031	0.000	0.002	0.000	0.002	0.061	0.007	0.000	0.040	0.015	0.018
Zr	48.495	39.526	42.292	43.690	43.864	42.605	42.241	42.573	42.943	40.590	39.806	39.344
Th	0.081	0.000	0.000	0.034	0.000	0.000	0.051	0.090	0.043	0.043	0.000	0.017
U	0.201	0.619	0.000	0.056	0.252	0.030	0.086	0.030	0.095	0.000	0.045	0.128
O	36.352	43.851	43.976	42.306	41.793	43.531	44.028	43.602	43.141	46.187	47.201	47.655
	100.001	100.001	99.999	100.000	100.000	100.000	99.998	100.001	100.000	100.000	100.000	100.001

APATITE PROBES

	PCJ_Zr6-Apt1	MP1_Zr11-dark2	IP1_Zr8-Core1	MP1_Zr8-rim1	MP1_Zr7-core1	MP1_Zr1-Edge1	MP1_Zr1-rim1	MP5_Zr1-core2	MP5_Zr1-rim1	MP5_Zr3-core1	MP5_Zr3-core2
Mg	0.000	0.029	0.000	0.005	0.000	0.000	0.000	0.000	0.000	0.000	0.000
Al	0.000	0.997	0.002	0.003	0.016	0.000	0.007	0.007	0.791	0.000	0.000
Si	0.086	4.775	0.114	0.189	0.201	0.333	0.707	0.206	7.938	0.000	0.759
P	18.664	1.371	12.686	12.474	12.524	15.820	11.603	12.683	4.320	11.878	10.987
Ca	39.506	0.434	1.855	1.981	2.020	0.196	2.253	1.732	1.279	0.034	1.124
Ti	0.000	0.027	0.000	0.024	0.000	0.001	0.023	0.010	0.150	0.000	0.000
Mn	0.052	0.000	0.000	0.000	0.000	0.000	0.000	0.050	0.106	0.000	0.000
Fe	0.040	0.303	0.000	0.000	0.000	0.000	0.000	0.000	0.791	0.000	0.000
Zr	0.000	13.255	0.000	0.000	0.000	0.000	0.000	0.636	32.330	0.000	0.000
Th	0.039	0.119	8.308	11.258	11.147	0.549	18.182	10.257	0.000	4.086	12.631
U	0.000	1.518	0.265	0.618	0.571	1.677	0.000	2.444	2.902	0.000	0.000
O	41.613	77.172	76.769	73.448	73.520	81.423	67.217	74.537	57.425	83.135	74.459
	100.000	100.000	99.999	100.000	99.999	99.999	100.000	100.000	99.999	100.001	100.000

APPENDIX H

Rb-Sr AND Sm-Nd RADIOGENIC ISOTOPE DATA

Lithology Sample No.	Mount Neill Granite				Augen-textured Gneiss				Biotite Granodiorite				
	A1015-HV-48	A1015-HV-57	A1015-HV-12	A1015-HV-13	A1015-HV-80	A1015-HV-86	A1015-HV-65	PCf (tail)	HSE (P. Plateau)	HV-60 (P. Plateau)			
Nd ppm	34.15	136.86	14.85	12.39	108.41	132.7122	80.076	14.653	8.145	3.797			
Sm ppm	6.98	32.93	3.86	3.38	19.83	27.77311	15.432	2.696	1.62	0.773			
143/144 Nd	0.511716	0.511722	0.511827	0.511865	0.511718	0.51157	0.511699	0.512034	0.512325	-			
2 sigma	0.000059	0.000059	0.0000422	0.0000852	0.000093	0.0000388	0.000172	0.000059	0.000059	-			
Sm/Nd	0.2044	0.2406	0.2599	0.2728	0.1829	0.2093	0.1927	0.1840	0.1989	0.2035			
147Sm/144Nd	0.1236	0.1455	0.1572	0.1650	0.1106	0.1266	0.1166	0.1113	0.1203	0.1231			
143/144Nd (470 Ma)	0.511335	0.511274	0.511343	0.511357	0.511377	0.511180	0.511340	0.511691	0.511955	0.511407519			
143/144Nd CHUR	0.512638	0.512638	0.512638	0.512638	0.512638	0.512638	0.512638	0.512683	0.512638	0.512638			
143/144Nd DM	0.513108	0.513108	0.513108	0.513108	0.513108	0.513108	0.513108	0.513108	0.513108	0.513108			
T mod:CHUR	1.92	2.71	3.11	3.69	1.63	2.31	1.78	1.08	0.63	-			
T mod:DM	2.29	2.99	3.31	3.70	2.01	2.62	2.16	1.57	1.25	-			
eps Nd (0)	-17.9854	-17.8684	-15.8201	-15.0789	-17.9464	-20.8334	-18.3170	-11.7822	-6.1057	-			
Sr ppm	56.42	46.94	38.57	33.44	74.96491	121.6859	95.56716	883	609.2	539.5			
Rb ppm	87.44	397.75	106.21	826.73	276.1867	252.333	360.609	177.4	90.9	77.1			
Sr87/86	0.792262	1.027965	0.8234	1.21092	1.070056	0.922266	0.899046	0.711922	0.709979	0.72			
2 sigma	0.000049	0.000049	0.000049	0.000049	0.000356	0.000172	0.000228	0.000049	0.000049	0.000049			
Rb/Sr	1.54981	8.47358	2.75369	24.72279	3.68421	2.07364	3.77336	0.20091	0.14921	0.1428			
frac 87	1.22075	1.24890	1.22447	1.27074	1.25392	1.23627	1.23350	1.21116	1.21093	1.212602566			
at wtSr	87.61100	87.59518	87.60887	87.58338	87.59242	87.60218	87.60374	87.61656	87.61670	87.6157			
87Rb/86Sr	4.52107	25.28434	8.05732	75.05059	11.03722	6.12551	11.12164	0.58151	0.43180	0.413904307			
87/86Sr (470 Ma)	0.761987443	0.858652956	0.769445634	0.708357144	0.996147229	0.881247641	0.824571936	0.708028008	0.707087497	0.721235364			

All samples pre-fixed A1086- except 980- (O'Halloran; 1992), 976- (Smith; 1992), A1015- (Schaefer; 1993), 948-92- (Foden, 1992 unpublished data)

Lithology Sample No.	British Empire Granite			Paralana Creek Metasediments			Freeling Heights Quartzite			
	Mix NC7	948-92-be1	948-92-be2	948-92-be3	948-92-be4	MP1	948-92-fhq1	948-92-fhq3	NC4	A1015-HV-55
Nd ppm	4.443	10.217	6.441	7.5345	5.649	10.312	19.686	20.146	18.863	16.881
Sm ppm	1.015	2.403	1.664	1.8803	1.37	2.603	3.467	3.467	3.34	2.995
143/144 Nd	0.511868	0.511826	0.511787	0.511865	0.511781	0.511858	0.51142	0.511509	0.511435	0.511493
2 sigma	0.000059	0.000059	0.000059	0.000059	0.000059	0.000059	0.000059	0.000059	0.000059	0.000059
Sm/Nd	0.2284	0.2352	0.2583	0.2496	0.2425	0.2524	0.1761	0.1721	0.1771	0.1774
147Sm/144Nd	0.1382	0.1423	0.1563	0.1510	0.1467	0.1527	0.1065	0.1041	0.1071	0.1073
143/144Nd (470 Ma)	0.511443	0.511388	0.511306	0.511400	0.511329	0.511388	0.511092	0.511189	0.511105	0.511163
143/144Nd CHUR	0.512638	0.512638	0.512638	0.512638	0.512638	0.512638	0.512638	0.512638	0.512638	0.512638
143/144Nd DM	0.513108	0.513108	0.513108	0.513108	0.513108	0.513108	0.513108	0.513108	0.513108	0.513108
T mod:CHUR	2.00	2.26	3.19	2.56	2.60	2.69	2.05	1.85	2.04	1.95
T mod:DM	2.43	2.65	3.36	2.91	2.91	3.00	2.35	2.18	2.34	2.26
eps Nd (0)	-15.0203	-15.8396	-16.6004	-15.0789	-16.7174	-15.2154	-23.7595	-22.0233	-23.4669	-22.3354
Sr ppm	178	35.36	38.603	47.744	61.706	52.5	5.366	6.93439	5.5	19.60018
Rb ppm	180.4	489.545	290.114	320.898	245.989	220.2	272.984	1056.15	137.5	102.306
Sr87/86	0.742951	0.979981	0.921056	0.901534	0.864247	0.838366	2.317549	4.429876	1.578829	0.967251
2 sigma	0.000049	0.000049	0.000049	0.000049	0.000049	0.000049	0.000049	0.000049	0.000049	0.000049
Rb/Sr	1.01348	13.84460	7.51532	6.72122	3.98647	4.19429	50.87290	152.30611	25.00000	5.21965
frac 87	1.21486	1.24317	1.23613	1.23380	1.22935	1.22626	1.40287	1.65508	1.31467	1.24165
at wtSr	87.61440	87.59894	87.60226	87.60357	87.60609	87.60785	87.51984	87.42673	87.56084	87.59918
87Rb/86Sr	2.94238	41.12289	22.19757	19.81495	11.71050	12.29025	170.36849	601.11803	78.49544	15.48521
87/86(470 Ma)	0.723247905	0.70460893	0.77241392	0.76884677	0.78582973	0.75609652	1.176706975	0.404596863	1.053198344	0.863557045

All samples pre-fixed A1086- except 980- (O'Halloran; 1992), 976- (Smith; 1992), A1015- (Schaefer; 1993), 948-92- (Foden, 1992 unpublished data)

APPENDIX I

RADIOGENIC ISOTOPE MIXING CURVES

Simple bulk mixing modelling

Radiogenic isotope modelling using Paralana Granodiorite and Freeling Heights Quartzite as the two endmembers indicates that simple bulk mixing can not account for the British Empire Granite isotopic signature. Plots of $1/\text{Sr}$ vs $87/86\text{Sr}$ at 470 Ma and $1/\text{Nd}$ vs $143/144\text{Nd}$ at 470 Ma indicate that the Nd ratios of the British Empire Granite can not be achieved in a bulk mixing scenario. Thus assimilation and fractional crystallisation models were considered.

Assimilation and fractional crystallisation modelling

The equation used for radiogenic isotopes (from DePaolo, 1981 in Wilson, 1989)

$$\varepsilon_L = \varepsilon_L^o + (\varepsilon_* - \varepsilon_L^o) \left(1 - \frac{C_L^o}{C_L} \int \right)$$

where:

ε_L = the isotopic ratio of the contaminated magma

ε_L^o = the isotopic ratio in the original magma

ε_* = the isotopic ratio in the contaminant

C_L^o = concentration of the trace element in the original magma

C_L = concentration of the trace element in the contaminated magma

$\int = F^{-(r-1+D)/(r-1)}$, where F = the fraction of magma remaining

r = ratio of the rate of assimilation to the rate of fractional crystallisation

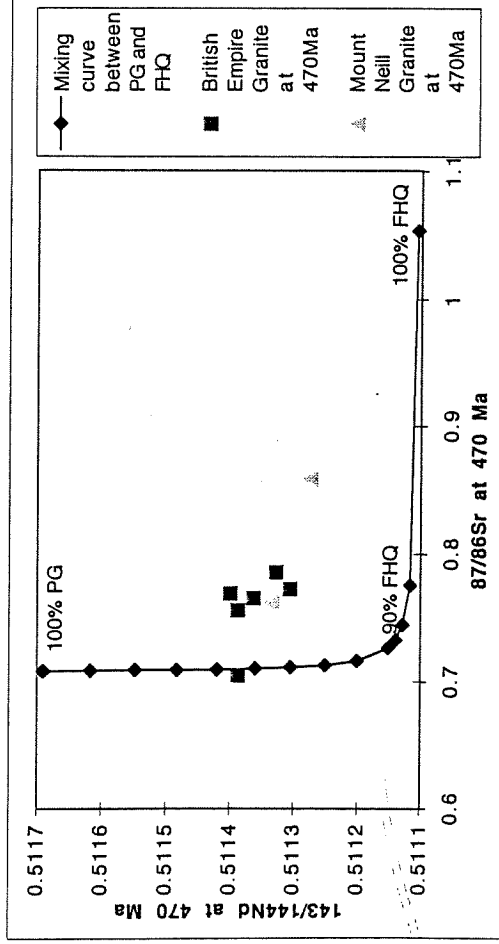
D = the bulk distribution coefficient for the fractionating assemblage.

Modelling using mineral/melt partition coefficients within accepted experimental range

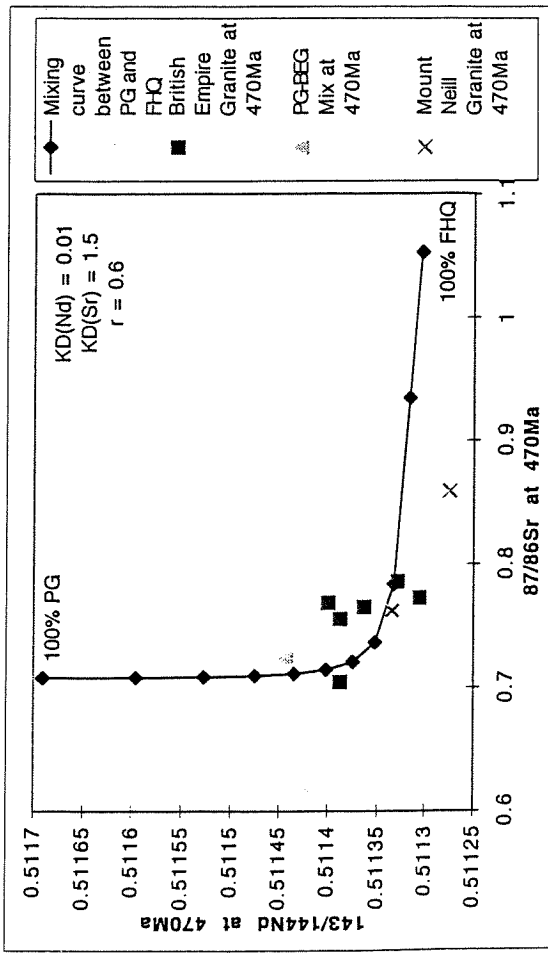
(Rollinson, 1993) indicate that AFC mixing with Paralana Granodiorite and Freeling Heights Quartzite as endmembers can produce the British Empire isotopic signature. Such a model requires approximately 60% Freeling Heights Quartzite and 40% Paralana Granodiorite, with the rate of assimilation to the rate of fractional crystallisation at 0.6.

Similar modelling using a mafic source (such as the Wooltana Volcanics) and Freeling Heights Quartzite as endmembers produces the isotopic signature required for the Paralana Granodiorite, with approximately 90% Wooltana Volcanics required. Further more, the British Empire Granite also lies on this mixing hyperbola, where such a scenario requires 70% Wooltana Volcanics and 30% Freeling Heights Quartzite, with the ratio of the rate of assimilation to the rate of fractional crystallisation much higher, at 0.9. However, it should be noted that the dominance of the mafic member in such a model is unlikely to produce the strong S-type characteristic of the British Empire Granite.

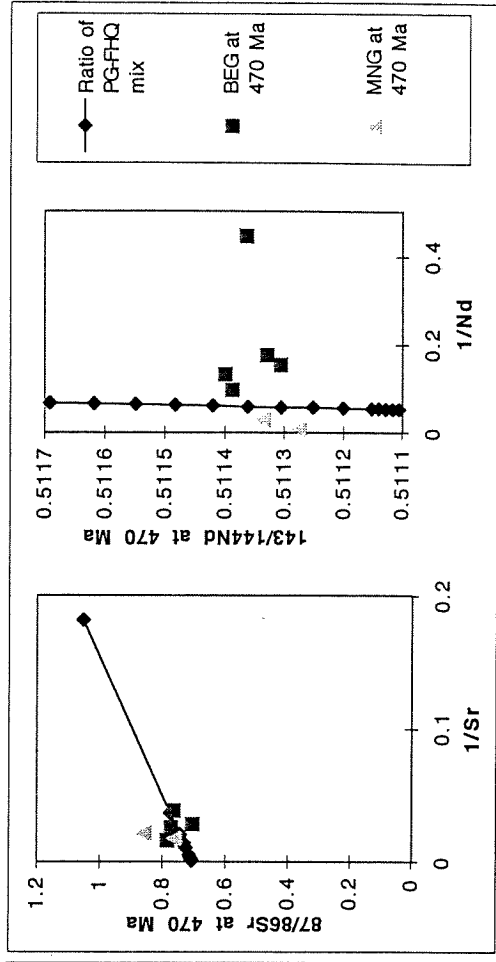
Simple bulk mixing for BEG with PG & FNQ endmembers



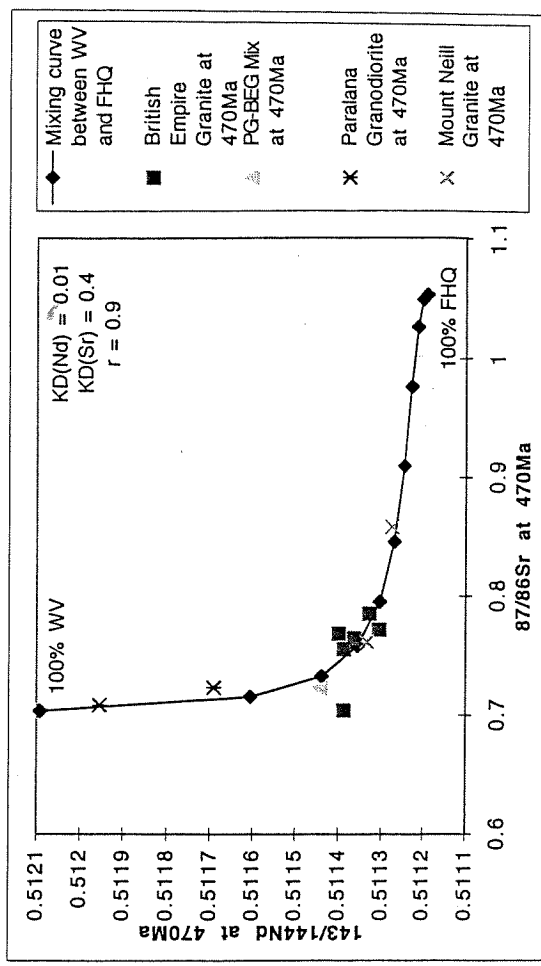
AFC mixing for BEG with PG & FHQ endmembers



Sr and Nd ratio comparisons for simple bulk mixing



AFC mixing for BEG with WV & FHQ endmembers



BEG=British Empire Granite, PG=Paralana Granodiorite, FNQ=Freeing Heights Quartzite, WV=Wooltana Volcanics

APPENDIX J

MAJOR, TRACE AND RADIOGENIC ISOTOPE ELEMENT

ANALYSIS TECHNIQUES

MAJOR AND TRACE ELEMENT ANALYSIS

Samples selected on the basis of freshness, size and lithological representation were cut by a diamond saw to remove all weathered surfaces. They were then crushed in a jaw crusher and milled to a powder in a tungsten carbide mill.

For major element analysis, fused discs were prepared by igniting approximately 2g of sample powder at 960°C for approximately 12 hours to determine the percentage loss of volatiles. 1 gram of ignited powder was then mixed with 4g of Lithium Tetraborate-Lithium Metaborate flux and fused with Ammonium Iodine on the Norrish Prometheus Fusion Apparatus.

Pressed pellets for trace element analysis were prepared by mixing the sample powder with a binding solution and compressed to produce a flat-surface disc.

Both pressed pellets and fused discs were then analysed by X-ray Fluorescence (XRF) methods on a programmable Phillips PW 1480 X-ray spectrometer.

Rb-Sr AND Sm-Nd ISOTOPIC ANALYSIS

Samples were crushed and mill as described above for element analysis. Sample dissolution was carried out in teflon vials using HF and HF-HNO₃. Samples were then converted to a chloride using 6N HCL and spilt, with half of the sample spiked with ¹⁵⁰Nd -¹⁴⁷Sm spike solution. The Rb-Sr fraction was separated using cation exchange columns with the residue collected and used on a second set of columns to extract the Sm and Nd fractions.

Sr samples were mounted onto single de-gassed tantalum filaments whereas Sm and Nd samples were mounted onto double de-gassed tantalum-rhenium filaments. Analysis was carried out on a Finnigan MAT 261 solid source Mass spectrometer, with measurements collected in data blocks of 11 scans. Measurement was continued until runs statistics were within standard operating conditions.

APPENDIX K

ZIRCON SEPARATION AND ANALYSIS TECHNIQUES

APPENDIX K : ZIRCON SEPARATION AND ANALYSIS TECHNIQUES

ZIRCON SEPARATION

Four samples were chosen for Pb-Pb analysis; British Empire Granite (A1086-MP1) from southeastern Mawson Plateau, Paralana Granodiorite-British Empire Granite mix (A1086-MP5) from the Body-Tail junction, Paralana Granodiorite from the southern Tail (A1086-PCf) and Paralana Granodiorite from Paralana Plateau (A1086-HSE).

2kg samples of the four chosen units were crushed through a jaw crusher until all the sample was <1 mm size, with the heavy fraction separated and collected by Wifley Table separation. A Frantz was then used to remove all magnetic material from the heavy fraction, with the zircon separate then extracted from the remaining sample using Sodium Polytungstate and Methylene Iodide heavy liquids. Clear, intact crack-free zircons of between 0.1 and 0.3 mm width were then hand picked and sketched for analysis.

ANALYTICAL METHODS

The procedures undertaken broadly correspond to that outlined by Kober (1987) and Dougherty-Page *et al.* (1996) where a zircon crystal is loaded into a 'canoe'-shaped rhenium filament. The evaporation filament is then aligned with a rhenium 'ionisation' filament. The zircon is then heated to remove surface contamination and unstable metamict zircon, with the ionisation filament heated to 2000°C to ensure that it is not contaminated with material emitted by the zircon. The zircon is then heated in a series of stages with emitted silica and Pb deposited on the cold ionisation filament. The evaporation filament is then cooled and the ionisation filament heated to produce a Pb beam, with the resulting Pb isotope ratios measured by a Finnigan MAT 261 mass spectrometer. Data was collected in 11 scan blocks with 208/206, 207/206 (first pair), 207/206 (second pair), 204/206, and first 206/second 206 ratios collected. Ten sets of these ratios (corrected for background and bilinear drift) were measured per block, with obvious ratio outliers rejected. The maximum possible number of blocks were measured for each disintegration step. Resulting ratios for each block, and then each step, were used to calculate ages which were then corrected for common Pb. These resulting values were then used to determine age plateaus and the true age of the zircon.

APPENDIX L

RADIOMETRIC IMAGE OF THE MOUNT PAINTER INLIER

RADIOMETRIC IMAGE OF THE MOUNT PAINTER INLIER

Radiometric survey of the Mount Painter and Mount Babbage Inliers conducted by CRA Exploration Pty Ltd. Within this image, red = Potassium, green = Thorium and blue = Uranium.

Note the high concentrations of K, Th and U of the Yerila Granite, Hot Springs Gneisses (equivalent to the Paralana Granite) and Box Bore Granite, as indicated by their white colour on the image. The red colour of the Terapinna Granite and Petermorra Volcanics corresponds to high K values, relative to U and Th concentrations, for these units. Proterozoic metasedimentary units (including Paralana Creek Metasediments and Freeling Heights Quartzite) are low in K, U and Th and thus appear dark on the image.

Corresponding K, Th and U concentrations (ppm) for selected regions obtained from geochemical analyses are listed, with the number of samples used also indicated (additional data from Wall, 1995 and Schaefer, 1993). These values are used to calculate heat production values at 500 Ma for specific Proterozoic units, with values ranging from 50 μWm^{-3} for the Yerila Granite to 6 μWm^{-3} for Petermorra Volcanics. Hot Springs Gneisses (equivalent to the Paralana granites) have heat production values of 40 μWm^{-3} at 500 Ma.

Petermorra volc. $\sim 6 \mu\text{W}/\text{m}^3$
5.8 32 11 11

Yerila granite
 $\sim 50 \mu\text{W}/\text{m}^3$
4.7 325 82 8

Terrapinna
granite
 $\sim 8 \mu\text{W}/\text{m}^3$
5.6 58 13 14

Box Bore gr.
 $\sim 25 \mu\text{W}/\text{m}^3$
7.2 112 58 8

Mt Neill gr.
 $\sim 10 \mu\text{W}/\text{m}^3$
5.2 60 20 8

Paralana gn.
 $\sim 40 \mu\text{W}/\text{m}^3$
3.4 266 77 12

20 km

Heat production values calculated for 500 Ma

APPENDIX M

HEAT PRODUCTION DATA FOR MOUNT PAINTER INLIER

**APPENDIX M : HEAT PRODUCTION CALCULATIONS THROUGH TIME
FOR SELECTED MOUNT PAINTER INLIER UNITS**

Sample No.	Lithology	Elemental concentration			Th/U	Calculated Heat Production (uWm-3)				
		U(ppm)	Th(ppm)	K (wt. %)		0Ma	470Ma	1050Ma	1540Ma	1670Ma
Mount Nellii Granite										
92-2-1A		20.8	62.8	4.88	3.0	10.5	11.0	11.8	12.4	12.6
62-2-1B		20.5	64.5	4.56	3.1	10.5	11.0	11.8	12.4	12.6
A1015-HV-12		18.4	81.6	3.26	4.4	11.1	11.6	12.3	12.9	13.1
A1015-HV-13		10.6	32.6	9.08	3.1	6.0	6.3	6.7	7.0	7.1
A1015-HV-32		9.5	82.3	6.71	8.7	9.1	9.5	9.9	10.3	10.4
A1015-HV-48		14.9	92.1	1	6.2	10.7	11.2	11.8	12.4	12.5
Average		15.8	69.3	4.9	4.8	9.6	10.1	10.7	11.3	11.4
Std		4.9	21.2	2.8		1.9	2.0	2.1	2.3	2.3
Hot Springs Gneisses										
H50	MK Gneiss	112.1	384.6	3.28	3.4	57.6	60.6	64.7	68.5	69.5
CS9	MK Gneiss	65.8	284.6	0.72	4.3	38.0	39.8	42.3	44.7	45.3
H5G	MK Gneiss	70.5	296.7	5.75	4.2	40.6	42.6	45.2	47.7	48.4
H5F	MK Gneiss	88.8	485.3	1.31	5.5	58.7	61.3	64.9	68.3	69.2
PCh	MK Gneiss	130	435.2	1.4	3.3	65.8	69.3	73.9	78.3	79.6
PCK	MK Gneiss	62.6	356.6	6.96	5.7	43.0	44.9	47.5	49.8	50.5
H5M	AT Gneiss	32.9	149.1	2.4	4.5	19.7	20.6	21.9	23.1	23.4
ECa	AT Gneiss	84.2	326	3.83	3.9	46.1	48.4	51.5	54.5	55.3
PCTa	AT Gneiss	118.7	423.2	7	3.6	62.5	65.7	70.0	74.1	75.2
A1015-HV-80	AT Gneiss	21.6	108.6	5.11	5.0	14.0	14.7	15.5	16.3	16.6
A1015-HV-87	AT Gneiss	68.4	177.1	0.11	2.6	30.8	32.5	34.9	37.1	37.7
92-2-3	Orthogneiss	71.5	451.8	0.69	6.3	51.6	53.9	56.9	59.7	60.5
A1015-HV-66	Orthogneiss	52	306.9	2.31	5.9	36.1	37.8	39.9	41.9	42.5
A1015-HV-86	Orthogneiss	90.9	435.7	3.74	4.8	55.8	58.5	62.0	65.3	66.3
Average		76.4	330.1	3.2	4.5	44.3	46.5	49.4	52.1	52.9
Std		30.7	118.5	2.3		15.7	16.5	17.5	18.5	18.8
Paralana Granodiorite										
H5D	Paralana Plateau	5.4	18.3	1.44	3.4	2.9	3.0	3.2	3.4	3.5
H5E	Paralana Plateau	1.5	3.3	1.1	2.2	0.7	0.8	0.8	0.9	0.9
H5K	Paralana Plateau	1.9	0.8	0.97	0.4	0.6	0.7	0.7	0.8	0.8
A1015-HV-60	Paralana Plateau	1.3	2.1	1.16	1.6	0.6	0.6	0.7	0.7	0.7
PP2	Paralana Plateau	8.4	10.8	4.37	1.3	3.4	3.6	3.9	4.1	4.2
PP18	Paralana Plateau	7.9	22.4	1.1	2.8	3.8	4.0	4.3	4.5	4.6
H5P	Paralana Plateau	7.2	38.6	1.21	5.4	4.8	5.0	5.3	5.6	5.7
A1015-HV-59	Paralana Plateau	2.8	9.7	0.31	3.5	1.5	1.5	1.6	1.7	1.8
H5N	Paralana Plateau	6.9	73.1	1.15	10.6	7.2	7.5	7.9	8.2	8.3
PCa	Tail	2.2	9.4	2.47	4.3	1.5	1.6	1.6	1.7	1.7
PCf	Tail	0.8	8.2	3.97	10.3	1.2	1.2	1.3	1.3	1.3
PCg	Tail	1.4	5.7	1.09	4.1	0.9	0.9	1.0	1.0	1.0
PCj	Tail	3.1	24.3	1.13	7.8	2.7	2.8	2.9	3.1	3.1
PCk	Tail	4.8	13.3	0.97	2.8	2.3	2.4	2.6	2.8	2.8
PCm	Tail	1.3	6.9	0.58	5.3	0.9	0.9	1.0	1.0	1.1
JF1	Tail	1	4.6	1.03	4.6	0.7	0.7	0.8	0.8	0.8
JF2	Tail	2.3	9.3	4.83	4.0	1.7	1.8	1.9	2.0	2.0
NC6	Tail	2.4	15.1	1.25	6.3	1.8	1.9	2.0	2.1	2.1
PCc	Tail	1.7	8.9	1.33	5.2	1.2	1.3	1.3	1.4	1.4
Average	Tail	3.4	15.0	1.7	4.4	2.1	2.2	2.4	2.5	2.5
Std		2.5	16.7	1.3		1.7	1.8	1.9	2.0	2.0
Paralana Granodiorite/British Empire Granite Mix										
NC5		2	6.6	6.18	3.3	1.6	1.7	1.7	1.8	1.8
NC7	Central Tail	1.9	5.2	3.17	2.7	1.2	1.2	1.3	1.4	1.4
NC9	Central Tail	10.3	15	1.94	1.5	4.0	4.2	4.5	4.9	4.9
NC8	Central Tail	3	10.2	3.3	3.4	1.8	1.9	2.0	2.1	2.2
MP5	Central Tail	19.6	13.1	4.85	0.7	6.6	7.0	7.6	8.1	8.3
MP8	Central Tail	24.5	14.5	5.27	0.6	8.0	8.5	9.3	10.0	10.2
Average	Central Tail	10.2	10.8	4.1	1.1	3.9	4.1	4.4	4.7	4.8
Std		9.8	4.1	1.6		2.9	3.1	3.3	3.6	3.7
British Empire Granite										
MP1		31.5	16.6	4.4	0.5	9.9	10.6	11.5	12.4	12.7
948-92-BE1		6.3	19.0	8.3	3.0	3.8	4.0	4.2	4.4	4.5
948-92-BE2		24.8	8.8	4.5	0.4	7.6	8.1	8.8	9.5	9.7
948-92-BE3		14.9	10.2	4.7	0.7	5.1	5.4	5.9	6.3	6.4
948-92-BE4		15.7	10.4	5.6	0.7	5.4	5.8	6.2	6.7	6.8
A1015-HV-56		4.0	4.8	3.2	1.2	1.7	1.8	1.9	2.0	2.1
Average		16.2	11.6	5.1	0.7	5.6	5.9	6.4	6.9	7.0
Std		10.6	5.2	1.7		2.9	3.1	3.4	3.7	3.8
Freeling Heights Quartzite										
NC3		1.3	6.5	1.47	5.0	1.0	1.0	1.0	1.1	1.1
NC4		1.5	8.7	2.26	5.8	1.2	1.3	1.4	1.4	1.4
A1015-HV-55		2.5	3.2	2.17	1.3	1.1	1.2	1.2	1.3	1.3
Average		1.8	6.1	2.0	3.5	1.1	1.1	1.2	1.3	1.3
Std		0.6	2.8	0.4		0.1	0.1	0.2	0.2	0.2
Paralana Creek Metasediments										
948-92-FHQ1	Metasediment	1.3	9.7	2.75	7.5	1.3	1.4	1.4	1.5	1.5
948-92-FHQ2	Paragneiss	1.4	9.8	2.73	7.0	1.3	1.4	1.4	1.5	1.5
948-92-FHQ3	Mica Schist	1.7	29.5	7.73	17.4	3.3	3.4	3.5	3.6	3.7
Average		1.5	16.3	4.4	11.1	2.0	2.1	2.1	2.2	2.2
Std		0.2	11.4	2.9		1.2	1.2	1.2	1.2	1.2

All samples prefixed A1086- except A1015- (Schaefer 1993) and 948- (Foden unpubl. data in Schaefer 1993)

Relative contributions of the two radiogenic uranium isotopes based on present isotopic composition of 99.2886% U238 & 0.7114% U235 (Fowler,1990)

Calculations of the amount of K present in the past are based on an assumed probability of decay to Ca40 and Ar40 occurring equally.